THE UNIVERSITY OF ALBERTA

PYROLYTIC GRAPHITE CONTAINING

SMALL CONCENTRATIONS OF TRANSITION METALS

by

Ⓒ   BRUCE EVART BALL

A THESIS

SUBMITTED TO THE FACULTY OF GRADUATE STUDIES AND RESEARCH

IN PARTIAL FULFILMENT OF THE REQUIREMENTS FOR THE DEGREE

OF DOCTOR OF PHILOSOPHY IN METALLURGICAL ENGINEERING

DEPARTMENT OF MINING AND METALLURGY

EDMONTON, ALBERTA

SPRING, 1973

ABSTRACT

Graphite alloys containing titanium, vanadium, manganese, and nickel were produced by pyrolytically decomposing propane and a metal-containing vapour onto a stationary graphite substrate. A deposition pressure less than 10 torr and a deposition temperature between 1500 and 2200°C were used in producing these alloys. The deposition kinetics of the alloy formation were examined by measuring the conductivity change of the alloy deposit with deposition time. Alloy formation was found to be linear with time under the deposition conditions employed.

The alloy density was measured using a sink float technique and crystallographic parameters were determined using X-ray diffraction. The microstructure of the alloys was examined by light microscopy, electron microscopy, electron diffraction, and by electron probe microanalyser. The mechanical properties of the alloys were examined by microhardness and bend testing. Some heat treating of the alloys was also conducted. A total of seventy-five deposits were investigated.

Titanium was found to enhance the pyrolytic deposition rate. The titanium containing alloys were found to be a two phase system down to the lowest concentration investigated (0.002 a/o Ti). The graphite phase was found to have

ABSTRACT

Graphite alloys containing titanium, vanadium, manga-
nese, and nickel were produced by pyrolytically decomposing
propane and a metal-containing vapour onto a stationary
graphite substrate. A deposition pressure less than 10
torr, and a deposition temperature between 1500 and 2100°C
were used in producing these alloys. The deposition
kinetics of the alloy formation were examined by measuring
the conductivity change of the alloy deposit with deposi-
tion time. Alloy formation was found to be linear with
time under the deposition conditions employed.

The alloy density was measured using a mini float.
technique and crystallographic parameters were determined
using X-ray diffraction. The microstructure of the alloys
was examined by light microscopy, electron microscopy,
electron diffraction, and by electron probe microanalyser.
The mechanical properties of the alloys were examined by
microhardness and bend testing. Some heat treating of the
alloys was also conducted. A total of seventy-five deposits
were investigated.

Titanium was found to enhance the pyrolytic deposition
rate. The titanium containing alloys were found to be a
two phase system down to the lowest concentration investi-
gated (0.002 a/o Ti). The graphite phase was found to have

an enhanced density but smaller crystal size than pure

pyrolytic graphite. Titanium carbide particles, 2,000 Å

in size, were preferentially aligned with their dense

packed (111) planes parallel to the graphite basal planes.

Evidence for dispersion hardening which reaches a maximum

at 0.020 a/o titanium was found.

Vanadium increased the pyrolytic deposition rate to

over four times that of pure pyrolytic graphite whereas

nickel enhanced the rate by one and one half times. Man-

ganese was found to have no effect. The alloys containing

either vanadium or nickel were found to have an increased

degree of graphitization with very little metal being

incorporated into the alloy deposits. The enhancement of

graphitization is significant in terms of codeposition

being employed to perfect the crystallinity of graphite

formed by the pyrolytic method.

In summary, the increased deposition rate, the enhanced

graphitization, and the possibility of dispersion hardening

are the most significant findings of this investigation.

Furthermore, it appears that any solid solubility of tran-

sition metals in graphite is very low.

an enhanced density but smaller crystal size than pure pyrolytic graphite. Titanium carbide particles, 2,000 Å in size, were preferentially aligned with their dense packed (111) planes parallel to the graphite basal planes. Evidence for dispersion hardening which reaches a maximum at 0,020 a/o titanium was found.

Vanadium increased the pyrolytic deposition rate to over four times that of pure pyrolytic graphite whereas nickel enhanced the rate by one and one half times. Manganese was found to have no effect. The alloys containing either vanadium or nickel were found to have an increased degree of graphitization with very little metal being incorporated into the alloy deposite. The enhancement of graphitization is significant in terms of composition being employed to perfect the crystallinity of graphite formed by the pyrolytic method.

In summary, the increased deposition rate, the enhanced graphitization, and the possibility of dispersion hardening are the most significant findings of this investigation. Furthermore, it appears that any solid solubility of transition metals in graphite is very low.

ACKNOWLEDGEMENTS

TABLE OF CONTENTS

LIST OF TABLES

LIST OF FIGURES

1.   INTRODUCTION

The use of graphite as an engineering material is rapidly expanding. This is due in part to the properties inherent to graphite and in part to a better understanding, achieved through research, of the structure-property relations which has led to the development of graphites with improved engineering properties. Graphite has the ability to retain its strength to approximately 2500°C. In fact, its tensile strength at 1400°C can be 75 percent higher than at room temperature.[1] This strength retention plus a relatively high conductivity (in the vicinity of 10^6 (ohm-cm)$^{-1}$)[2] are utilized in electrical applications such as electrodes and brushes. Good machinability plus an excellent resistance to thermal shock make graphite a desireable material for some machine components. A low neutron absorption cross-section makes graphite useful as a nuclear reactor moderator and structural material. Aerospace applications make use of graphite's anisotropy and high temperature stability. Hot pressing dies made from graphite make high density and high strength ceramics possible. These are only a few of the more recent uses that research and development have contributed to for graphite materials.

Factors which have restricted a more wide spread use of bulk graphite are its permeability, low ductility and relatively low strength. These limiting factors are caused by imperfections of the crystal lattice, the presence of voids, and the weak bonds between crystallographic layer planes. Before examining possible means of improving or altering graphite's properties, a review of the natural and man made forms of graphite is in order.

Natural graphite is found in various locations throughout the world and occurs as either single crystals or crystal aggregates, generally possessing a low degree of perfection. The primary source of industrial graphite is not these natural crystals but commercially made graphite which comes in two forms: that made by the Acheson Process, and that made by a pyrolytic decomposition and deposition process. The Acheson Process begins with a carbonaceous material such as petroleum coke, anthracite or lampblack. This material is calcinated and then crushed and screened to produce a range of particle sizes and a flour material. The particles and flour are mixed with coal tar pitch, formed into shapes, and then baked. This resulting "green" material is impregnated with pitch and subsequently graphitized at a temperature of approximately 3000°C. The final graphitized product has a very complex structure consisting of graphite particles held together

by a semi-graphitic binder. There are many shrinkage cracks and voids present in this product. Figure 1 shows a typical microstructure of an Acheson graphite.

Pyrolytically formed graphite is more dense and contains fewer voids than the Acheson graphite. Pyrolytic graphite also is highly anisotropic and displays a range of crystallinity. This form of graphite can be made by thermally decomposing a carbonaceous gas or liquid to give a graphite deposit on a heated substrate.

Graphite single crystals can be made using a pyrolytic process also, but it is more common to obtain single crystals by growing them in a molten metal or carbide bath.[3] The crystals so produced display structural defects such as twins. Thus, regardless of the source of the graphite, it contains a number of different defects which affect its properties.

Improvement in properties may be achieved by the following techniques:

1.   Infiltration of graphite.

This involves introducing a second phase (metallic or nonmetallic) into the graphite pores resulting in

(a)   an increased density,

(b)   an increased load-bearing cross-section,

(c)   a second phase which may hinder crack propagation.

2. Graphite-metal combinations (cermets).

    This is essentially a powdered graphite matrix held together by a metal binder. The binder is more ductile than the graphite and should:

    (a) form a strong bond between the graphite particles,

    (b) reduce stresses resulting from anisotropy,

    (c) serve as a hinderance to crack propagation.

3. Alloying of graphite.

    Both solid solution and multiphase alloys are theoretically feasible. Such alloying may:

    (a) increase the degree of graphitization and perfection of the crystal lattice,

    (b) increase the crystallographic layer plane bonding strength,

    (c) increase the ductility,

    (d) conceivably result in segregation of solute atoms to boundaries causing relaxation in boundary areas and an increase of the bonding between particles,

    (e) reduce submicroscopic porosity,

    (f) possibly cause precipitation hardening or dispersion hardening.

    The alloying behaviour has implications for the formation of both infiltrated graphite and cermets. It is for this reason that alloying will be investigated in this

thesis and that phase relationships will be of importance.

1.1 Alloying Additions to Graphite.

Natural graphite is known to contain a number of metal-
lic impurities. The presence of these metallic elements
in artificial graphites possibly promotes crystallization
of the graphite as well as modifying other properties. In
most cases, additions of metal to graphite have been in-
vestigated only at large metal concentrations. However,
in recent years there has been an increasing interest in
graphite-metal relationships for small metal concentrations.
Studies of graphite-metal systems are more complex than
metal-metal systems because graphite begins to sublime at
approximately 2500°C and can only be melted above 100 atmos-
pheres and 3800°C and, therefore, cannot be readily equilib-
rated in the liquid state.

There are, however, four methods of adding metals or
compounds to graphite to facilitate graphite-metal phase
studies. These methods are: powder blending and sinter-
ing, molten bath mixtures, graphite infiltration, and
pyrolytic codeposition.

The cermet forming technique of powder blending and
sintering results in a multi phase system--graphite with
one or more phases bonding graphite particles together.
Electrical brushes are commercially made by this process

to give brush material which is high in conductivity and wear resistance. Common bonding materials are copper, copper oxide and silver. Graphite electrodes for various uses can also be made in this manner. Other graphite base materials with iron and cobalt have been found to have improved mechanical properties over graphite.[4] No phase studies have been conducted with alloys produced using the technique of powder blending and sintering.

The method used to produce graphite single crystals in molten metal baths has, however, been employed in graphite-metal phase studies. Commonly, nickel or iron melts are used as these molten metals are capable of dissolving sufficient amounts of carbon for precipitation as graphite. Other melts such as tungsten, chromium, rhodium, molybdenum, zirconium carbide and titanium boride have also been used.[5] Austerman[3] reports that entrapment of the solvent can readily occur in graphite crystals grown from a melt and the degree of such entrapment varies directly with the crystal growth rate. Micrographs produced by Austerman show graphite cleavage planes decorated with iron and nickel beads. No information on the mechanical properties of the graphite so produced is available as this technique has been employed to produce highly crystallized but very small single crystals for electronic studies.

Using the method of growing crystals from solution,

Strong and Hanneman[6] were among the first investigators to
suggest that there is any sort of measureable solid solu-
bility of metallic elements in graphite. In their investi-
gation of the nickel-carbon phase diagram, they employed
an electron probe micro-analyser for chemical analysis of
small graphite crystals frozen into a nickel matrix. They
found that the distribution of nickel was uniform through-
out each graphite crystal. The temperature at which the
graphite crystals were grown ranged between 1350°C and
1510°C. Pressures of 1 atmosphere and 26 or 54 kilobars
were employed. The concentration of nickel possibly cor-
responding to the solubility limit in the graphite phase
was found to be 0.3 $\pm$ 0.1 atomic percent (a/o) nickel. The
graphite crystals were observed in an electron microscope
and were found to be uniform to a resolution of at least
100 Å. Pressure effects on solubility could not be detect-
ed within experimental error. Carbide formation and high
melting temperatures have restricted further use of this
technique.

The graphite infiltration technique has been used to
form mixtures and alloys between graphite and other mater-
ials viz. elements, compounds, and radicals. Infiltration
can usually be achieved by exposing graphite to the appro-
priate medium (either liquid or gas) and allowing the
reactant material to diffuse into the graphite. In some

cases a catalyst has been found necessary to obtain any infiltration. Using the infiltration technique, a wide range of crystal compounds called intercalation or lamellar compounds have been formed with graphite. Intercalation compounds contain an element or compound in the interstitial space in the graphite lattice while the basic lattice structure of the graphite is preserved. Compounds are formed between graphite and one or more of the following chemical forms:

bisulphates	halides
nitrates	metal oxides
perchlorates	metal sulphides
arsenates	metal amides
halogens	alkali metals
phosphates	

Not all derivatives of the above form intercalation compounds as it is necessary for a transfer of electrons between the graphite and the reactant to occur before a compound is formed.[7,8] An intercalation compound can exist in several concentration stages which differ in the number of carbon layers alternating in a periodic sequence with single layers of reactant. A large number of these compounds are stable only in the presence of excess reactant. A considerable amount of work has been done with these systems; primarily to determine the electronic behavior of

the intercalation compounds.[7,9,10,11]

When the intercalation compound is heated to drive out the reactant, an equilibrium concentration of the reactant remains. The system achieved in this manner is called a residual compound, although this is probably a misnomer as the compound aspect no longer exists. The reactant is probably trapped at crystal defects in the graphite.[7]

The infiltration-diffusion technique was employed by Lowell to determine the extent of boron solid solution in graphite.[12] Natural graphite crystals were heat treated in a boron atmosphere between 1800°C and 2500°C. Analysis by X-rays of the resultant graphite showed a maximum solubility of 2.35 a/o at an eutectic temperature of 2350°C. The solid solution was shown to be substitutional. Enhancement of strength, density and crystallinity over ordinary graphite have been achieved by the formation of graphite-boron materials.[13,14]

Fitzer and Kegel[15] also employed infiltration (or diffusion) to determine vanadium solubility in graphite. An electron probe microanalyzer was used to study glassy carbon and graphite samples upon which vanadium carbide had been melted. They found that between 2650°C and 3000°C, the solubility of vanadium in well ordered graphite

is 0.088 $\pm$ 0.007 a/o vanadium. Vanadium also enhanced the crystallinity of the graphite.

The technique of pyrolytically codepositing graphite and an element or compound has become prominent in the last twenty years. Originally, codeposition was used to enhance the properties of pyrolytic graphite used as a protective coating material[16] but it can now be used to form free standing alloys. That is, it is no longer necessary to retain a back up substrate or skeleton frame for the final graphite form.

Codeposition usually involves the thermal decomposition of two gas phases or, alternatively, the thermal decomposition of a single gas phase over an appropriate substrate, to give the desired product. This technique has been the basis of forming the alloys described in some patents[17,18] and alloy studies.[19-25]

Most of these studies were concerned with the strong carbide-forming transition metals and their effects on graphite strength and oxidation resistance. This work has been oriented towards heat shielding and nozzle materials for rocketry applications.[19,20] Other researchers[21-25] have employed the codeposition technique to improve the crystallinity of the graphite formed by pyrolysis. In most of the aforementioned work, the metal additive concentration has been greater than one weight percent. This

often results in a two phase system: a carbide and graphite. Generally, it has been found that the carbide is uniformly distributed throughout the graphite matrix.[24]

There have also been some studies using the pyrolytic codeposition method to study solid solubility in graphite. By far the largest number of these studies has been on the boron-carbon system. Katz and Gazzara[13] studied graphite-boron deposits by light microscopy, X-ray diffraction, and flexural strength measurements. They proposed that on the basis of all available evidence, the solubility limit of boron in graphite lies between 0.44 and 1.1 a/o boron. Structural changes observed at higher concentrations were explained by a coherent/noncoherent boron carbide deposition mechanism. Marinkovic et al[26] evaluated deposits of graphite and boron formed at 1400, 1500 and 1600°C. Deposits were evaluated by X-ray diffraction, oxidation behavior, density and microscopy. They concluded that boron can occupy both substitutional and interstitial positions in the graphite lattice. The limit of boron solubility at the temperatures previously cited was thought to be in the vicinity of 1 percent. The bend strength of the alloys was found to be a maximum of 23 KSI compared to 15 KSI for pyrolytic graphite.[13] The oxidation rate of the alloys was found to be lower than that of graphite and the density greater.[26]

The silicon-carbon system has also been investigated by the pyrolytic codeposition technique. At silicon concentrations of 0.006 to 0.30 a/o, silicon carbide particles having a dimension of approximately 1000 Å have been identified.[27] Yajima and Hirai[28,29,30] produced siliconated pyrolytic graphite alloys containing 0.001 to 1.8 a/o silicon over the temperature range of 1400 to 2000°C. Based on data from X-ray analysis, surface oxidation, electron diffraction and electron microscopy, they concluded that the major portion of the silicon is present as β-SiC which is uniformly distributed throughout the graphite.[29] No evidence of the carbide was found in samples of low silicon concentration (below approximately 0.015 a/o silicon).

Marinkovic et al[31] analyzed carbon-silicon deposits formed between 1340 and 1630°C in the same manner as they evaluated the carbon-boron system.[26] They found that silicon enters the graphite lattice only in the substitutional mode and the limit of this solid solution is 0.065 - 0.085 a/o silicon. Silicon above this concentration forms β-SiC. In addition, they found[32] that with a silicon concentration of up to 0.085 a/o, the microhardness of the deposit was unaffected but at higher silicon concentrations and higher deposition temperatures, areas could be found where the hardness corresponded to that of silicon carbide.

Marinkovic et al[33] have also applied their vapor codeposition technique[26,31] to the uranium-carbon system. Uranium was found to be nonuniformly distributed throughout the deposit. No solid solubility was detected. Alloys containing less than 0.015 a/o uranium were not studied. The presence of uranium was found to promote crystallization of the graphite.

Other studies which are of significance in phase relationships and thus in property development, are those concerning the distribution of impurities in graphite. Both natural and commercial graphites contain impurities such as sulphur derivatives, pure metals or metal compounds as well as boron and silicon and their compounds.[34] The distribution of these impurities in graphite electrodes has been examined using radiography, ash patterns and sulphur prints.[35] This distribution was found to be nonuniform with clustering in the intersticies of coke grains. The release energies of some metallic impurities from graphite were studied by George.[36] For the metallic elements calcium, barium, strontium, and aluminum, the release energies were found to be greater than the known vaporization energies of the same atoms from their parent metals. These energies, however, are lower than the release energy for carbon atoms from graphite. The alkali metals are known intercalation compound formers and it appears that bonding

in such compounds is reasonably strong. Aluminum is not known to form an intercalation compound and thus its high release energy could indicate strong metal-carbon bonds being formed in a possible solid solution of aluminum in graphite.

In summary, the preceding has shown that some work has been done on phase relationships with graphite. Most of the published data deals with compound formation, two-phase studies (graphite plus a carbide), and solid solubility of boron and silicon. The two reported metal solid solubilities in graphite of 0.088 a/o vanadium and 0.3 a/o nickel are large enough to be of commercial manufacturing importance. These reported solubilities are of even more significance when the solid solution effects of boron and silicon are examined. Such solid solution alloys display higher flexural strength[13], better erosion resistance[20], and better oxidation resistance[26] than pure graphite. This leads to the possibility that transition metals might also enhance the properties of graphite. It is, therefore, of interest to extend the knowledge of transition metal-graphite systems and associated property changes particularly at small metal concentrations.

2. THE GRAPHITIC FORM OF CARBON

2.1 Graphite and its Crystal Lattice.

Graphite has been found to exist in two crystal struc-
tures. The hexagonal form is the normal structure, but a
rhombohedral structure has been identified in severely
cold-worked graphite.[38] This rhombohedral structure read-
ily transforms to hexagonal graphite upon heat treatment.

In graphite, carbon is sp_2 hybridized. The electronic
configuration of the carbon atoms is $1s^2 \ sp_2^1 \ sp_2^1 \ sp_2^1 \ p^1$.
Sigma bonding between the sp_2 hybrid orbitals results in a
hexagonal planar network of covalently bonded carbon atoms.
The remaining electron in the unhybridized p orbital is
also available for bonding. As this orbital is at right
angles to the planar net, these planar networks are bonded
together by the formation of van der Waals type pi bonds
between the p orbitals. The result is a highly anisotropic,
layered structure.

Within the layer planes, the carbon-carbon distance
is 1.415 $\overset{\circ}{A}$, while the distance between layer planes is
3.354 $\overset{\circ}{A}$. The unit cell is hexagonal with a c dimension of
6.708 $\overset{\circ}{A}$ and an a parameter of 1.415 $\overset{\circ}{A}$. The theoretical
density is 2.265 gm/cc.

2.2   Concept of Degree of Graphitization.

Carbon is an extraordinary element in that it exists in a number of metastable forms under standard conditions. Graphite is the stable form of carbon. Chars and soots are amorphous solids displaying various degrees of crystalline properties. Other carbons vary in crystallinity from amorphous to crystalline graphite. Metastable diamond is a highly crystalline carbon solid. This ability to exist in various states of crystallinity has resulted in terminology confusion, particularly between the carbons and graphite. Graphite is the material with the hexagonal lattice discussed previously. Most materials that are called graphite are actually carbons which exhibit a crystallinity approaching that of graphite. In fact, true graphite is a rare material. However, in this text and as is commonly accepted, we shall refer to graphite as any carbon material having a c lattice spacing between 6.71 Å and 6.90 Å.

With an increase in the lattice parameter of graphite comes a decrease in the bond strength which is almost certain to have an effect on alloying behavior. Thus the degree of graphitization (crystallinity) and the actual graphitization process is fundamentally different from recrystallization in metals since in graphite the nucleation and growth of new perfect crystals does not generally occur

below the melting temperature. Fischbach[39] discusses
graphitization in terms of a progressive improvement in an
initially very defective structure. Thus the existence of
a layer plane structure and the concentration and distri-
bution of defects in the original structure are of import-
ance.

The structure of disordered carbons is readily studied
by X-rays. X-ray examination of a poorly crystallized
graphite shows the presence of (ool) peaks and (hko) peaks.
No three dimensional (hkl) peaks appear. The peaks that
are present are quite broad and, in such cases, the lattice
spacing, c, is larger than that of true graphite. The size
of the semi-crystallized regions, called crystallites, can
be estimated from Scherrer's line broadening formula.[40,41]
At a higher degree of graphitization (crystallization),
X-ray peaks sharpen and three-dimensional ordering peaks
appear. A model in which poorly crystallized graphites are
called turbostratic carbons was proposed by Warren.[42] The
turbostratic term was coined to cover the manner in which
the layer planes are displaced relative to each other by
small translations or rotations about the c axis of the
layered region.

There has been a considerable number of studies[39,43,44]
on the graphitization process and how it is affected by
heat treatment, pressure application, plastic deformation
and catalyst addition. To graphitize, a temperature greater

than 2000°C is generally required (although carbons formed at temperatures as low as 1500°C by the pyrolytic method do display some crystallinity). High temperature plastic deformation[45] and high pressures are found to be effective in increasing the rate and the degree of graphitization.

Enhancement of the rate and degree of graphitization by the use of metals as catalysts is important in phase studies of graphite-metal systems. Schwartz and Bokros[24,25] studied the catalytic effect of titanium on pyrolytic graphite by codepositing titanium and graphite. They found 5 to 7 weight percent titanium was necessary to cause catalysis. Fitzer and Kegel[15] proposed a mechanism for the catalytic effect of metals on graphite. They felt that the reaction proceeded via one of the following paths as the metal diffused through the carbon:

$$MC_{1-x} + C \rightarrow MC_{1-x+\varepsilon} \rightarrow MC_{1-x} + \varepsilon G$$

or

$$M + (1-x)C \rightarrow MC_{1-x} \rightarrow M + (1-x)G$$
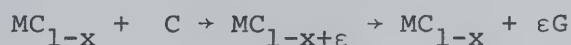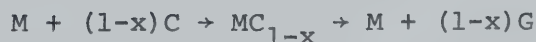
Derbyshire et al[46] experimented with graphite films deposited on nickel and found that the above diffusion-precipitation model explained the observed enhanced graphitization.

In a study of the formation of pyrolytic carbon on metal substrates between 870 and 1030°C,[23] an enhancement of

deposition and graphitization was found. The metals used were iron and nickel and the aforementioned diffusion-carbide mechanism was employed to explain the enhanced graphitization. In a similar study at 1000°C,[47] carbon films showed an increasing crystallinity with the order of the following metal substrates: molybdenum, tungsten, platinum, and tantalum. In yet another study,[48] metals were assumed responsible for promoting graphitization of artificial resins between 1400 and 2300°C. Thus in a study of metal-graphite phase relations, the concept of catalyzed graphitization is important as most graphites are actually carbons which display some graphitic character and the presence of metal atoms affects this degree of graphitization.

3. EXPERIMENTAL PROGRAM

The experimental program of this study concerns the production of graphite-metal alloys, and the evaluation of their structure and properties.

3.1 Alloy Production.

Alloys were formed by the pyrolytic codeposition technique. This method was selected in preference to the liquid metal-graphite methods as it was felt that melt techniques could involve extremely high pressures which may significantly affect any possible solid solubility.[49] This was substantiated by Walker and Imperial,[50] who concluded that graphite crystals grown in an iron melt are subjected to pressures in the order of 100 Kgm/cm^2. With melt techniques, there is also the problem of wettability of graphite by molten metals.[4]

Pyrolytic deposition can be achieved either from a liquid phase or a gaseous phase. Gas phase deposition, which is considerably better documented,[51-61] was selected to minimize the amount of necessary work on pure pyrolytic carbon. Pyrolytic deposition can be done on a fluidized bed substrate or on a stationary substrate.[62] A stationary substrate was selected for this experimental program. Although a variety of carbon source gases can be employed,

propane was chosen as it is reported to have a high depo-
sition rate[20] relative to other readily available gases.
The high deposition rate was required to minimize alloy
formation time which was in excess of three hours. An
analysis of the Matheson Natural Grade propane used in
the deposition experiments is given in Table 1. To achieve
a carbon deposit that resembled graphite according to the
earlier stated limits, a deposition temperature greater
than 1500°C and a deposition pressure less than 10 torr
were generally employed.

Two series of deposition experiments were run: one
series was straight graphite deposition and the other a
graphite-metal codeposition. Pure graphite was formed as
it was felt necessary to characterize graphite deposited
with the equipment design employed and also to form a com-
parison base from which alloy deposits could be evaluated.

3.2 Selection of Alloying Elements.

The choice of metals that could be employed was limited
by the following considerations:
1.   The vapor pressure of the metal in the graphite must
     be less than the deposition pressure at the employed
     deposition temperature. That is, the product of the
     equilibrium vapor pressure of the metal times its
     activity must be less than the existing vapor pressure

of the codeposited metal.

2.   A volatile compound which would be economically feasible to use had to exist for the metal to give the required metal vapor. Furthermore, this compound must be thermally unstable at the deposition temperature involved. The compound should also contain no oxygen, nitrogen or other elements which might interfere in such a manner as to give an unwanted phase.

3.   The selection of metals employed should be such that a general indication of phase and property trends for transition metals might be achieved.

Not all of the above criteria could be met in the selection of metals and metal compounds. Top priority was given to Condition Three and the resultant metal choices were: titanium, vanadium, manganese, and nickel. These metals are all from the fourth row of the periodic table and should indicate any trend related to the increasing atomic number. Titanium and vanadium are strong carbide formers. Manganese forms a variety of metastable carbides and nickel possibly forms only a very unstable carbide, Ni_3C. Solubilities of 0.088 a/o for vanadium in graphite[15] and 0.3 a/o for nickel in graphite[6] have been reported. No solubility data for titanium and manganese in graphite is available.

Titanium tetrachloride, vanadium tetrachloride, methyl-
cyclopentadienyl manganese tricarbonyl, and nickel carbonyl
were the chemical compounds selected for the codeposition
experiments.

3.3 Deposition Equipment.

Figure 2 is a schematic representation of the equipment
which was designed, constructed, and employed in the pyro-
lytic codeposition experiments. Figure 3 is a photograph
of this equipment. In essence, the equipment consisted of
à feed gas train, a deposition chamber in which an electric
resistance heated substrate was located, and an exhaust gas
train.

The feed gas train is the equipment between the propane
source (A) and the inlet orifice (H). Here, the pressure
was maintained at approximately 760 mm Hg by a low pressure
regulator (B). The temperature of the water bath (E) could
be varied to control the vapor pressure of the metal com-
pound and thus the pressure of the propane. The inlet
orifice (H) controlled the flow rate of the gases entering
the deposition chamber.

The pressure in the deposition chamber and the exhaust
gas train was kept at 10 torr or less. The deposition
chamber was constructed from a Balzer's stainless steel
vacuum cross-piece which was immersed in a water bath. At

right angles to the gas stream in the chamber was a graphite
substrate whose approximate dimensions are given in Figure
4. The substrate was made from Speer RC4 graphite (Fig. 1)
and was designed such that thermal gradients would be mini-
mized. The design is given in Figure 4, where it is shown
that the actual deposition surface was cut at different
lengths on opposite sides of the substrate. Only alloy
deposits formed in the centre region of the substrate were
used for examination.

The temperature of the substrate was monitored through
a quartz glass window by a Latronics Infred Pyrometer (L).
In addition to temperature monitoring by the pyrometer, a
stainless steel sheathed, chromel-alumel thermocouple was
inserted into the deposition chamber to within 20 mm of the
deposition substrate. On some occasions, despite a protec-
tive shutter covering the sight glass, the glass became
coated with soot and the thermocouple had to be used to
maintain a constant substrate temperature. This increased
the error in temperature control which is discussed in
Appendix A. A Hobart-Electric-Motor-Driven welding gener-
ator capable of producing 36 kilowatts of d.c. power was
used as a power source for the electrical resistance heated
substrate. Controls on the welder were quite coarse and
only a temperature tolerance of $\pm$ 50°C could be achieved in
most deposition experiments.

In the exhaust gas stream, a water cooled condensing tower (J) was used to condense any volatiles passing from the deposition chamber. In addition, the condensing tower was packed with glass wool which acted as a solids filter for any gas-born soot particles. A sodium hydroxide solution (M) was used as a chlorine gas scrubber in the titanium and vanadium codeposition experiments. This was done to protect the vacuum pump from the chlorine gas generated by the decomposing chlorides.

3.4   Methods of Deposit Evaluation.

3.4.1   Deposition Kinetics

Information on the variation of the deposition rate as a function of time or stage of deposition was obtained by measuring the electrical resistance change of the substrate and deposit.[63] In a first approximation, it was assumed that the deposition is uniform over the test length and that prolonged heating of the deposit has no effect on its electrical resistance. Measurements indicating the order of the deposition and whether the kinetics of the reaction changed as deposition progressed were then obtained by considering the following development.

It was assumed that a power relation exists between the total weight of the deposit and time, thus

$$W^n = Ct \qquad\qquad (1)$$

where W = weight of the deposit

     C = a constant

     t = deposition time

     n = weight exponent

The following symbols are further defined:

     ℓ, w, s = length, width and thickness of deposit

         ρ = resistivity of deposit

         d = density of deposit

       R_D = resistance of deposit

       R_S = resistance of substrate

       R_T = resistance of substrate plus deposit

Now,

$$W = \ell wsd \tag{2}$$

and

$$R_D = (\ell\rho)/(ws) \tag{3}$$

hence

$$W = (\rho\ell^2 d)/R_D = C_2/R_D .$$

Substituting (3) in (1) gives

$$W^n = R_D^{-n}C_3 = C_1 t$$

where $C_3 = C_2^n$.

Further simplifying gives

$$(1/R_D)^n = C_4 t = (1/R_T - 1/R_S)^n$$

where $C_4 = C_1/C_3$.

The effect of changing deposition surface condition was thus obtained by measuring the resistance of the substrate plus deposit and plotting the changing conductance of the substrate plus deposit on a logarithmic scale against time; the slope of this plot being the weight exponent.

3.4.2 Chemical Composition

The chemical composition of the deposit was determined by using different techniques for different alloy deposits. Only manganese concentrations were determined by a commercial laboratory. In all other cases, approximately 100 milligrams of the powdered alloy deposit was placed in a platinum crucible and ashed at 750°C in air. From here, the treatment for different metals varied.

a.   Titanium

The spectrophotometric method outlined by Weissler[64] was approximately followed to determine titanium concentrations as low as 20 ppm by weight. Approximately 50 mg of ammonium sulphate and 5 cc of concentrated sulphuric acid were added to the ashed graphite. This mixture was gently heated for one hour to dissolve all oxide matter. Five millilitres of 70% perchloric acid was then added and the total solution diluted to 25 cc. To 5 cc of this solution were added two drops of 30% hydrogen peroxide and

the intensity of the solution measured at a wavelength of 410 mμ in a spectrophotometer. The results were compared against a calibration curve prepared as outlined by Weissler.

b. Vanadium

The 3,3'-dimethylnaphthidine colorimetric method as outlined in ASTM specifications C560, Chemical Analysis of Carbon and Graphite,[65] was followed. However, only approximately 10 mg of ash was used instead of the specified 50 mg. The photometric measurements were done at a wavelength of 550 mμ and calibration curves were prepared as specified in the standard.

c. Nickel

Nickel analysis was done by dissolving the ashed graphite in 2 ml of 1:1 HNO_3. This solution was diluted to 10 ml and the nickel content determined by atomic absorption spectrometry. Analysis[66] was done at 2,320 Å on a Perkin Elmer Model 290B atomic absorption spectrometer. Standards were prepared from Fisher Certified Atomic Absorption Standard for Nickel.

3.4.3 Density Measurements

The apparent density of the deposit was measured by the sink-float technique. A mixture of carbon tetrachloride and tetrabromoethane or carbon tetrachloride and methanol was used. A piece of the deposit was allowed to remain in

the liquid for 45 minutes before the final balance was made
in order to standardize penetration of the liquid into the
graphite's pores.[67]

3.4.4   Microstructure Examination

The microstructures of the deposits were studied both
by light and electron microscopy. For light microscopy,
samples were prepared by cutting sections of the deposit
plus substrate from the parent substrate and mounting the
resulting section in bakelite. As different alloy deposits
exhibited different degrees of ease of polishing, a variety
of standard metallographic polishing techniques had to be
employed to achieve a satisfactory polished surface. The
specimen was generally observed under polarized light to
obtain contrast between different structures.

Samples for the electron microscope were prepared by
two different methods. One method was to glue acetate tape
to the deposit, allow it to dry and then peel off the tape
along with some of the deposit. The acetate tape was sub-
sequently dissolved in acetone to leave behind the thin
specimens peeled from the deposit. The other method was to
grind the deposit until pieces were thin enough to be
transparent to electrons. Due to the anisotropy of graphite,
all specimens formed in the preceeding two ways were basal
plane specimens and no non-basal plane samples were examined.

A Hitachi HU11 microscope was used in the investigations and an accelerating voltage of 75 KV was found to be the most useful for examining the graphite. Some electron diffraction was also done on the microscope.

3.4.5 X-ray Structure

The structure of the deposit was examined using both an X-ray diffractometer and a Debye Scherrer camera. In most cases copper radiation was used; however, chromium radiation was also used to examine those deposits which contained vanadium in order to avoid the problem of excess absorption of copper radiation by vanadium.[68] Diffractometry was done on a Philips model PW1380 horizontal goniometer.

The lattice parameter, c, was obtained wherever possible from the (004) peak of a powdered sample obtained by filing the deposit. If the deposit was too thin to be powdered, a solid piece of the deposit was analyzed. The (004) peak position was not corrected for polarization and absorption as such corrections would be very small for a flat specimen at a two theta angle of 53°.[69] The degree of ordering or the crystallite size in the C direction, L_c, was determined using Scherrer's formula for line broadening:[40]

$$L_c = \frac{K \lambda}{B \cos \theta}$$

where K = 0.94 for the (002) peak of graphite,[70] and λ is the radiation wavelength, B is the peak broadening at half peak height, and Θ is the diffraction angle. Peak broadening due to lattice strain was not separated from crystallite size broadening as it was found to be very small. The root mean square lattice strain perpendicular to the basal planes, $(\overline{\eta^2}_c)^{1/2}$, was evaluated for some of the deposits by considering the broadening of both the (004) and the (002) peaks[71] of a solid specimen. A change in the crystallite height and the root mean square lattice strain has been used as an indication of solid solubility limits in the graphite-boron system[13,26] and the graphite-silicon system.[31]

3.4.6 Bend Strength Evaluation

Bend strength measurements were conducted on an Instron testing machine. Deposit samples approximately 4 mm long X 1.5 mm wide X 1 mm thick were removed from the substrate and tested in three point bending. The samples were tested with the top surface of the deposit facing the single point load. The results were analyzed by the relationship:[72]

$$\sigma = \frac{3P\ell}{2wt^2}$$

where σ is the bend rupture stress (rupture modulus), P is the applied load at failure and ℓ, w and t are the sample length, width and thickness respectively. Teflon was used

on the stationary end supports to reduce sticking friction.
Bend strength measurements were used by Katz and Gazzara[13]
to indicate microstructural changes in the boron-graphite
system. These changes were interpreted by other investi-
gators[26] as the limit of solid solubility of boron in
graphite.

3.4.7 Deposit Microhardness

Microhardness is a well known technique for determin-
ing phase limits and structural changes in metal systems
and in many cases is more reliable than X-rays.[73] Previous-
ly, abrupt changes in bend strength have been interpreted
as indicating solid solubility limits[13,26] and as micro-
hardness varies in an identical manner as bend strength in
pyrolytic alloy codeposits,[17] microhardness should also be
useful to indicate any solid solubility limits. Further-
more, microhardness results can be used to complement bend
strength findings as an indication of mechanical properties.

The previously prepared metallographic samples were
vapor coated with a coating of aluminum thick enough to
enable hardness indentations to be seen yet thin enough
that the graphite structure was still visible. A 100 gm
load applied for 5 seconds on a Reichert microhardness
tester was used.

3.4.8 Distribution of Alloying Element

The distribution of the alloying additions was deter-
mined by examining deposits of various compositions and
orientations using an ARL electron probe microanalyzer
which has a resolution of slightly less than 1 micron.[74]

3.4.9 Stability of Alloying Element

The stability of the alloying element was examined by
heat treating deposits of various concentrations at the
temperature of deposition for twenty hours in a Brew vacuum
furnace. Heat treated deposits were subsequently examined
as to density, microstructure, X-ray structure, microhard-
ness, and alloy element distribution. Chemical analysis
was also carried out on some of the heat treated samples.

4. EXPERIMENTAL RESULTS

4.1 Deposition Kinetics.

4.1.1 Pyrolytic Graphite

Figure 5 shows that for pyrolytic graphite deposited at 5 ± 1 torr, the growth rate is constant. Values for n ($W^n = kt$) vary from 0.9 to 1.2 indicating that the deposition growth is, to a good approximation, a linear function of time at a given constant pressure. For this reason, the deposition growth rate perpendicular to the substrate was also determined by measuring the actual thickness of the deposit and dividing this by the deposition time. Figure 6 shows that the growth rate of pyrolytic graphite increases with increasing deposition temperature for a deposition pressure of 5 ± 1 torr. Other researchers[62] have found similar trends for other carbonaceous gases and different deposition conditions. Graphical analysis in Figure 5 was done by linear regression.

4.1.2 Pyrolytic Graphite-Titanium Alloys

Figure 7 shows that the addition of titanium does not produce changing deposition surface conditions which change the linearity of the deposition growth as values of n are found to be between 0.9 and 1.0. Data for alloys formed at $1975 \pm 35°C$ and 5.5 ± 1.5 torr also show an n value of

approximately one. The presence of titanium tetrachloride
or its derivatives in the deposition gas, immediately re-
sults in a growth rate approximately one and one half times
that of pure pyrolytic graphite. In addition, the growth
rate further increases with increasing titanium concentra-
tion in the alloy deposit. Figure 8 indicates that with
increasing titanium concentration in alloy deposits formed
at 1675 $\pm$ 75°C, the growth rate increases from 54 x 10^{-4}
mm/min at 0.001 a/o titanium to 96 x 10^{-4} mm/min at 0.280
a/o titanium.

4.1.3 Pyrolytic Graphite-Vanadium Alloys

Vanadium additions cause the growth rate to be at
least four times the growth rate of pyrolytic graphite.
Figure 9 shows that the growth rate in the presence of
vanadium increases with an increasing propane flow rate.
This is not the case in pyrolytic graphite and graphite-
titanium deposits where the same propane flow rates were
used as in the graphite-vanadium experiments. In these
experiments, propane flow rates were sufficient so that
carbonaceous gas supply did not control the deposition
rate. Temperature effects on the deposition rate for the
vanadium alloys can not be singled out from combined temp-
erature and flow rate effects.

4.1.4 Pyrolytic Graphite-Nickel Alloys

The deposition rate of graphite-nickel alloys is con-
stant and the deposition growth linear with time as is
seen in Figure 10. Evaluation of a 0.003 a/o nickel alloy
shows a growth rate of approximately 0.005 mm/min at
1590 $\pm$ 30°C and 5.5 torr. This growth rate is approxi-
mately one and one half times that of pyrolytic graphite
formed under similar conditions.

4.2 Pyrolytic Graphite Deposition

4.2.1 Metallography of Pyrolytic Graphite

The top view of a pyrolytic graphite deposit and its
substrate is shown in Figure 11. The centre of the deposit
is smooth and has a grey metallic lustre. In the cooler
regions of the deposition surface (end sections), the
pyrolytic graphite is often bumpy as is shown in the figure.

Figures 12 and 13 present two types of microstructure
observed in the deposits. These micrographs were taken of
cross sections with the direction of deposit growth verti-
cal. Figure 12 shows what is commonly called a singularly
nucleated pyrolytic growth, while the growth in Figure 13
is called polynucleated. Growth cones are visible in both
figures and it is from the appearance of these growth cones
that the microstructures are so named. In Figure 12, the
apexes (nucleation point) of the majority of these cones

are on the deposition substrate. Subsequent growth stems in a continuous manner from the cone apex. The pyrolytic growth in Figure 13 contains areas which are rougher in appearance due to the presence of larger secondary growth nuclei . These nuclei are thought to be less graphitic than the rest of the deposit.[62] The larger growth cones are also seen in Figure 13. In extreme cases of poly-nucleated microstructure, these larger cones are not vis-ible.[62] Both of the figures represent different graphites that were formed at 1650°C and 5 torr. The difference in the microstructure is understandable when the work of Yajima et al on pyrolytic graphite microstructure[63] is con-sulted. The conditions previously cited are in a transi-tion region between singularly nucleated and polynucleated microstructures and thus either polynucleated, singularly nucleated, or a combination of both microstructures is possible.

Figure 1 shows the substrate material for comparison with the pyrolytic graphite. The substrate graphite is made by the Acheson Process and consists of cylindrical filler grains (which were pyrolytically formed in a fluid-ized bed) bonded together to give a resultant porous struc-ture. No growth cones are visible in the filler grains.

Growth cones are readily seen in Figure 14 which shows the polished surface taken at right angles to Figures 12

and 13, or parallel to the deposition plane. These cones
are of various sizes with the larger cones being visible as
bumpy growths on unpolished deposits as was seen in Fig-
ure 11.

X-ray examination of the deposits shows that the basal
planes of the pyrolytic graphite are aligned parallel to
the plane of the deposition substrate. Some curvature of
the basal planes does occur as can be seen from the cracks
parallel to the basal plane in Figure 12.

4.2.2 Property and Structure Variation of Pyrolytic Graphite

Table 2 lists the deposition conditions and some of
the properties of the pyrolytic graphite deposits that were
examined. Figure 15 shows that from 1490 to 1650°C, the
apparent density of the deposit increases rapidly from 1.65
to 2.17 gm/cc. Beyond 1650°C the density levels off at
approximately 2.195 gm/cc and then remains relatively con-
stant. Results by Yajima et al[63] from similar deposition
conditions are included in Figure 15. These results show
a similar trend to the experimental values obtained. The
slight differences are due to different propane flow rates.
Yajima et al[63] found that different propane flow rates pro-
duced a slight shift in the density curve.

In Figure 16, the lattice constant, c, of the graphite
is shown to remain constant at a value of 6.86 Å up to a

deposition temperature of 2200°C. This compares with a value of 6.71 Å for true graphite and a value of approximately 6.85 Å found by Hirai and Yajima.[69] Figure 17 shows that the crystallite size follows a trend similar to that observed in the density. The range of ordering of the basal plane stacks (crystallite size, L_c) rapidly increases from approximately 100 angstroms to 300 angstroms over the temperature range 1500°C to 1650°C. The size then slowly increases to approximately 350 Å at 2000°C. These findings are comparable to those found by other researchers.[63,69,75]

Table 3 presents the microhardness results. The microhardness of the planes perpendicular to the basal plane remains relatively constant at an average value of approximately 73 Kgm/mm^2 with a scatter of $\pm$ 11%. Data on basal plane microhardness are inconsistent.

4.3 Pyrolytic Alloy Codeposition.

4.3.1 Graphite-Titanium Alloy Codeposition

The known phase diagram[76] for the carbon-titanium system is given in Figure 18. At a concentration of greater than 50 a/o carbon, a two phase system is indicated-- titanium carbide and graphite. No information on the phase system is given beyond 80 a/o carbon.

a. Metallography of Graphite-Titanium Alloy Codeposits.

The alloys prepared of pyrolytic graphite and tita-
nium all have singularly nucleated microstructures. Very
little structural difference can be detected among alloys of
different concentrations and different forming conditions.
This is seen in Figures 19 and 20. Figure 21, however, shows
that the frequency of occurrence of the larger cones increases
with increasing metal concentration. It is more difficult to
obtain a scratch-free surface for metallographic examination
with the graphite-titanium alloys than with pure graphite.

Electron microscopy was performed on a wide range of
alloy compositions. Hexagonal shaped precipitates were found
distributed throughout all specimens. Figure 22 shows that
the precipitates are approximately 2,000 $\overset{\circ}{A}$ across. A dif-
fraction pattern and the area from which it was obtained are
presented in Figure 23. Analysis of the diffraction pattern
shows that it is compatible with the precipitate being
titanium carbide (TiC) and that the diffraction spots are
from planes belonging to the [111] zone.

b. Properties and Structure of Graphite-
    Titanium Alloy Codeposits.

Table 4 lists some of the alloys examined and their
properties. Alloys were formed at 1675°C containing from
0.007 to 0.285 a/o titanium (0.029 to 1.127 w/o), at 1975°C
containing from 0.002 to 0.012 a/o titanium (0.009 to
0.046 w/o), and at 2200°C containing 0.001 a/o titanium

(less than 0.005 w/o). As the deposition temperature was increased, the amount of titanium that could be introduced into the codeposit decreased because of the increase in the titanium vapor pressure with increasing temperature. Figures 24 and 25 indicate that the density of the alloy increases with increasing titanium concentration at deposition temperatures of 1675°C and 1975°C. This increase is at a rate many times greater than a calculated density increase for direct titanium addition to graphite. Data from Figures 24 and 25 were analyzed by linear regression. The maximum deviation is only $\pm$ 0.5% and the scatter on the graphs appears large because of the scale used on the ordinate. Four figure reliability was found to be reasonable for densities determined by the sink-float technique.

The lattice parameter and the root mean square of the lattice strain in the c direction, as determined by X-ray analysis, are relatively constant as can be seen in Table 4-- the lattice parameter at 6.86 $\overset{\circ}{A}$ and the strain at 0.003 to 0.004 for deposits formed at 1675°C. The lattice strain is approximately 0.001 for the higher temperature deposits. Figures 26 and 27 show that the crystallite height, L_c, immediately decreases with the introduction of the titanium and then remains constant with increasing titanium concentration. The experimental scatter is quite large with some values being $\pm$ 10% of the mean.

X-ray diffractometry shows a peak corresponding to the (111) peak of titanium carbide. Detection is possible at a concentration as low as 0.012 a/o titanium in the alloys. Such detection requires the use of solid samples so that preferred orientation effects can be employed to best advantage. That is, in the extremely low concentration alloys no non-graphite peaks are detected in powdered samples. In solid samples, however, alignment of second phase particles makes diffraction from (111) carbide peaks strong enough to be detectable. No other peaks are detected and the (111) planes of the carbide are aligned with the basal planes of graphite because this peak can only be detected when the basal plane orientation of the graphite is examined.

The size of the titanium carbide particles in the [111] direction is estimated to be 2,000 $\overset{\circ}{A}$ using the Scherrer formula. This compares with the 2,000 $\overset{\circ}{A}$ diameter of the precipitates' (111) planes observed by electron microscopy (Fig. 22).

Flexural strength tests were done on most of the alloy deposits, but the technique was abandoned due to the inconsistency of the results achieved from tests conducted on any one specimen. Table 5 gives some indication of the variation in strengths obtained from an alloy containing 0.014 a/o titanium. It is thought that the presence of micro cracks prevents a true bend rupture strength from being determined.

Figure 28 presents the rupture strengths where only the highest values or average of highest values are plotted for each alloy. This was done to avoid consideration of pre-cracked alloy samples. Very little difference between the alloyed and the unalloyed graphite is indicated. It should be noted that microhardness results were more consistent than bend strength data. These results are presented in Figures 29 through 32.

In Figure 29, the microhardness of the planes at right angles to the basal planes increases from 75 to approximately 90 kgm/mm^2 between pure graphite and a titanium concentration of 0.020 a/o. The microhardness then rapidly decreases to 70 kgm/mm^2 where it remains constant with increasing titanium. In higher temperature deposits, the microhardness on the non-basal planes remains relatively constant although a linear regression analysis of the points indicates a decrease in hardness with an increasing titanium concentration (Fig. 30). For the alloy deposits formed at 1675°C, the microhardness on the basal plane decreases from 85 kgm/mm^2 to approximately 61 kgm/mm^2 where it remains constant with increasing titanium additions beyond 0.03 a/o. The deposits formed at 1975°C (Fig. 32), however, show a slight increase in basal plane hardness with increasing titanium. In Figure 31, as in Figure 29, a higher hardness is indicated at a concentration of approximately 0.020 a/o titanium.

The electron microprobe showed the titanium in the deposits to be distributed throughout the alloy. Figure 33 does shown some slight clustering of the titanium as does Figure 34. Figure 33 also shows a band of higher concentration along the right hand side of the figure. This band occurs in an area very close to the bottom of the deposits; i.e., the apex area of the growth cones. Fluorescent radiation pictures from the electron microprobe analyzer represent a metal distribution in three dimensions as the probe excites radiation from a depth of approximately 1μ below the sample surface.[77]

c. Stability of Graphite-Titanium Alloy Codeposits.

A series of alloy deposits was heat treated in a vacuum of 10^{-5} torr at 1600 $\pm$ 100°C for 20 hours. The heat treated samples were then evaluated as to density, X-ray structure, microhardness, microstructure, and titanium distribution. Table 6 indicates that the density remains approximately unchanged with the heat treatment. The alloy does, however, appear to have become more graphitic with the lattice parameter showing a slight decrease and the mean crystallite height possibly showing a slight increase. Chemical analysis of samples after heat treatment showed that a maximum loss of 15% titanium can be expected as is indicated in Table 7. Both light and electron microscopy indicate no detectable structure changes. The carbide

particles are still found to be aligned with the (111)
planes parallel to the graphite basal planes and the size
of the particles are unchanged at 2,000 Å. X-rays picked
up a stronger (111) peak of titanium carbide than was
detected in the unheat-treated deposits. Figure 35 shows
that the (111) peak is stronger in a heat treated sample
of lower titanium concentration than a sample which is of
higher titanium concentration but which had received no
heat treatment.

Figures 36 and 37 show that the microhardness of the
samples which were heat treated has changed slightly. The
microhardness on the planes perpendicular to the basal
planes increased from 70 kgm/mm^2 in the unheat-treated
samples to 76 kgm/mm^2 in the heat treated samples. The
increase in hardness peak observed in the unheated deposits
at a composition around 0.020 a/o titanium is not as
obvious in the heat treated samples. This is because there
are fewer data points at an approximate concentration of
0.020 a/o titanium in Figure 36 (heat treated alloys) than
in Figure 29 (as-deposited alloys). For this reason, and
also because other microhardness plots of alloys deposited
at 1675 $\pm$ 75°C (Figs. 29 and 31) show higher hardness read-
ings in the vicinity of 0.020 a/o titanium, the high hard-
ness value in Figure 36 should not be dismissed as
experimental scatter. The microhardness on the basal planes

shows an increase from 61 kgm/mm^2 to 78 kgm/mm^2 in the heat
treated samples over the as-deposited samples.

Figures 38 and 39 show that there is no change in the
titanium distribution during heat treatment. Figure 38 was
obtained from the same alloy deposit as that of Figure 33
and can therefore be compared directly with it. As in
Figure 33, a band of higher titanium concentration appears
in an area which was formed in the initial stages of the
alloy deposit. Figure 39 is of a lower concentration alloy
and indicates uniform distribution of the titanium with no
isolated areas of high concentration.

4.3.2 Graphite-Vanadium Alloy Codeposition

The phase diagram for the carbon-vanadium system[78] is
presented in Figure 40. Beyond a composition of 47 a/o
carbon, a two phase system exists--vanadium carbide (VC)
and graphite. A solubility of 0.088 a/o vanadium in
graphite is reported.[15]

Difficulties occurred in preparing alloys of pyrolytic
graphite with vanadium. The deposit growth rate is very
high as discussed previously. It was not possible to form
alloys containing more than 0.001 a/o vanadium under the
range of deposition conditions investigated.

a.   Metallography of Graphite-Vanadium Alloy Codeposits.

Figure 41 shows a singularly nucleated pyrolytic

graphite-vanadium alloy. This alloy is somewhat different in appearance than other singularly nucleated deposits as there is no pronounced "stringy" substructure. (See Figures 12, 13, 19, and 20.) The structure in the lower region of the deposit is also different from that in the upper region as indicated by the appearance of a band in the lower region when the deposit is examined under polarized light. The microstructure shown in Figure 42 is more characteristic of pure graphite formed at a higher deposition pressure.[63] It has large growth cones which contain many smaller cones. Figure 43 shows a plume-like carbon growth on the deposition substrate. Such plume growths are found at higher deposition pressures in pure pyrolytic graphite.[63] Figure 44 shows that minute vanadium or vanadium compound additions result in an increase in the diameter of the growth cones. The presence of a vanadium addition along with a slight pressure increase results in the appearance of secondary growth cones inside larger ones.

b.   Properties and Structure of
     Graphite-Vanadium Alloy Codeposits.

The results of some of the alloy codeposition experiments are given in Table 8 which indicates that the alloy deposits are more graphitic than pyrolytic graphite formed under similar conditions. The lattice parameters for the alloys average 6.85 Å compared with 6.86 Å for

pyrolytic graphite. The table also indicates that the crystallite height, L_c, is on the average 320 Å with some lower values being observed.

Although the alloy deposits are more graphitic than pure pyrolytic graphite, the alloys exhibit lower aniso-tropy. This is evident from the strengthening of (hko) peaks and the weakening of (ool) peaks in diffractometer scans. This increase in isotropy is due to a higher depo-sition rate. Figure 45 indicates that the higher deposi-tion rate also produces a decrease in apparent density with a density of 2.195 gm/cc only being achieved at a deposition temperature of 1850°C. This density (2.195 gm/cc) is reached at approximately 1700°C in pyrolytic graphite. Figure 45 further shows that the apparent density of pyro-lytic graphite-vanadium alloys varies linearly with temper-ature between 1770°C and 1850°C. At 1770°C, the alloy deposit has a density of 1.71 gm/cc.

Although it was expected that second phase particles would not be detectable even if they were present, chromium radiation was used in X-ray diffractometer scans for pre-cipitates in solid alloy specimens. As anticipated, no additional peaks were found.

Microhardness results are presented in Table 9 from which it can be seen that hardness values on the non basal planes are approximately 76 kgm/mm^2 for alloys formed at

5 torr. The alloys formed at higher pressure show a sig-
nificant increase in hardness (as much as 230%). This
increase in hardness is also evident when filing the deposits
to obtain powder samples.

   4.3.3 Graphite-Manganese Codeposition.

   One alloy of pyrolytic graphite and manganese was
formed at 1500 $\pm$ 30°C and 5 torr. Formation of an alloy at
1200°C was also attempted but the graphite formation rate
was so slow that a sample of sufficient size for examination
could not be produced.

   Manganese has an equilibrium vapor pressure of 10 mm
Hg at 1510°C.[2] This vapor pressure is greater than the
deposition pressure, nevertheless, the alloy deposit at
1500°C contains 1 x 10^{-4} a/o manganese.* This alloy has a
density of 1.701 gm/cc and a crystallite height of 156 Å.
The c lattice spacing is not determinable as the (004)
peak cannot be resolved. This indicates a very low degree
of graphitization.

   4.3.4 Graphite-Nickel Alloy Codeposits.

   The carbon-nickel phase diagram has not been estab-
lished with certainty. Difficulties arise around the

---

* Analysis done by Chicago Spectro Service Laboratory, Inc.,
  Chicago, Illinois.

existence and stability of the carbide phase Ni_3C. Most researchers agree that this compound exists but the stability of it and its crystal structure are not definite.

a.   Metallography of Graphite-Nickel Alloy Codeposits.

Alloys formed between pyrolytic graphite and nickel have a very high metallic lustre. In addition, the deposit surface is very smooth and contains few growth cone bumps. Figure 46 shows the alloy deposit microstructure to be singularly nucleated. Also, as with vanadium but even more so with nickel alloys, there is no "stringy" substructure present in the growth cones. The metallographic specimens are relatively easy to polish.

Examination of the graphite-nickel alloys in the electron microscope showed the possible existence of precipitates. One diffraction pattern was observed which contained spots that did not correspond to diffraction from graphite planes. However, the area from which the diffraction pattern was obtained was too thick to be resolved for precipitates.

b.   Properties and Structure of
     Graphite-Nickel Alloy Codeposits.

It was found that alloys containing more than 0.003 a/o nickel could not be formed with the range of deposition techniques being used. Table 10 gives some of the properties of the alloys formed. The trend to a decreasing density with a lower deposition temperature is similar

to that found for pyrolytic graphite over this temperature
range. (See Figure 15.) The lattice parameter, c, and the
crystallite height, L_c, also show values similar to those
found in pure graphite. The lattice parameters, however,
appear to be somewhat smaller than those of pure graphite
but more data is required to state with certainty that this
is so. Microhardness on the planes perpendicular to the
basal planes is 78.9 $\pm$ 4.2 kgm/mm^2. This is slightly
higher than values obtained for pyrolytic graphite formed
under similar conditions.

Debye-Scherrer diffraction patterns were obtained using
copper radiation to examine two powdered samples obtained
from alloy deposit #2PCNi. Exposure times of approximately
140 hours are required to detect second phase materials.
In patterns obtained from both samples, a very faint dif-
fraction ring corresponding to an unknown with a d value of
2.50 $\pm$ 0.01 $\overset{\circ}{A}$ is detected. All other rings present can be
associated with graphite diffracting planes.

Electron microprobe examination of the nickel distri-
bution in one of the alloys (#2PCNi) shows nickel to be
distributed throughout the area examined. Figure 47 shows
a band of higher concentration near the top face of the
deposit.

5. DISCUSSION

5.1 Evaluation of Pyrolytic Deposition.

The deposition growth of all deposited materials is concluded to be linear with time; i.e., n = 1 for the assumed power growth law W^n = kt. Deposition temperature and alloy additions do not affect deposition surface conditions such that the surface changes the linearity of the deposition for deposition pressures of 5.5 $\pm$ 1.5 torr.

The alloy additions, however, do enhance the rate of deposition. The deposition rate was shown to increase with increasing titanium concentration in the alloy. Whether or not any of the enhancement is due to the presence of the titanium in the deposition chamber is not clear as $TiCl_4$ was used in the codeposition and the presence of chlorine is known to increase the deposition rate of pyrolytic graphite.[79] However, in the vanadium alloys, the enhancement of the deposition rate is several times that of the titanium alloys and since vanadium tetrachloride is very similar to titanium tetrachloride, the pronounced enhancement is concluded to be caused by the presence of the vanadium.

To test the catalytic effect of vanadium on graphite deposition further, vanadium was melted onto part of a

substrate on which pyrolytic graphite was subsequently deposited. No deposit formed on the molten vanadium. Furthermore, as very little vanadium was found incorporated in the pyrolytic alloy deposits, the catalytic effect of vanadium must occur in the gaseous phase. This would also help explain why the characteristics of vanadium alloy deposition were similar to those of pyrolytic graphite formed at a higher pressure. The effect of vanadium must therefore be such that it catalyses the gas phase reaction in a manner similar to increased pressure.[56] This finding differs somewhat from those of other researchers[21,61,80,81] studying different metals where the deposition rate over metal substrates has been found to be increased by as much as five times.[80] The substrates employed were nickel, iron, platinum, molybdenum, tungsten, titanium and tantalum. This indicates that both gas phase and surface reactions can be of importance in controlling the pyrolytic deposition rate.

5.2 Discussion of Alloy Deposition Results.

5.2.1 Graphite-Titanium Alloys

The presence of chlorine in a pyrolytic deposition chamber is known to enhance the density of the resultant graphite.[79] This enhancement occurs as a shift in the density minimum to a lower temperature, (see Figure 15)

the density at higher formation temperatures remaining un-
changed, and hence it is concluded that the density
increase displayed in Figures 24 and 25 is a result of the
presence of titanium. This must be a catalytic effect as
the density increase in the deposit is greater than a cal-
culated density increase for direct titanium addition.
The density increase is greater in deposits formed at
1975°C than those formed at 1675°C indicating that the
catalytic effect of the titanium is a function of temp-
erature. Just exactly how this enhanced densification has
taken place is not clear. The lattice parameter, c,
remains constant and the crystallite height decreases.
This could possibly mean that the crystallite diameter is
greater in a graphite-titanium alloy as compared to pure
graphite deposits. No measurement of the crystallite
diameter could be obtained as the (110) and (100) peaks of
the deposits were not strong enough to allow measurements
to be taken. However, if the perfection of the graphite
lattice was extended in the radial direction, some enhance-
ment of the (110) and (100) peaks should have been observed.
This was not found to be the case.

Alternatively, the enhanced densification could be a
result of the forming characteristics of the deposit.
Diefendorf[52] concludes that the structure of a pyrolytic

graphite is largely controlled by gas phase reactions and surface mobility. He further states that with a temperature increase, the deposition rate increases and the density of the deposit decreases until such a temperature that surface mobility would allow rearrangement of the deposit and thus a density increase. It is quite possible that the presence of titanium enhances surface mobility and allows for a more dense packing of graphite crystals. It is known[24,25] that during heat treatment, the presence of titanium at concentrations greater than 5 w/o enhances graphitization and induces structural changes. However, the density is affected only slightly, any change in density being less than the change in density of pure graphite given an identical heat treatment.[25] Thus, density must be most strongly affected by crystallite arrangement, and titanium must enhance this arrangement upon deposition.

The presence of second phase particles whose electron diffraction and X-ray patterns correspond to reflecting planes of titanium carbide leads to the conclusion that any solid solubility of titanium in graphite must be below 0.002 a/o titanium which is the lowest concentration examined in this program. In codeposition, the carbide forms so as to have its dense packed planes ((111) planes) parallel to the dense packed basal planes of the graphite. The titanium carbide particles are approximately 2,000 Å

in size and appear to be equiaxed. It is thought that the presence of these carbide particles also explains why it was difficult to obtain a scratch free surface for metallographic examination. The carbide particles are removed from the deposit during polishing operations and thus are available to abrade the softer graphite sample.

The other results of the investigation along with the observation of precipitates, indicates that there has been no extensive solid solution alloy formed. The structure of the alloy deposits appears to be very similar to the structure of singularly nucleated pyrolytic graphite. The root mean square of the lattice strain in the c direction remains unchanged from that of pyrolytic graphite as does the lattice c parameter. The decrease in the crystallite height can be viewed as a consequence of an enhanced deposition rate.

Figure 48 presents some of the results of Marinkovic et al[31] on the silicon-graphite system where changes in crystallite size and density have been interpreted as indicating the extent of solid solubility of silicon in graphite. In this instance, property changes increase to a maximum--the solubility limit, and then decrease. Both the density and crystallite size showing maximization at the same silicon concentration. Changes or lack of changes observed in density and structural parameters of graphite-

titanium alloys are not consistent as in the graphite-
silicon case and thus property changes are not interpreted
as phase changes.

Although a change in microhardness values as shown in
Figures 29, 31, and 36 could be taken to indicate that the
limit of solid solubility of titanium in graphite is
0.020 a/o, the previously discussed data do not support
this interpretation. Instead, it is proposed that disper-
sion strengthening accounts for the microhardness peak. A
two phase system--titanium carbide and graphite, is thus
believed to exist down to concentrations as low as 0.002
a/o titanium. Figure 49 shows that the free energy of
formation for titanium carbide is highly negative (-40
Kcal/mole C) which indicates that the carbide formation is
energetically favourable at the temperatures under consid-
eration, pressure effects being neglected. It is also
feasible that the free energy of formation would be essen-
tially unchanged if the pressure effect was known as the
pressure is not thought to be a significant variable at
the 5 torr pressure involved.

The theory that the alloy is dispersion strengthened
is supported by a number of facts. Titanium has a rela-
tively large atomic radius (1.458 $\overset{\circ}{A}$) and hence its diffus-
ivity in graphite at 1600°C is expected to be low. The
carbide is also particularly stable at this temperature.

Thus, heat treatment of a 0.020 a/o titanium alloy should result in little loss of dispersion hardening which was found to be the case (Figure 36). The electron microprobe analysis confirmed the stability of the titanium distribution. The dispersion strengthening is thought to occur in part by coherency effects. An enhancement of (111) peaks of the carbide in the heat treated alloys was observed. The size of the carbide particles was found to be unchanged in the heat treated samples which was confirmed by electron microscopy and diffraction peak broadening. Some reorientation of carbide particles in the graphite, possibly altering coherency effects, is thought to have occurred with heat treatment. A diffraction pattern of a carbide crystal in which the planes of the [110] zone were at right angles to the basal planes of graphite was observed for a non-heat treated sample. This pattern is presented in Figure 50. Heat treatment could allow this particle to become reorientated so that the (111) carbide planes become parallel to the graphite basal planes.

Titanium carbide has a rock salt lattice structure and hence the (111) plane can be thought of as a dense packed plane of titanium atoms as is seen in Figure 51. Figure 51 further shows how the interface between the carbide and the graphite may be considered semi coherent. The hexagonal shape of the carbide is also accounted for in this two

dimensional mode. Similarly, spacings of approximately
2.5 Å between (111) carbide planes and 3.4 Å between
graphite basal planes could lead to a highly strained
semi coherent interface. (Basal plane spacings of 2.5 Å
have previously been found in graphite.[83]) Semi coherent
interfaces are known to be responsible for strengthening
in metal-metal systems.[84] Also size and distribution of
precipitates affect strength[84] and the subsequent decrease
in hardness of alloys with a titanium concentration
greater than 0.020 a/o could be due to these factors. A
more detailed study is, however, required to verify the
proposed hardening mechanism in graphite-titanium alloys.

5.2.2 Graphite-Vanadium Alloys

The results of the codeposition experiments using
vanadium clearly indicate that vanadium catalyzes pyrolytic
deposition. Also, it appears that the alloy formed is more
highly graphitized than pyrolytic graphite formed under
comparable conditions. The increase in the isotropy of
the alloys does not mean that the deposit is less graphitic.
The enhancement of graphitization by vanadium has been
studied previously and the carbide diffusion mechanism was
used to explain the observed behavior.[15]

Under the experimental conditions, no alloys contain-
ing more than 0.001 a/o vanadium were formed. Vanadium
carbide has previously (1931) been formed by vapor phase

deposition from the tetrachloride and toluene at 1500 to 2000°C.[85] The deposition conditions, however, were different from those used in this study.

The soot formed in the deposition chamber was examined by X-rays and no evidence of the carbide was found there; however, X-ray diffraction peaks from a vanadium oxychloride complex were present.[86] The concentration of vanadium in the soot was found to be 0.5 w/o. This supports the theory that alloys are most readily formed from materials of low graphite character. As the degree of graphitization in the vanadium alloys is reasonably high, positions for vanadium or vanadium carbide in the alloy deposit are limited. This results in alloy deposits with a low vanadium concentration.

5.2.3 Graphite-Manganese Alloys

Little can be said about the one pyrolytic graphite-manganese alloy formed other than that no obvious catalyzation of deposition or enhancement of graphite properties could be seen. It is surprising that any manganese at all was found to be present in the alloy as the vapor pressure of manganese at 1500°C far exceeds the total deposition pressure. Possibly the manganese has been trapped or a strong bond has been formed within the graphite. Manganese which has an outer electronic configuration of $3p^6\ 3d^5\ 4s^2$ could be a good candidate for forming bonds with the pi electrons of carbon in graphite. A number of manganese

carbides are thought to exist although numerous contradic-
tory results are reported[76,78,87] indicating highly meta-
stable conditions in the carbon-manganese system. The
concentration of manganese in the alloy formed was too low
for X-ray diffraction to detect any possible carbide peaks
if they had been present.

5.2.4 Graphite-Nickel Alloys

Nickel is well documented as being a graphitizing
catalyst.[24,46,48,88] The uniformity and metallic-like
appearance of the graphite codeposited with nickel seem to
bear this out. However, other parameters examined do not
provide sufficient evidence of enhanced graphitization.

The evidence for the presence of a second phase mater-
ial in the alloy deposit is strong. The spots observed in
the electron diffraction pattern did not fall on existing
graphite rings and therefore are due to the presence of a
second phase material. The extra ring observed in the
Debye-Scherrer patterns could be due to nickel-iron oxide
$(NiFe_2O_4)$.[86] The purity of the nickel carbonyl used to
form this alloy is not known; furthermore, the carbonyl
was supplied in a steel pressure vessel and thus the possi-
bility of iron carbonyl being present is strong.

As with vanadium, nickel alloy deposits which contained
greater than a certain percentage (0.003 a/o) of nickel

would not be formed. In the case of nickel, the low metal concentration could be due to the premature decomposition of the carbonyl to give nickel and carbon monoxide and leave the decomposing gas in the vicinity of the substrate deficient in nickel. Significant amounts of nickel, nickel oxide and possibly some nickel carbide were found in an X-ray analysis of soot formed in the deposition chamber during graphite-nickel alloy formation.

Alternatively, we can again assume that alloy formation or solid trapping is greatest in graphite of low perfection and as nickel enhances graphitization, very little metal would be expected in deposits of graphite formed in the presence of nickel. Figure 47 shows the nickel concentration is greatest at the top surface of the deposit. It is probable that the outer surface of the deposit will be the least graphitized. For comparison, the density of surface layers of a pyrolytic graphite-titanium deposit was found to be 2.140 gm/cc compared with a middle layer density of 2.146 gm/cc. (See Appendix A, Item 3.)

5.3 Phase Relationships in Alloys.

The alloys formed in these experiments appear to be two phase systems even though the metal concentration in the alloys is quite low and there is a possibility of solid solutions existing at these concentrations. This

conclusion is supported by the presence of precipitates in the titanium-graphite and nickel-graphite systems. Other work concerned with different transition metal and graphite systems also tends to support this conclusion. The two reported solubilities of 0.088 vanadium[15] and 0.3 nickel[6] in graphite are probably too high and this point is discussed in Appendix B.

Wolf et al[89] studied diffusion of silver, nickel, uranium, thorium, and radium in various types of graphite. These researchers felt that substitutional and interstitial diffusion are negligible and that all mass transport proceeds via subgrain boundaries. This was shown by examining diffusion in a number of graphites, each presenting a different degree of crystal perfection, and finding that diffusion is the least in graphites having the smaller subgrain boundary area. Hummond[90] and Riedinger et al[91] also found that diffusing species do not use substitutional or interstitial diffusion mechanisms but rather diffuse primarily via grain boundaries and pores. The Hummond study was an examination of niobium diffusion in pyrolytic graphite while Riedinger et al studied the diffusion of cesium and barium through graphites of low helium permeability. All three of the above studies indicate or state that the solubilities of foreign atoms within the graphite lattice are small.

In a study of carbon deposited on metal substrates at 650 to 750°C, Robertson,[92] using the microprobe, found no evidence of nickel, cobalt, or iron in regions of high crystal perfection. Oxidation studies, however, did indicate that possibly these elements were present. This led Robertson to conclude that metal concentrations in crystalline regions of graphite were too small to be detected by the electron microprobe. Such concentrations must certainly be below 0.001 a/o, for absorption effects will be small when detecting a heavy metal in a light matrix like carbon. The work of Courtney and Duliere[93] also showed no iron present in a highly crystalline area of graphite; however, iron was present in adjacent carbon material.

The existence of two phase alloy systems can be explained by examination of alloying principles for metal-metal systems where the solubility limit is reached in cases when the Fermi surface makes contact with the Brillouin zone boundaries.

The band model developed for graphite is a simplified two band approach which neglects layer plane interactions. It is found that there is a band overlap of 0.03 to 0.04 eV[94] between the conduction and the valence bands.

The Brillouin zone of graphite is hexagonal in k space. Theoretical calculations[94,95] indicate that the Fermi surfaces will be located at the corners of the Brillouin zone.

Thus there is little chance that any extensive solid solutions can be formed between graphite and transition metals.

The Hume Rothery electronegativity rule[96] which states that the extent of solid solution is limited where large electronegativities exist between solute and solvent, also helps explain the limited solubility. Carbon has a Pauling electronegativity of 2.5 eV[97] while that of transition metals is 1.3 to 2.4 eV with the majority of the elements having an electronegativity around 1.6 eV. An electronegativity difference of more than 0.3 eV is quite large and thus solid solutions become more restricted.

5.4 Engineering Significance of Alloys.

5.4.1 Deposition Rates

The formation of alloys has been shown to enhance the rate of pyrolytic deposition. In some instances, this enhancement has been at the expense of preferred orientation which could be of advantage or undesirable depending on the degree of anisotropy wanted in the final alloy. In the case of the vanadium alloys formed using VCl_4, highly enhanced deposition rates can be achieved with limited contamination of the graphite while with titanium alloys, higher rates of enhancement can only be achieved by the incorporation of more titanium in the deposit. Nickel was found to enhance the deposition rate by 1.5 times which is

not as significant an enhancement as that produced by titanium and vanadium. Moreover, this rate is only one third that reported for deposition over the metal foil. This higher rate was, however, achieved at a lower deposition temperature.[80]

5.4.2 Enhanced Graphitization

Alloy additions by the pyrolytic codeposition method have been shown to enhance graphitization. Such a realization allows for the formation of massive, highly graphitic forms of carbon at lower formation temperatures. Titanium enhances the densification of graphite markedly. This enhancement is a function of titanium concentration in the alloy.

Vanadium additions to graphite give a lower c lattice spacing and a higher L_c crystallite size thus indicating a higher degree of graphitization. However, the overall density of vanadium-containing alloys is somewhat less than that of pyrolytic graphite; probably as a result of the enhanced deposition rate. Nickel also appears to promote a smaller lattice spacing.

5.4.3 Second Phase Hardening

The results of the microhardness tests on graphite-titanium alloys show the possibility for dispersion hardening in graphite-transition metal systems. Data plotted in

Figure 52 also indicates the possibility of an alloy hardening and strength improving mechanism occurring in the graphite-niobium system. Such findings are of significance in improving the relatively low strength of graphite.

5.5 Summary.

The pyrolytic codeposition process was used to form graphite alloys at 5 torr pressure and between 1500 and 2200°C. The findings of the alloy studies are summarized below.

1. Titanium carbide was found in graphite alloys at concentrations as low as 0.002 a/o titanium.

2. Evidence of solid solubility of vanadium in graphite was not found for alloys which contained 0.001 or less atomic percent vanadium.

3. Graphite-nickel alloys containing 0.003 a/o nickel were found to contain precipitates.

4. Carbide particles cause dispersion hardening in graphite-titanium alloys up to a concentration of 0.020 a/o titanium.

5. Pyrolytic deposition growth is linear with time and alloy additions do not change the linearity of the deposition for deposits formed at 5.5 ± 1.5 torr.

6. The deposition rate in pyrolytic graphite-titanium alloys increases with increasing titanium concentration in the alloy.

7. The presence of vanadium tetrachloride in the vapour phase enhances the rate of pyrolytic deposition by a factor of at least four times the rate of pure pyrolytic graphite deposition.

8. The rate of pyrolytic deposition was not affected by manganese.

9. Nickel increases the rate of pyrolytic deposition by 1.5 times that of the pure pyrolytic graphite deposition rate.

10. Titanium, vanadium, and nickel promote graphitization in pyrolytic codeposition.

11. Titanium enhances densification of pyrolytic graphite.

6.   CONCLUSIONS

From the experimental data presented in this report,
it is concluded that improvement of pyrolytic graphite
properties can be achieved by codeposition of graphite and
an appropriate transition metal. Areas of property im-
provement are the degree of graphitization and the micro-
hardness. It is probable that the strength of the
codeposited material can also be improved.

Changes in the rate of pyrolytic deposition can be
achieved by codepositing graphite and a transition metal.
Different metals have different effects on the deposition
rate. It is also not necessary for large metal concentra-
tions to be taken into the graphite for a highly enhanced
deposition rate to occur.

Any solid solubility of transition metals in graphite
is very limited. Even though large interstitial spaces
are present in the graphite lattice, interstitial solubil-
ity is very low. In some cases, large electronegativity
differences between transition metals and carbon mean that
competition between the carbide phases and the solid solu-
tion phase results in a very restricted solid solution.
Theoretical calculations of the electronic structure of
graphite indicate that solubility may be limited because of
the possibility of the Fermi surface making contact with

the Brillouin zone boundary with the addition of solute
metal atoms.

It is further concluded that the uptake of metals in
graphite is a function of the degree of graphitization
(crystallinity). Excess bonding electrons are available at
crystal defects in graphite. These electrons can be used
to form bonds with foreign metal atoms and thus solubility
will increase with an increasing defect concentration.
This is not true matrix solid solubility but it must be
considered in a material which displays a range of crystal-
linity as does graphite.

REFERENCES

1. J. Rappeneau and G. Jouquet, Les Carbones, Tome I,
    A. Pacault (ed.), Masson et Cie, Paris, 1965, p. 527.

2. Handbook of Chemistry and Physics, 50th Edition,
    R.C. Weast (ed.), The Chemical Rubber Company,
    Cleveland, Ohio, 1969.

3. S. B. Austerman, Chemistry and Physics of Carbon,
    Vol. 4, P.L. Walker, Jr. (ed.), Marcel Dekker Inc.,
    New York, 1968.

4. M. Humenik, Jr., D. W. Hall and R. L. Van Alsten,
    "Graphite-Base Cermets", Metal Prog., April 1962,
    p. 101.

5. P. C. Li, "Preparation of Single Crystal Graphite
    from Melts", Nature 192, 1961, p. 864.

6. H. M. Strong and R. E. Hanneman, "Crystallization of
    Diamond and Graphite", J. Chem. Phys. 46, 1967,
    p. 3668.

7. G. R. Henning, Progress in Inorganic Chemistry 1, 1959,
    p. 125.

8. R. C. Croft, Proceedings of the Third Conference on
    Carbon, Pergamon Press, 1957.

9. A. R. Ubbelohde and F. A. Lewis, Graphite and Its
    Crystal Compounds, Oxford University Press, London,
    1960.

10.   R. C. Croft, "Lamellar Compounds of Graphite", Quart.
      Revs. London 14, 1960, p. 1.

11.   W. Rudolf, Advances in Inorganic Chemistry and Radio-
      chemistry 1, 1959, p. 233.

12.   C. E. Lowell, "Solid Solution of Boron in Graphite",
      J. Am. Ceram. Soc. 50, 1967, p. 142.

13.   R. N. Katz and C. P. Gazzara, "The Influence of Boron
      Content on the Fine Microstructure of Pyrolytic Graph-
      ite", J. Mat. Sc. 3, 1968, p. 61.

14.   F. Tombrel, "Effet du Bore sur la Structure et les
      Propriétés Mécaniques a Haute Température du Pyro-
      carbone", Rev. Hautes Tempér. et Réfract., t. 3,
      1966, p. 79.

15.   E. Fitzer and B. Kegel, "Reaktionen Von Kohlenstoff-
      gasattigter Vanadiumcarbidschmelze met Ungeordnetem
      Kohlenstoff", Carbon 6, 1968, p. 433.

16.   C. F. Powell, J. H. Oxley and J. M. Bocher, Vapor
      Deposition, J. Wiley and Sons, New York, 1966.

17.   U.S. Patent #3,464,843; Sept. 2, 1969.

18.   British Patent #967,565; 1964.

19.   Raytheon Company, Final Progress Report, U.S. Navy
      Contract NORD 19135, Nov. 1959 - Jan. 1963.

20.   R. Francis, Arthur D. Little Inc., Final Progress
      Report, Contract DA 19-020-ORD-5490, June 1961 -
      June 1962.

21. A.E.B. Presland and P. L. Walker, Jr., "Growth of Single Crystal Graphite by Pyrolysis of Acetylene over Metals", Carbon 1, 1969, p. 1.

22. A. E. Karu and M. Beer, "Pyrolytic Formation of Highly Crystalline Graphite Films", J. Appl. Phys. 37, 1966, p. 2179.

23. Y. Tamai, Y. Nishiyana and M. Takahashi, "Carbon Deposition on Iron and Nickel Sheets from Light Hydrocarbons", Carbon 6, 1968, p. 593.

24. A. S. Schwartz and J.C. Bokros, "Catalytic Graphitization of Carbon by Titanium", Carbon 5, 1967, p. 325.

25. R. J. Price and J. C. Bokros, "Isochronal Annealing Kinetics and Neutron-Induced Dimensional Changes of Titanium Doped Pyrolytic Carbons", Carbon 9, 1971, p. 205.

26. S. Marinkovic, C. Suznjevic and I. Dezarov, "Simultaneous Pyrolytic Deposition of Carbon and Boron", Carbon 7, 1969, p. 185.

27. J. L. Kaae and T. D. Gulden, "Structure and Properties of Codeposited Pyrolytic C-SiC Alloys", J. Am. Ceram. Soc. 54, 1971, p. 605.

28. S. Yajima and T. Hirai, "Siliconated Pyrolytic Graphite, Part 1", J. Mat. Sc. 4, 1969, p. 416.

29. S. Yajima and T. Hirai, "Siliconated Pyrolytic Graphite, Part 2", J. Mat. Sc. 4, 1969, p. 424.

30. S. Yajima and T. Hirai, "Siliconated Pyrolytic Graphite, Part 3", J. Mat. Sc. 4, 1969, p. 685.

31. S. Marinkovic, C. Suznjevic, I. Dezarov, A. Mihajlovic and D. Cerovic, "Simultaneous Chemical Vapour Deposition of Carbon and Silicon", Carbon 8, 1970, p. 283.

32. A. Tukovic and S. Marinkovic, "Microhardness of Silicon-containing Pyrolytic Carbon", J. Mat. Sc. 5, 1970, p. 541.

33. S. Marinkovic, C. Suznjevic and I. Dezarov, "Simultaneous Chemical Vapor Deposition of Carbon and Uranium", J. Nuc. Mat. 33, 1969, p. 103.

34. M. Millet, Les Carbones, Tome 1, A. Pacault (ed.), Masson et Cie, Paris, 1965.

35. M. Inagaki and T. Noda, "Distribution of Inorganic Impurities in Graphite Electrodes", Japan Chem. Soc. Bull., Vol. 36, 1963, p. 112.

36. D. W. George, "On the Release of Metallic Impurities from Graphite at Temperatures Above 1750°C", Carbon 3, 1965, p. 43.

37. S. Sklarew and M. J. Albom, "Pyrolytically Derived Refractory Materials", Met. Prog., Feb. 1965, p. 102.

38. W. N. Reynolds, Physical Properties of Graphite, Elsevier Publishing Company, London, 1968.

39. D. B. Fischbach, Chemistry and Physics of Carbon, Vol. 7, P. L. Walker, Jr. (ed.), Marcel Dekker Inc., New York, 1971.

40. P. Scherrer, Nachr. Ges. Wissensch Gottingen 2, 1918, p. 98.

41. M. A. Short and P. L. Walker, Jr., "Measurement of Interlayer Spacings and Crystal Size in Turbostratic Carbons", Carbon 1, 1963, p. 3.

42. B. E. Warren, Phys. Rev. 59, 1941, p. 693.

43. A. Pacault, Chemistry and Physics of Carbon, Vol. 7, P. L. Walker, Jr., (ed.), Marcel Dekker Inc., New York, 1971.

44. J. Maire and J. Mering, Chemistry and Physics of Carbon, Vol. 6, P. L. Walker, Jr. (ed.), Marcel Dekker Inc., New York, 1970.

45. D. B. Fischbach, "The Influence of High Temperature Plastic Deformation on the Kinetics of Graphitization of Pyrolytic Carbons", J. Chem. Phys., 1969, p. 121.

46. F. J. Derbyshire, A.E.B. Presland and D. L. Trimm, "The Formation of Graphite Films by Precipitation of Carbon and Nickel Foils", Carbon 10, 1972, p. 114.

47. S. M. Irving and P. L. Walker, Jr., "Interaction of Evaporated Carbon with Heated Metal Substrates", Carbon 5, 1967, p. 399.

48. C. Yokokawa, K. Hosokawa and Y. Takegami, "Low Temperature Catalytic Graphitization of Hard Carbon", Carbon 4, 1966, p. 459.

49. L. Kaufman, Solids Under Pressure, W. Paul and D. M. Warschauer (eds.), McGraw Hill Co., 1963.

50. P. L. Walker and G. Imperial, "Structure of Graphites", Nature 180, 1957, p. 1184.

51. A.R.G. Brown and W. Watt, "The Preparation and Properties of High-Temperature Pyrolytic Carbon", Industrial Carbon and Graphite, Soc. of Chem. Ind., 1958, p. 86.

52. R. J. Diefendorf, "The Deposition of Pyrolytic Graphite", J. Chim. Phys. 57, 1960, p. 817.

53. J. C. Bokros, "The Structure of Pyrolytic Carbon Deposited in a Fluidized Bed", Carbon 3, 1965, p. 17.

54. R. O. Grisdale, "The Formation of Black Carbon", J. App. Phy. 24, 1953, p. 1082.

55. B. Banerjee, T. Hirt and P. Walker, "Pyrolytic Carbon Formation from Carbon Suboxide", Nature 192, 1961, p. 450.

56. S. Yajima, T. Satow and T. Hirai, "Mechanism of the Pyrolytic Graphite Formation", J. Nuc. Mat. 17, 1965, p. 116.

57. T. J. Hirt and A. B. Palmer, "Kinetics of Deposition of Pyrolytic Carbon Films from Methane and Carbon Suboxide", Carbon 1, 1964, p. 65.

58. D. B. Murphy, H. B. Palmer and C. R. Kinney, "A Kinetic Study of the Deposition of Pyrolytic Carbon Films", Industrial Carbon and Graphite, Soc. of Chem. Ind., 1957, p. 77.

59. K. W. Carley-Macauly and M. MacKenzie, "Studies on the Deposition of Pyrolytic Carbons", Proceedings of the 5th Conference on Carbon, Pergamon Press, 1961.

60. S. Marinkovic, C. Suznjevic, M. Gasic and I. Dezarov, "Aparatura za Dobijanje Pirolitickog Karbona", Hemijski Industrija 2, 1967, p. 326.

61. A. E. Karu and M. Beer, "Pyrolytic Formation of Highly Crystalline Graphite Films", J. Appl. Phys. 37, 1966, p. 2179.

62. F. Tombrel and J. Rappeneau, Les Carbones, Tome II, A. Pacault (ed.), Masson et Cie, Paris, 1965.

63. S. Yajima, T. Satow and T. Hirai, "Microstructure and Density of Pyrolytic Graphite", J. Nuc. Mat. 17, 1965, p. 127.

64. A. Weissler, "Simultaneous Spectrophotometric Determination of Titanium, Vanadium, and Molybdenum", Ind. and Eng. Chem., 1945, p. 695.

65. Annual Book of ASTM Standards, Part 13, American Society for Testing and Materials, Philadelphia, Pa., 1970.

66. Perkin-Elmer, "Analytical Methods for Atomic Absorption Spectrophotometry", Perkin-Elmer Corp.

67. R. E. Franklin, "A Study of the Fine Structure of Carbonaceous Solids by Measurement of True and Apparent Densities", Trans. Faraday Soc. 45, 1949, p. 274.

68. B. D. Cullity, <u>Elements of X-ray Diffraction</u>, Addison-Wesley Publishing Co., Reading, Mass., 1956.

69. T. Hirai and S. Yajima, "Structural Features of Pyrolytic Graphite", J. Mat. Sc. <u>2</u>, 1967, p. 18.

70. J. C. Bokros, <u>Chemistry and Physics of Carbon</u>, Vol. 5, P. L. Walker, Jr., (ed.), Marcel Dekker Inc., New York, 1969.

71. G. K. Williamson and W. H. Hall, "X-ray Line Broadening from Filed Aluminum and Wolfram", Acta Met. <u>1</u>, 1953, p. 22.

72. E. R. Maurer and M. O. Withey, <u>Strength of Materials</u>, 2nd ed., John Wiley and Sons, Inc., New York, 1940.

73. E. R. Petty, <u>Techniques of Metals Research</u>, Vol. 2, pt. 2, R. F. Bunshah (ed.), Interscience Publishers, New York, 1971.

74. Personal communication with D. Tomlinson, Department of Geology, University of Alberta.

75. J. C. Bokros and R. J. Price, "Deformation and Fracture of Pyrolytic Carbons Deposited in a Fluidized Bed", Carbon <u>3</u>, 1966, p. 503.

76. R. P. Elliot, <u>Constitution of Binary Alloys</u>, First Supplement, McGraw Hill Co., New York, 1965.

77. I. Adler, <u>X-ray Emission Spectrography in Geology</u>, Elsevier Publishing Co., New York, 1966.

78. F. A. Shunk, <u>Constitution of Binary Alloys</u>, Second
    Supplement, McGraw Hill Co., New York, 1969.

79. P. H. Higgs, R. L. Finicle, R. J. Bobko, E. J. Seldin
    and K. J. Zeitsch, WADD Tech. Report 61-72, Vol. 37,
    May 1964, Wright-Patterson AFB.

80. Y. Tamai, Y, Nishiyana and M. Takahashi, "Carbon Depo-
    sition on Iron and Nickel Sheets from Light Hydrocar-
    bons", Carbon <u>6</u>, 1969, p. 593.

81. S. M. Irving and P. L. Walker, "Interaction of Evap-
    orated Carbon with Heated Metal Substrates", Carbon <u>5</u>,
    1967, p. 399.

82. L. H. Ván Vlack, <u>Elements of Materials Science</u>, 2nd
    ed., Addison-Wesley Publishing Co., Reading, Mass.,
    1964.

83. G. Mathews, Philips Electronics Industries Ltd.,
    Scientific and Electronic Equipment Department,
    EM 300 Micrograph.

84. J. W. Martin, <u>Precipitation Hardening</u>, Pergamon Press,
    1968.

85. C. F. Powell, I. E. Campbell and B. W. Gonser (eds.),
    <u>Vapor Plating</u>, John Wiley and Sons, New York, 1955.

86. J. V. Smith (ed.), <u>Index to the Powder Diffraction
    File 1967</u>, American Society for Testing and Materials,
    Philadelphia, Pa., 1967.

87.   M. Hansen, Constitution of Binary Alloys, 2nd ed.,
      McGraw Hill Co., New York, 1958.

88.   V. R. Dietz and E. F. McFarlane, "Hydrogen Reaction
      with Carbon and Nickel Evaporated Films", Carbon 1,
      1964, p. 117.

89.   J. R. Wolf, D. R. McKenzie and R. J. Borg, "The
      Diffusion of Non Volatile Metallic Elements in
      Graphite", Lawrence Radiation Laboratory, Contract
      Number W-7405-eng-48, April 1964.

90.   M. L. Hummond, "Diffusion of Nb-95 in Pyrolytic Graph-
      ite", Paper presented 7th Conference on Carbon, Case
      Institute of Technology, Cleveland, 21-25 June 1965.

91.   A. B. Riedinger, C. E. Milstead and L. R. Zumwalt,
      "Experiments on the Diffusion of Cesium and Barium
      Through Graphites of Low Helium Permeability", Proc.
      of the 5th Conf. on Carbon 2, Pergamon Press, London,
      1963, p. 405.

92.   S. D. Robertson, "Carbon Formation from Methane Pyro-
      lysis Over Some Transition Metal Surfaces", Carbon 8,
      1970, p. 365.

93.   R. L. Courtney and S. F. Duliere, "The Catalytic
      Graphitization of Naphthalenediol and a Urethane
      Foam--A Feasibility Study", Carbon 10, 1972, p. 65.

94. J. W. McClure, "Energy Band Structure of Graphite",
     I.B.M. Journal of Research and Development 8, 1964,
     p. 255.

95. M. S. Dresselhaus and J. G. Mavroides, "The Fermi Sur-
     face of Graphite", I.B.M. Journal of Research and De-
     velopment 8, 1964, p. 262.

96. W. Hume Rothery and G. V. Raynor, The Structure of
     Metals and Alloys, 4th ed., Institute of Metals,
     London, 1962.

97. B. E. Douglas and D. H. McDaniel, Concepts and Models
     of Inorganic Chemistry, Blaisdell Publishing Co.,
     Waltham, Mass., 1965.

TABLES

TABLE 1

Analysis of
Matheson Natural Grade Propane
Used in Deposition Experiments*

Gas	Weight Percent	Mole Percent
Propane	91.15	90.88
Propylene	7.88	8.25
Isobutane	0.88	0.66
Neon	0.08	0.17
Methane	0.02	0.04

* Analysis done by gas chromotography.

3

TABLE 2

Pyrolytic Graphite Properties

Sample Number	Deposition Temperature (°C)	Deposition Pressure (torr)	Density (gm/cc)	c_0 (Å)	L_c (Å)
1PC	1670 ± 50	5	2.163	6.860	284
2PC	1670 ± 50	5	2.179	6.868	299
4PC	1650 ± 25	4.5	2.183	6.852	279
8PC	2200 ± 40	4	2.202	6.858	334
9PC	1970 ± 30	4	2.184	6.863	348
10PC	1970 ± 30	4	2.194	6.862	355
11PC	1875 ± 45	4	2.200	6.864	275
12PC	1890 ± 20	4	2.199	6.857	316
13PC	1490 ± 50	5	1.662	6.846	119

TABLE 3

Microhardness of Pyrolytic Graphite

Sample Number	Deposition Temperature (°C)	Microhardness On Basal Plane (Kgm/mm^2)	Microhardness Perpendicular To Basal Plane (Kgm/mm^2)
1PC	1670 ± 50		72.7 ± 5.8
2PC	1670 ± 50	85.4 ± 11.9	
4PC	1650 ± 25		76.6 ± 7.8
8PC	2200 ± 40		71.6 ± 3.5
9PC	1970 ± 30	52.6 ± 5.3	64.8 ± 2.7
11PC	1875 ± 45		78.9 ± 4.5

TABLE 4

Properties of Graphite-Titanium Alloys

Deposition Temperature 1675 ± 75°C

Deposition Pressure 5 ± 1 Torr

Sample Number	a/o Titanium	Density (gm/cc)	C_o (Å)	L_c (Å)	$(\bar{\eta}^2)^{\frac{1}{2}}$
1PC	0.000	2.163	6.860	284	0.0033
2PC	0.000	2.179	6.868	299	0.0041
4PC	0.000	2.183	6.852	279	0.0034
6PCTi	0.007	2.171	6.844	258	0.0043
37PCTi	0.012	2.184	---	---	-----
19PCTi	0.013	2.193	6.866	262	0.0032
15PCTi	0.015	2.180	6.865	243	0.0033
32PCTi	0.016	2.161	---	---	-----
14PCTi	0.018	2.170	6.867	251	0.0038
36PCTi	0.034	2.184	---	---	-----
39PCTi	0.037	2.182	6.846	---	-----
38PCTi	0.049	2.181	---	---	-----
18PCTi	0.078	2.185	6.876	254	0.0032
34PCTi	0.095	2.178	---	---	-----
7PCTi	0.110	2.176	6.860	270	0.0032
13PCTi	0.128	2.172	6.870	230	0.0042
9PCTi	0.152	2.191	6.871	237	0.0033
35PCTi	0.157	2.180	---	---	-----
33PCTi	0.172	2.179	---	---	-----
16PCTi	0.178	2.184	---	---	-----
17PCTi	0.187	2.171	---	---	-----
11PCTi	0.241	2.192	6.869	275	0.0037
12PCTi	0.260	2.189	6.898	270	0.0042
8PCTi	0.285	2.193	6.884	254	0.0034

$(\bar{\eta}^2)^{\frac{1}{2}}$ is the root mean squared of the lattice strain.

TABLE 4 (Continued)

Properties of Graphite-Titanium Alloys

Deposition Temperature 1975 ± 35°C

Deposition Pressure 5.5 ± 1.5 Torr

Sample Number	a/o Titanium	Density (gm/cc)	C (Å)	L_c (Å)	$(\overline{\eta^2})^{\frac{1}{2}}$
9PC	0.000	2.184	6.863	348	0.0005
10PC	0.000	2.174	6.862	355	0.0011
27PCTi	0.002	2.192	6.860	341	0.0008
25PCTi	0.002	2.195	6.863	294	0.0013
28PCTi	0.003	2.196	6.860	332	0.0003
29PCTi	0.004	2.193	6.863	334	0.0015
30PCTi	0.007	2.195	---	---	----
24PCTi	0.009	2.204	6.861	363	0.0004
26PCTi	0.011	2.198	6.860	334	0.0007
31PCTi	0.012	2.188	---	---	----

Deposition Temperature 2200 ± 100°C

Deposition Pressure 4 Torr

Sample Number	a/o Titanium	Density (gm/cc)
8PC	0.000	2.202
20PCTi	0.001	2.200
21PCTi	0.001	2.198

$(\overline{\eta^2})^{\frac{1}{2}}$ is the root mean squared of the lattice strain.

TABLE 5

Bend Strength Test Results
for Sample #15PCTi

Sample	Length (mm)	Width (mm)	Thickness (mm)	Failure Load (Kgm)	Rupture Stress (Kgm/mm^2)
A	4.01	1.152	0.753	1.56	14.37
B	4.01	1.005	0.737	0.98	10.80
C	4.01	1.040	0.724	2.12	23.39
D	4.01	1.208	0.745	2.58	23.15

TABLE 6

Properties of Heat Treated
Titanium Alloy Codeposits

Sample Number	A/o Titanium	Density (gm/cc)	C (Å)	L_c (Å)
1PC	(0.000)	2.162 (2.163)	6.850 (6.860)	299 (284)
37PCTi	(0.012)	2.187 (2.184)	------	----
19PCTi	(0.013)	2.180 (2.193)	6.849 (6.866)	262 (262)
32PCTi	(0.016)	2.159 (2.161)	------	----
39PCTi	(0.037)	2.194 (2.182)	6.831 (6.846)	255
34PCTi	(0.095)	2.182 (2.178)	6.854	254

Brackets ( ) denote values of deposit
prior to heat treatment.

TABLE 7

Chemical Analysis of Heat Treated
Graphite-Titanium Alloys

Sample Number	A/o Titanium Before HT	A/o Titanium After HT	Apparent Loss
19PCTi	0.013	0.011	15.4%
39PCTi	0.037	0.032	13.5%

TABLE 8

Pyrolytic Carbon-Vanadium System Properties

Sample Number	Deposition Temperature (°C)	Deposition Pressure (Torr)	Apparent Density (gm/cc)	C_0 (Å)	L_c (Å)
1PCV	1770 ± 30	5	1.710	6.845	216
2PCV	1800 ± 20	5	2.020	6.847	310
3PCV	1790 ± 50	5	1.748	6.862	328
4PCV	1850 ± 50	5	2.197	6.852	322
7PCV	1550 ± 100	14	1.400	---	---
8PCV	1700 ± 30	8+	1.263	---	174

All alloy samples contain less than 0.001 a/o Vanadium.

TABLE 9

Microhardness of Pyrolytic
Graphite-Vanadium Alloys

Sample Number	Deposition Temperature (°C)	Deposition Pressure (Torr)	Microhardness on Planes Perpendicular to Basal Planes (Kgm/mm^2)
1PCV	1770 ± 30	5	84.6 ± 7.9
2PCV	1800 ± 20	5	73.4 ± 3.4
4PCV	1850 ± 50	5	71.4 ± 4.0
7PCV	1550 ± 100	14	166.9 ± 9.8
8PCV	1700 ± 30	8+	103.2 ± 3.6

All samples contain less than 0.001 a/o Vanadium.

TABLE 10

Pyrolytic Graphite-Nickel System Properties

Sample Number	Deposition Temperature (°C)	Deposition Pressure (Torr)	a/o Nickel	Apparent Density (gm/cc)	C (Å)	L_c (Å)
1PCNi	1620 ± 20	6.5	0.000	2.186	6.849	275
2PCNi	1590 ± 30	5.5	0.003	2.155	6.843	299
3PCNi	1500 ± 30	5	0.003	1.539	---	---

FIGURES
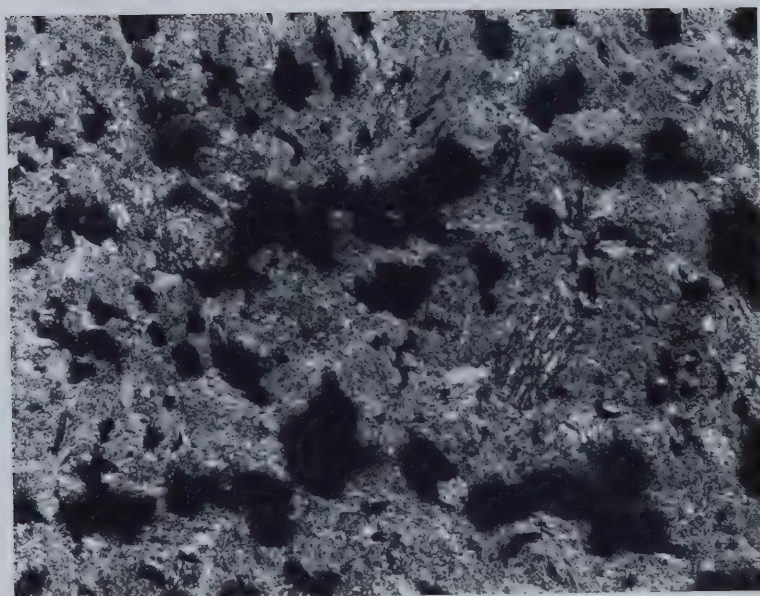
FIGURE 1.   Speer RC4 graphite.
80X

A. propane
B. low pressure regulator
C. dessicant
D. manometer
E. flowmeter
F. water bath
G. metal compound container
H. inlet orifice
I. deposition chamber
J. condensing tower
K. air inlet
L. pyrometer
M. NaOH
N. control valves
P. vacuum pump
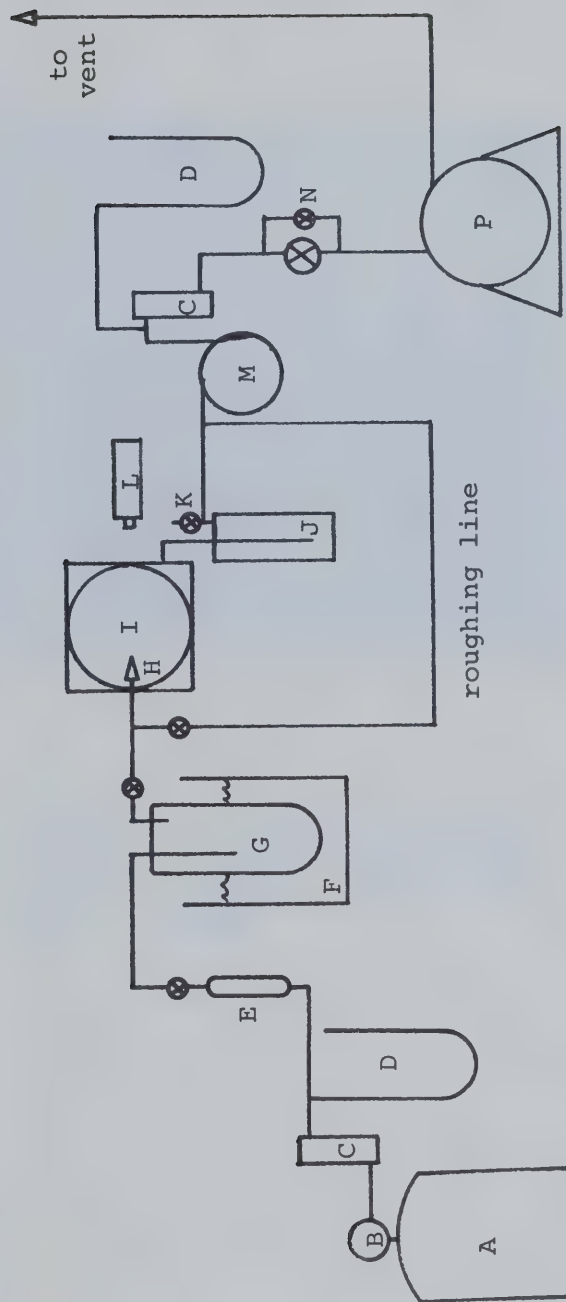
FIGURE 2. Flow sheet for pyrolytic codeposition apparatus.
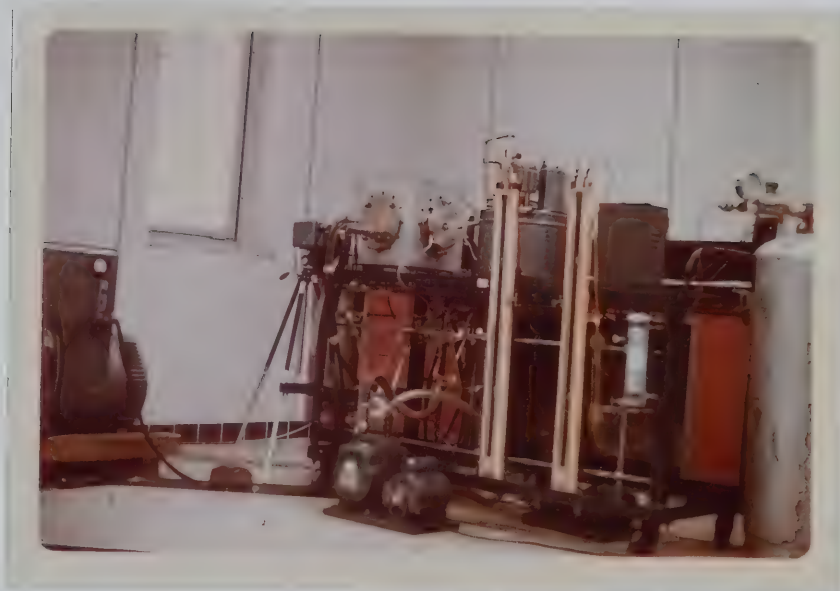
FIGURE 3.   Pyrolytic codeposition equipment.
L to R: D.C. welder, pyrometer,
deposition chamber, vacuum pump,
constant temperature bath, mano-
meters, propane.
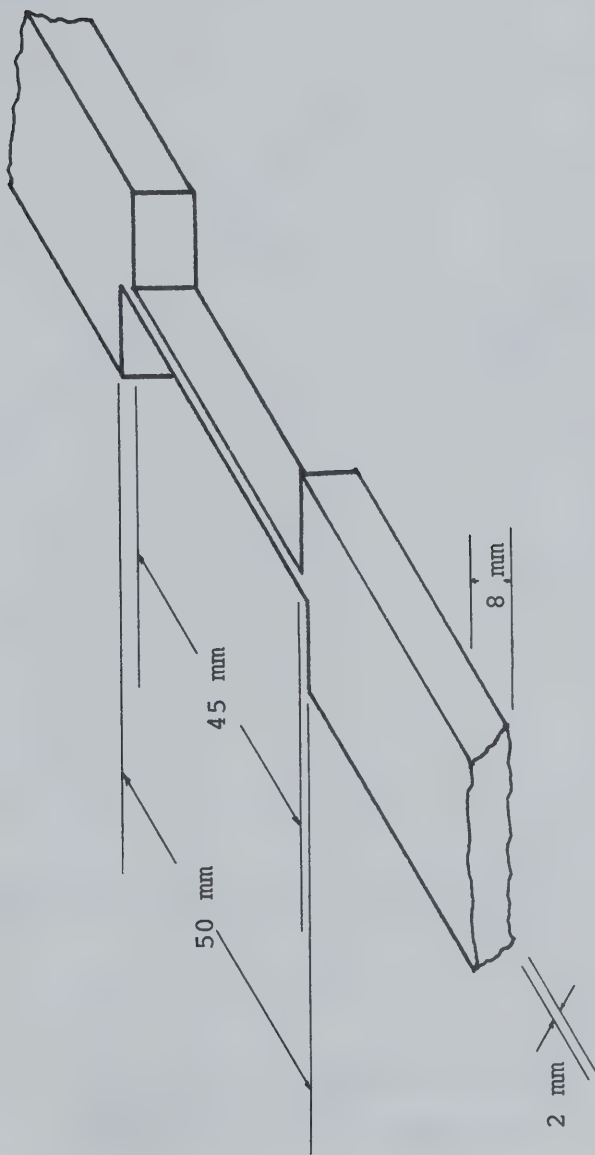
FIGURE 4. Graphite substrate design.
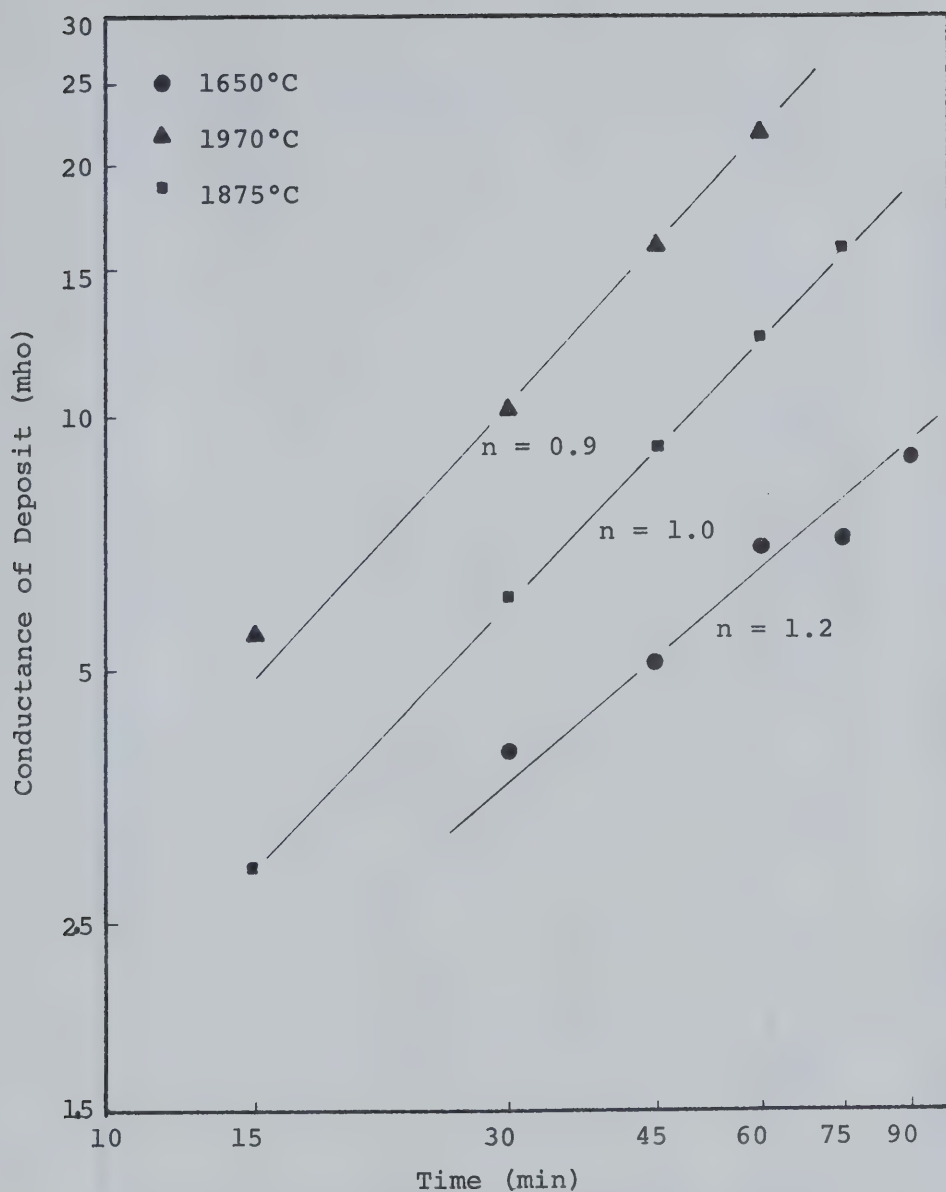
FIGURE 5. Conductance change of graphite deposit with time. Pyrolytic graphite deposited at 5 ± 1 torr.
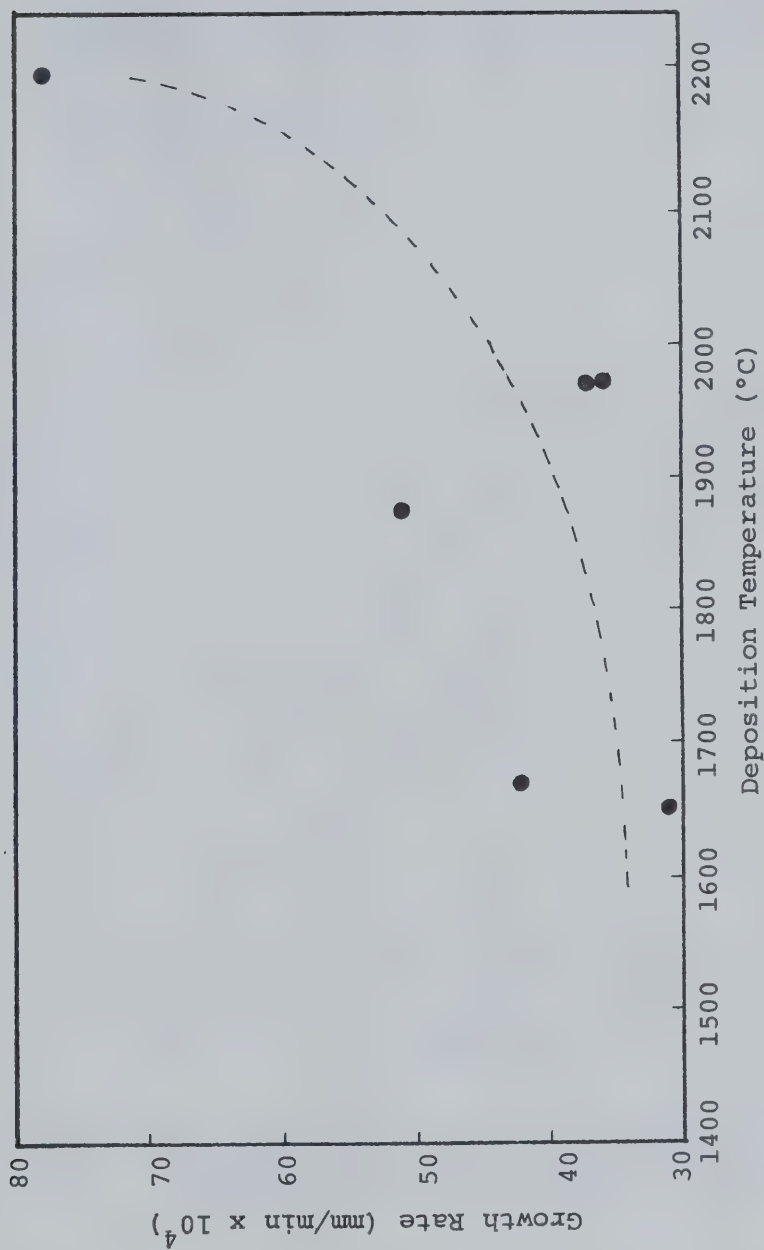
FIGURE 6. Growth rate of pyrolytic graphite as a function of
deposition temperature for a deposition pressure
of 4.5 ± 0.5 torr.
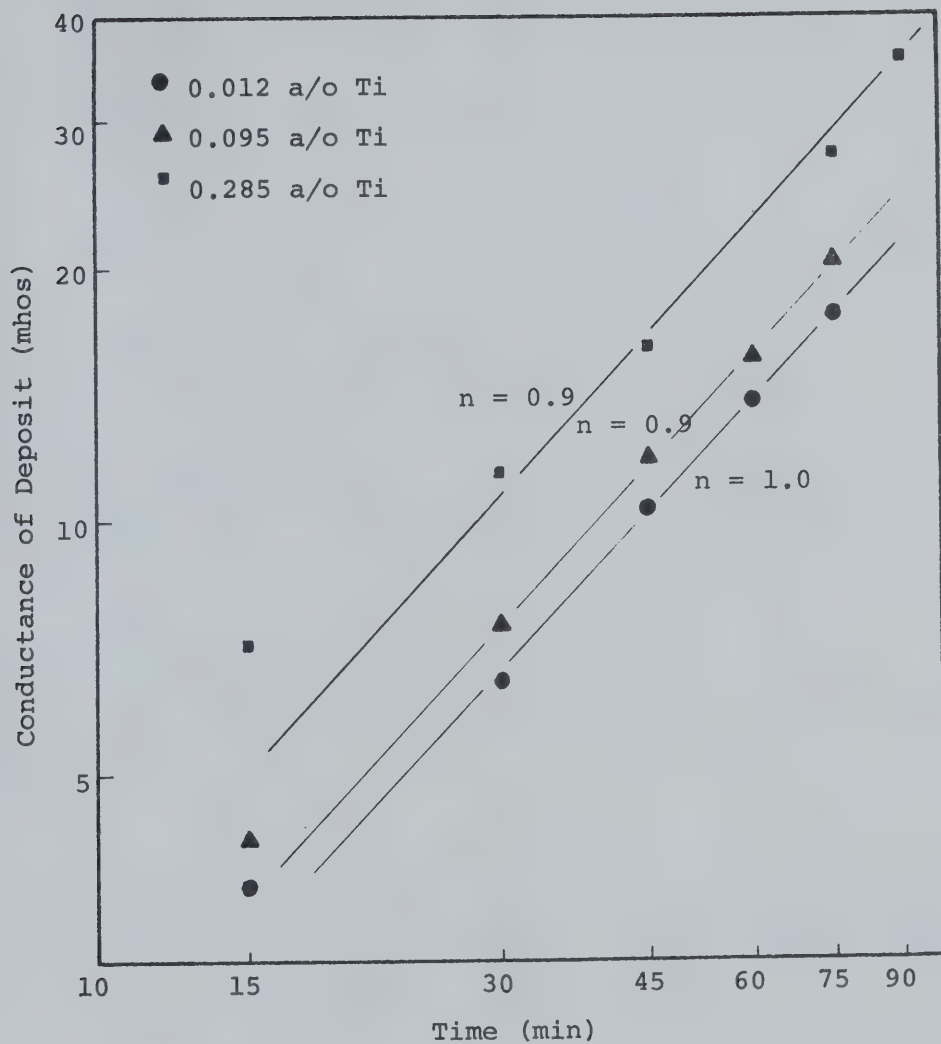
FIGURE 7. Conductance of graphite-titanium deposits formed at 1675 ± 75°C and 5 ± 1 torr.
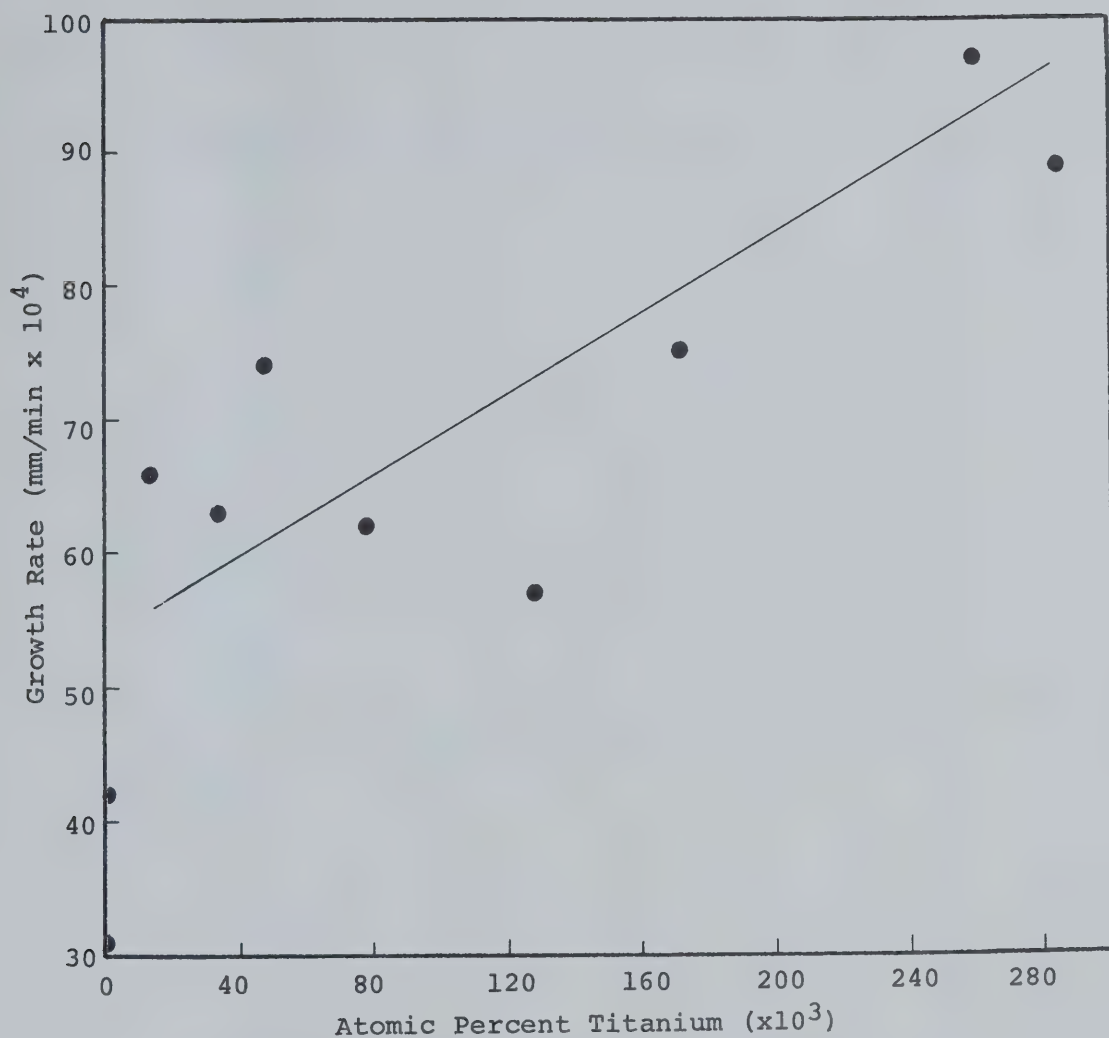
FIGURE 8. Growth rate as a function of titanium
concentration for alloys formed at
1675 ± 75°C and 5 ± 1 torr.
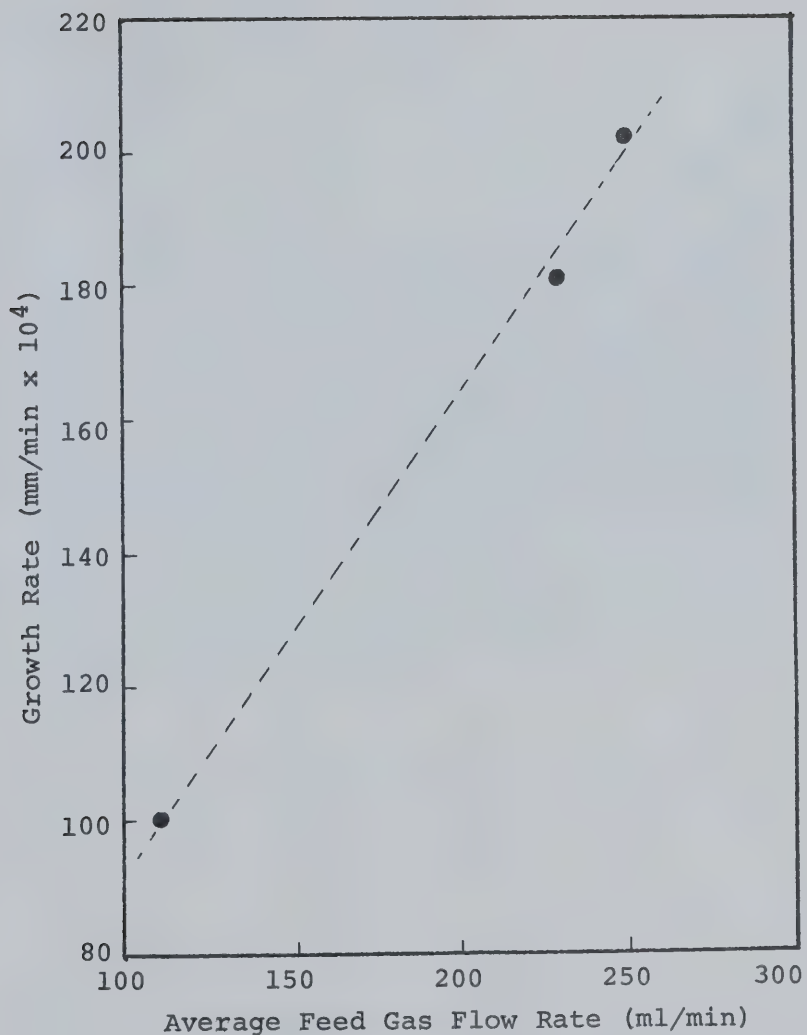
FIGURE 9. Effect of feed gas flow rate on the
growth rate of pyrolytic graphite-
vanadium alloys.
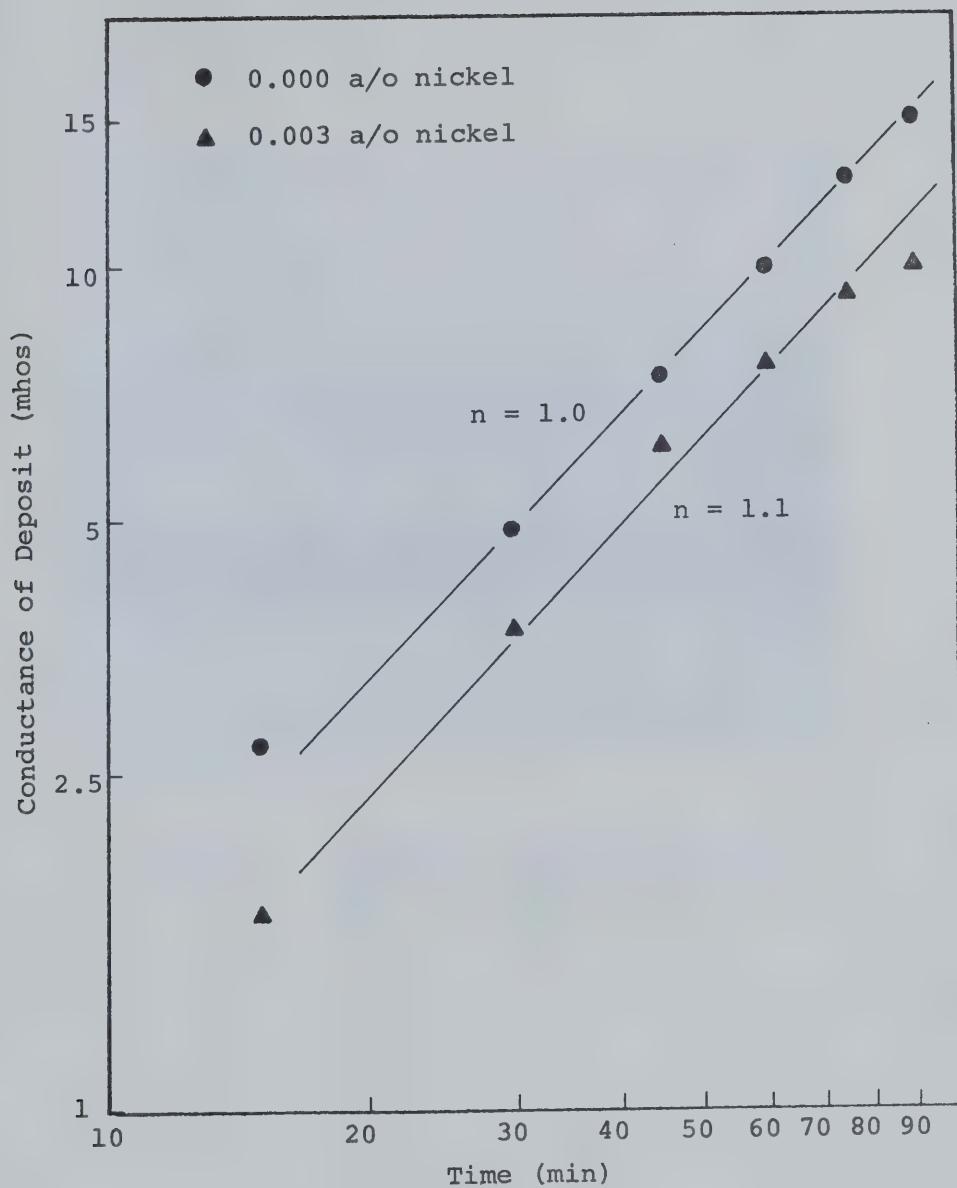
FIGURE 10. Conductance of graphite-nickel alloy
deposits formed at 1600 ± 40°C and
6 ± 0.5 torr.

FIGURE 11. Substrate with top view of
pyrolytic graphite deposit.
1X
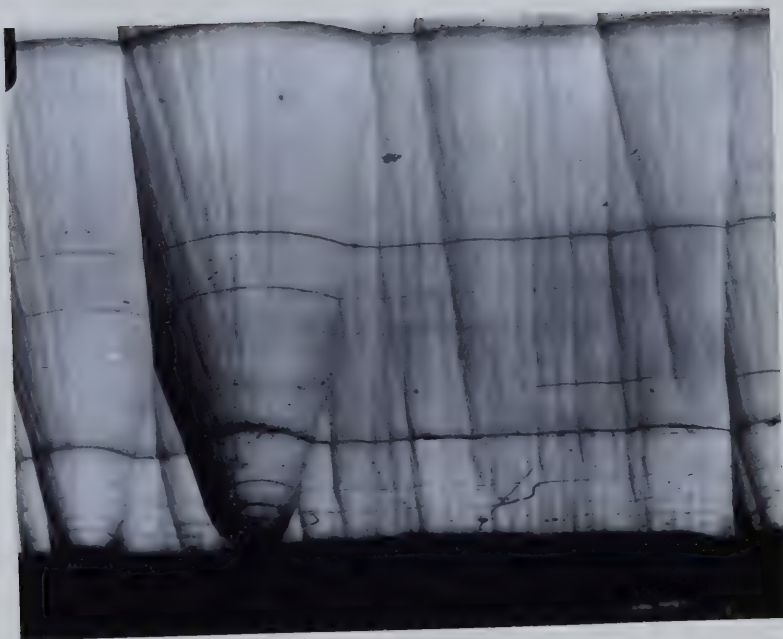
FIGURE 12. Singularly nucleated pyrolytic graphite. 100X polarized light.

FIGURE 13.   Polynucleated pyrolytic graphite.
80X polarized light.
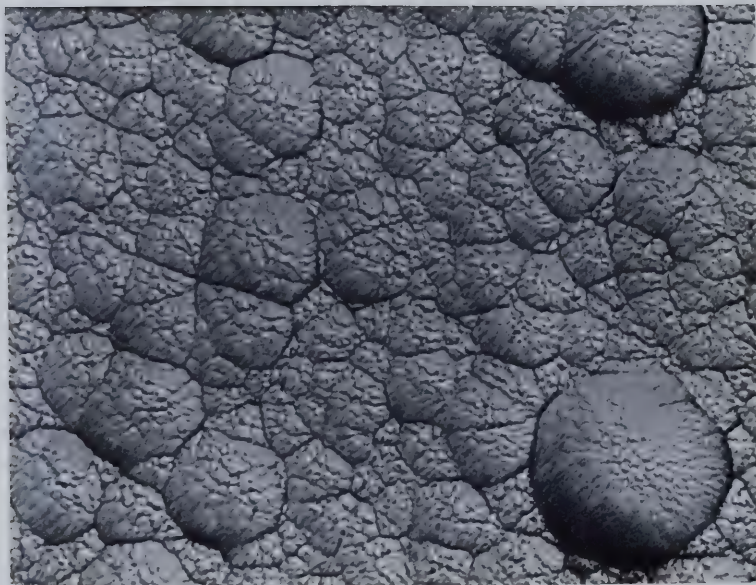
FIGURE 14.   Deposition surface parallel
to deposition substrate.
Mechanically polished.   100X
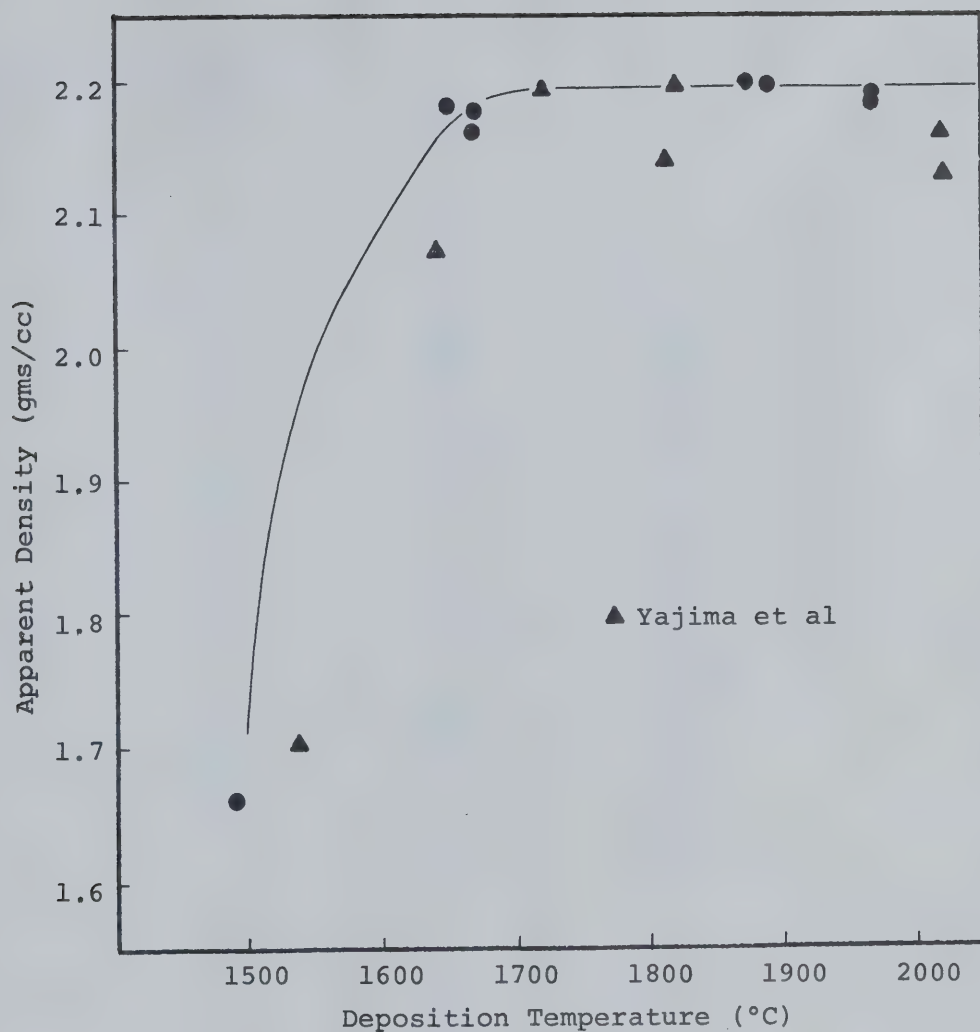
FIGURE 15. Apparent density of pyrolytic graphite
            as a function of deposition temperature.
            Deposition pressure constant at
            4.5 ± 0.5 torr.
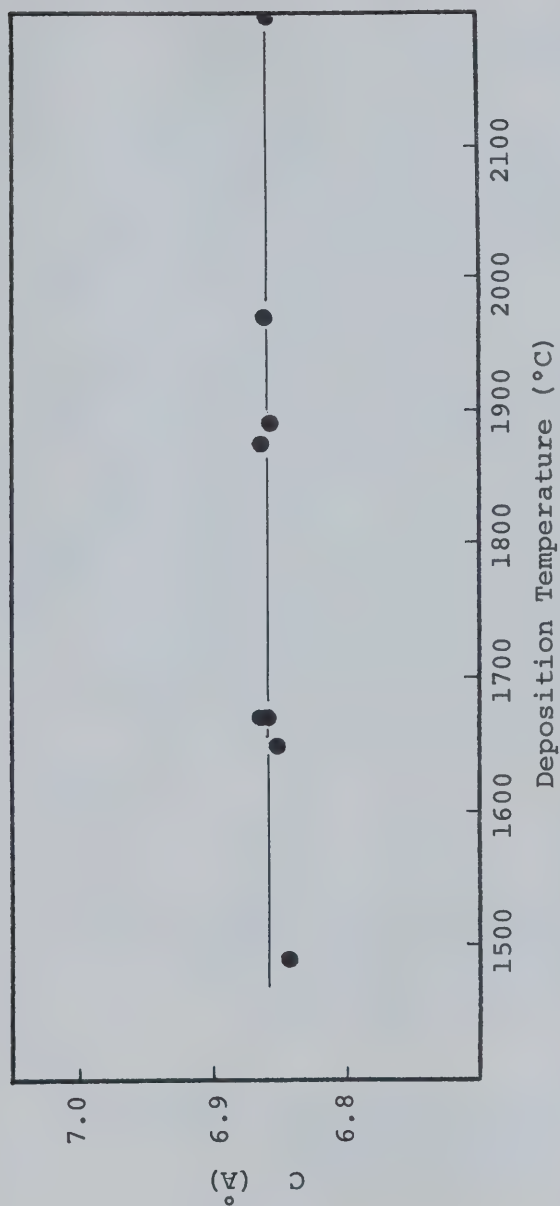
FIGURE 16. Lattice constant, C, as a function of deposition temperature for pyrolytic graphite formed at a pressure of 4.5 ± 0.5 torr.
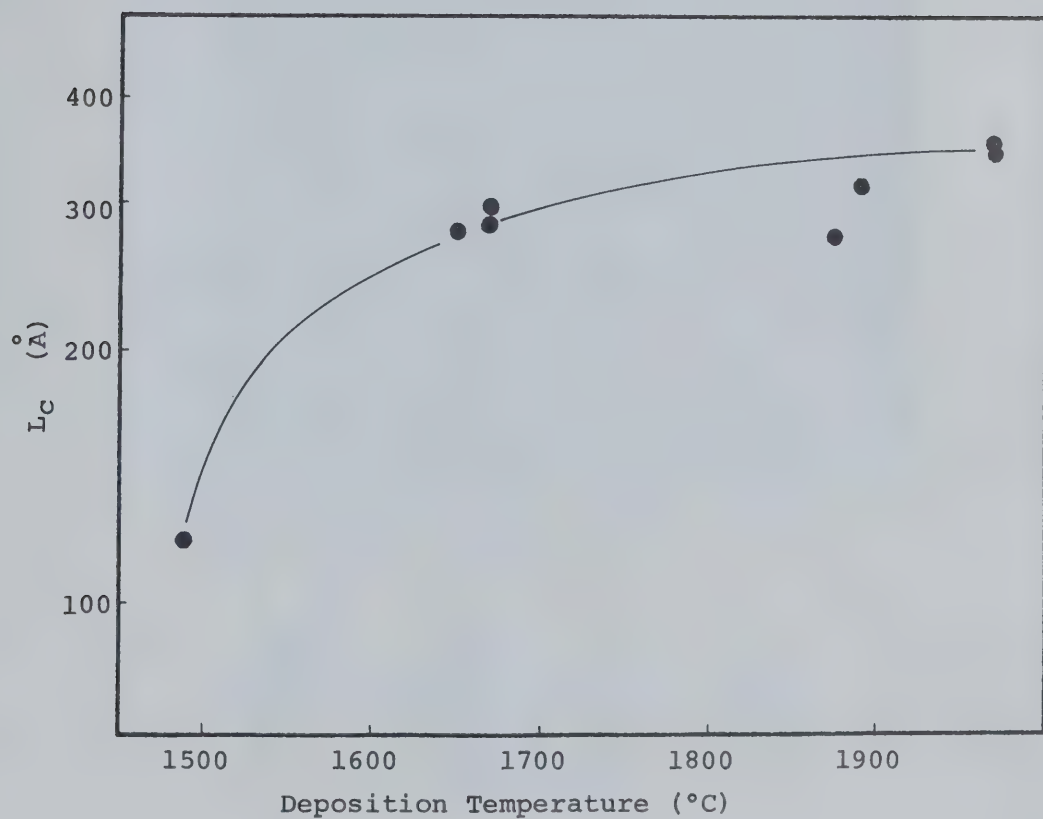
FIGURE 17. Crystallite size, L_C, as a function of
deposition temperature of pyrolytic
graphite formed at 4.5 ± 0.5 torr.
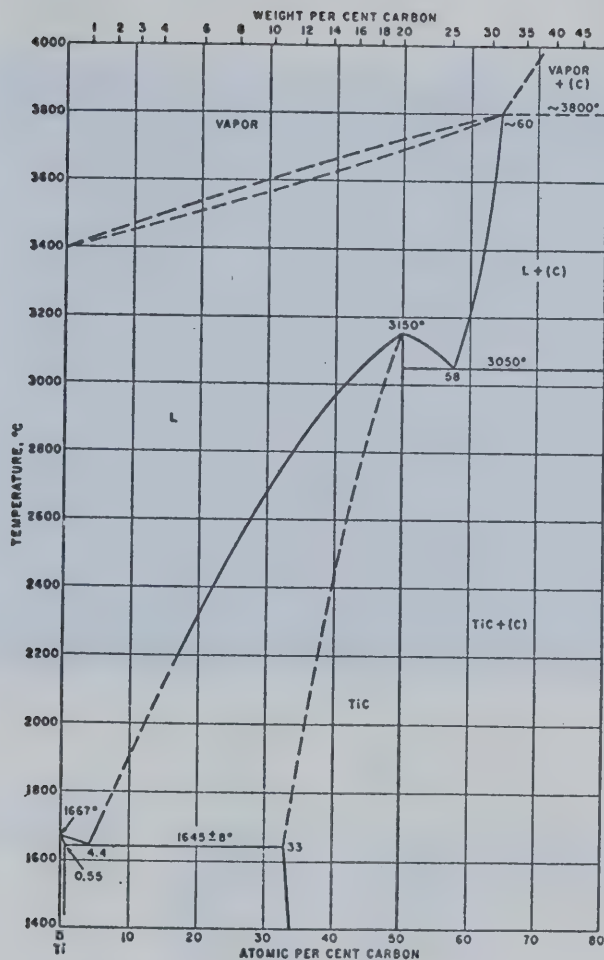
FIGURE 18. Carbon-titanium phase diagram.

Taken from R.P. Elliot, Constitution
of Binary Alloys, First Supplement,
McGraw Hill Co., New York, 1965.

FIGURE 19.   Singularly nucleated alloy of
             pyrolytic graphite and 0.285
             a/o titanium formed at 1625 ±
             25°C and 4 torr.
             80X polarized light.

FIGURE 20. Singularly nucleated alloy of
            pyrolytic graphite and 0.002
            a/o titanium formed at 1980 ±
            30°C and 4 torr.
            80X polarized light.

(a)

(b)

(c)
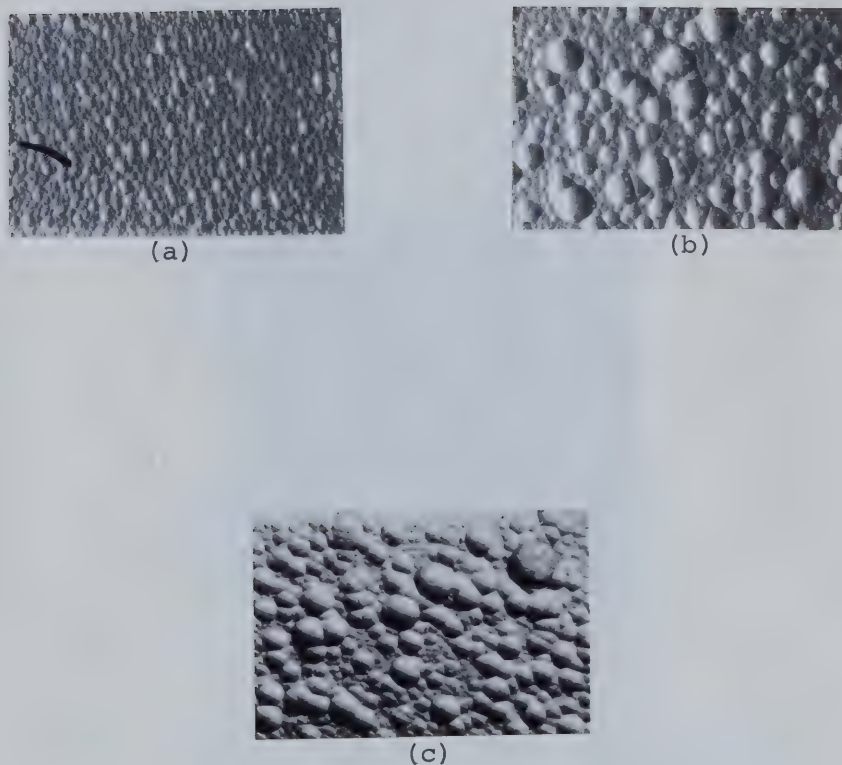
FIGURE 21.   Top view of basal plane growth cones in
pyrolytic graphite-titanium alloys
deposited at 1675 ± 75°C and 5 ± 1 torr.

(a)   0.012 a/o titanium
(b)   0.078 a/o titanium
(c)   0.187 a/o titanium

6X

FIGURE 22.   Precipitate in pyrolytic graphite-
0.012 a/o titanium alloy deposited
at 1660 ± 20°C and 5 torr.

(a)

(b)
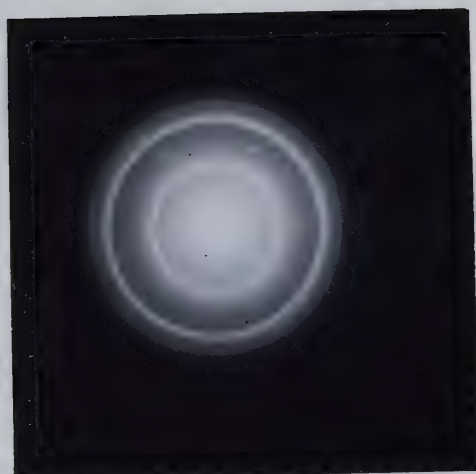
FIGURE 23. Pyrolytic graphite-0.285 a/o titanium
            alloy formed at 1625 ± 25°C and 4 torr.

            (a) Diffraction pattern.
            (b) Area from which diffraction
                 pattern obtained.
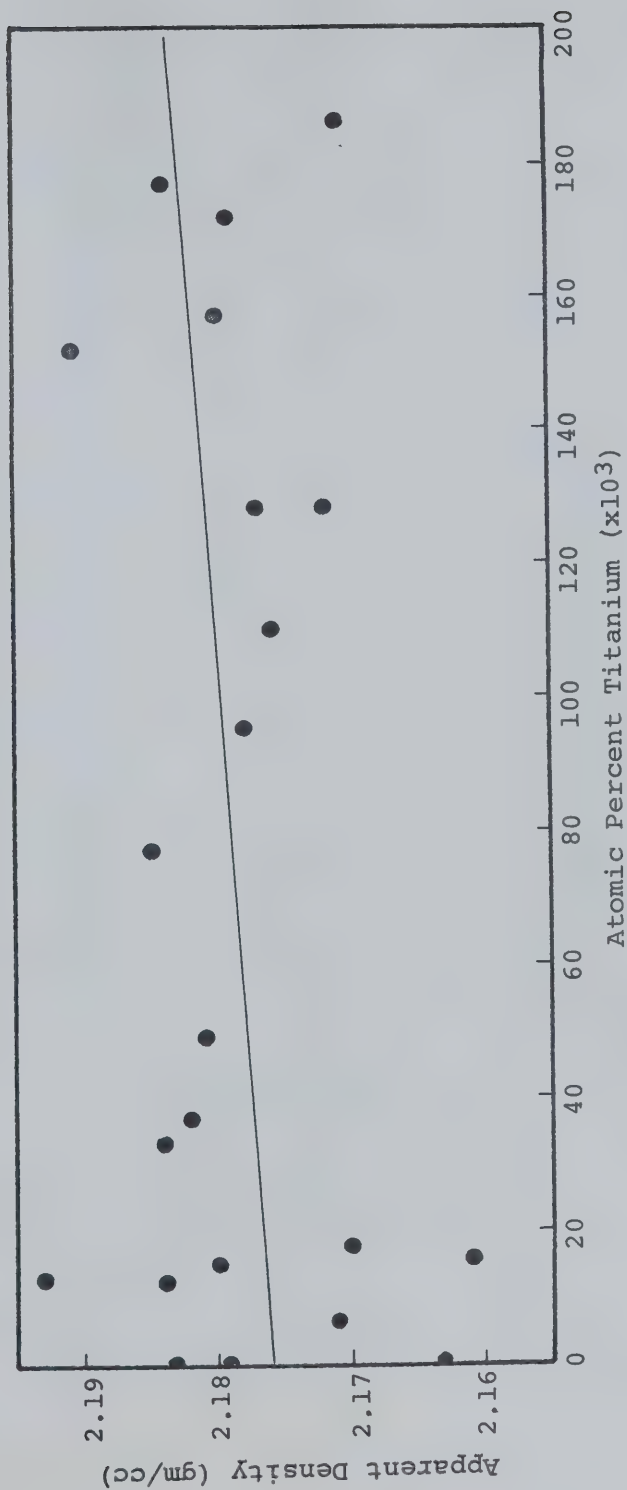
FIGURE 24. Apparent density of alloy deposits as a function of titanium concentration. Deposits formed at 1675 ± 75°C and 5 ± 1 torr.
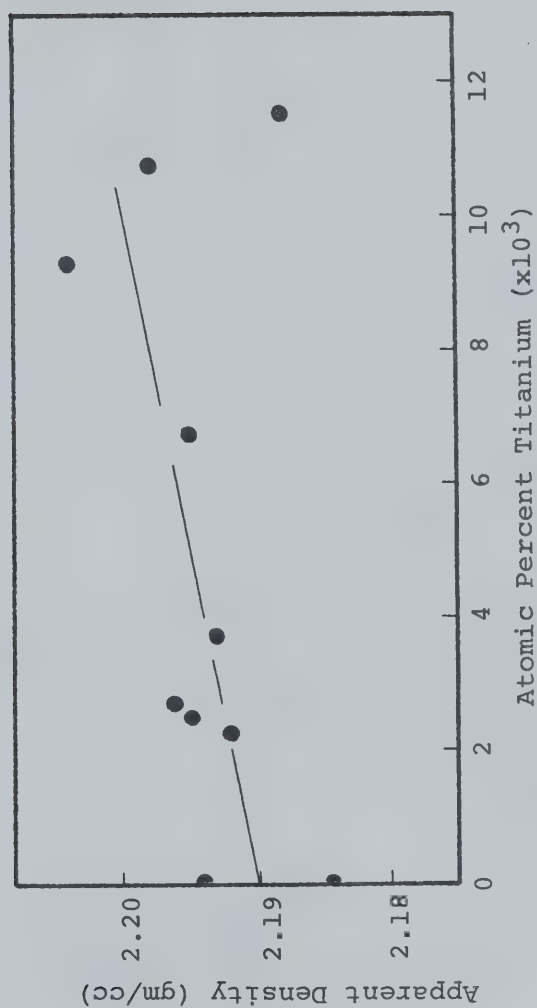
FIGURE 25. Apparent density of alloy deposits as a function of titanium concentration. Deposits formed at 1975 ± 35°C and 5.5 ± 1.5 torr.
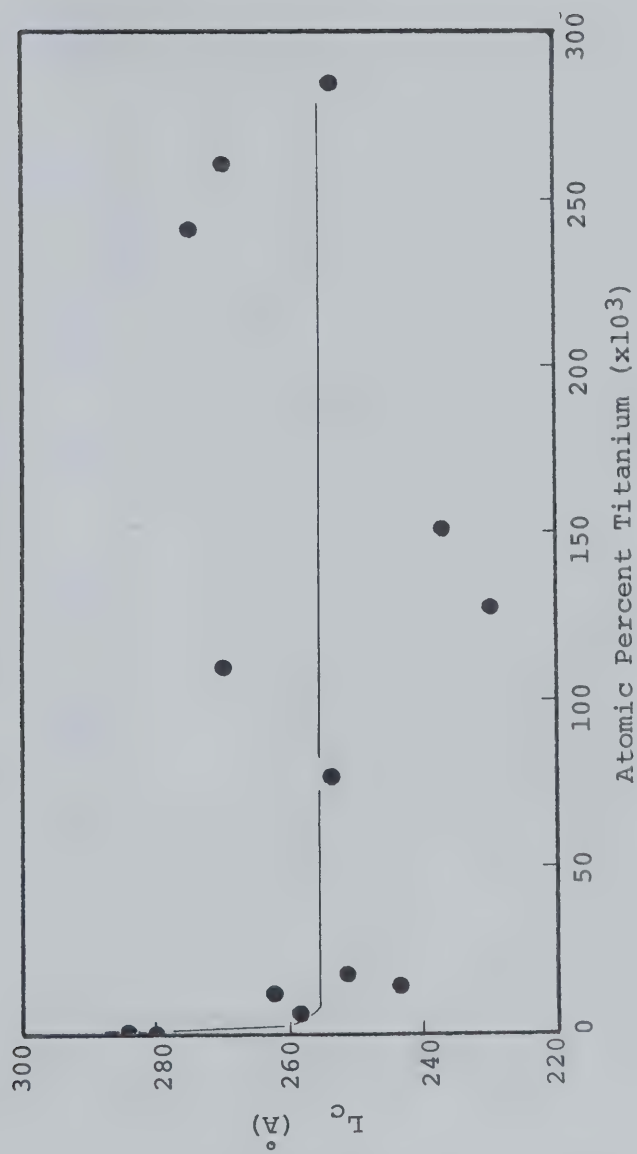
FIGURE 26. Crystallite height, L_c, as a function of composition. Alloys formed at 1675 ± 75°C and 5 ± 1 torr.
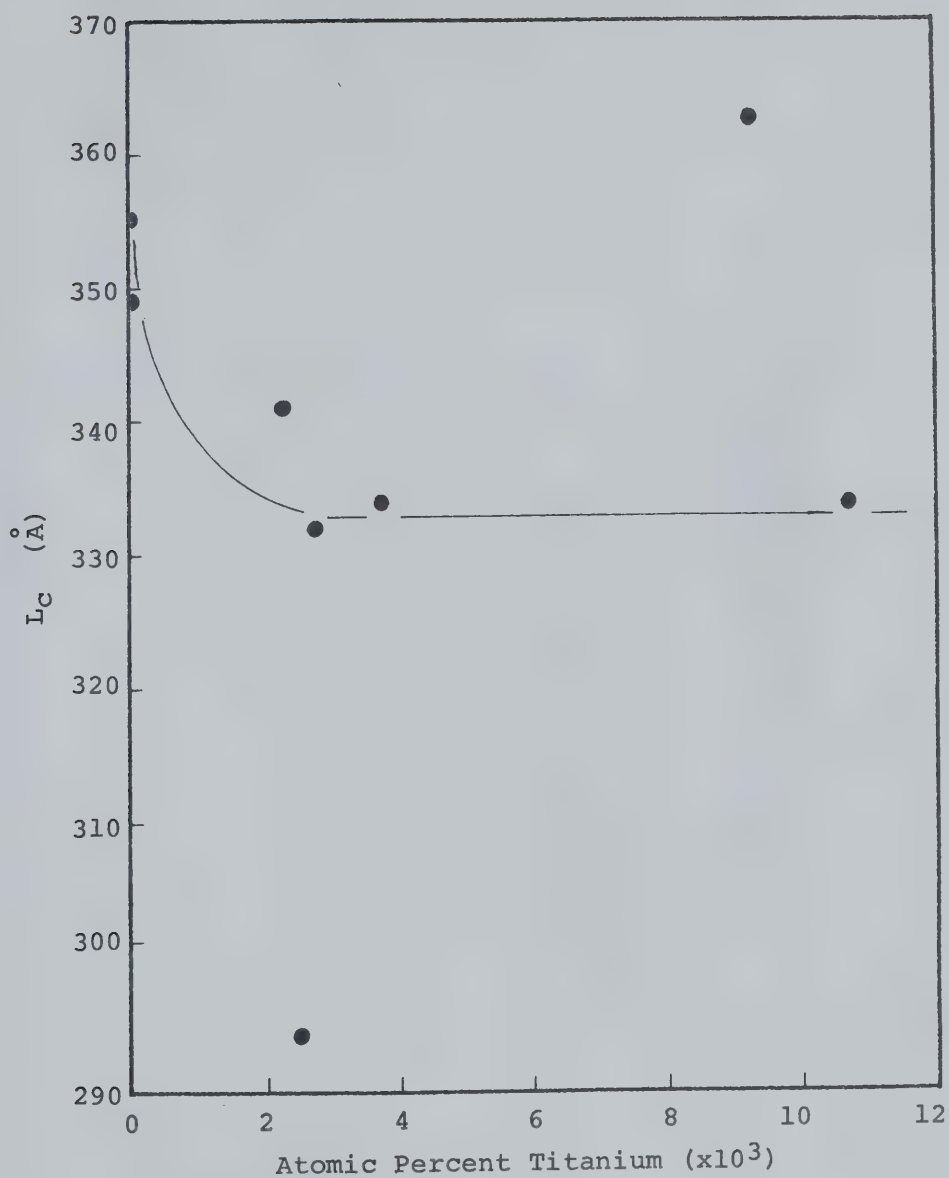
FIGURE 27. Crystallite height, L_C, as a function
of titanium concentration. Alloys
formed at 1975 ± 35°C and 5.5 ± 1.5 torr.
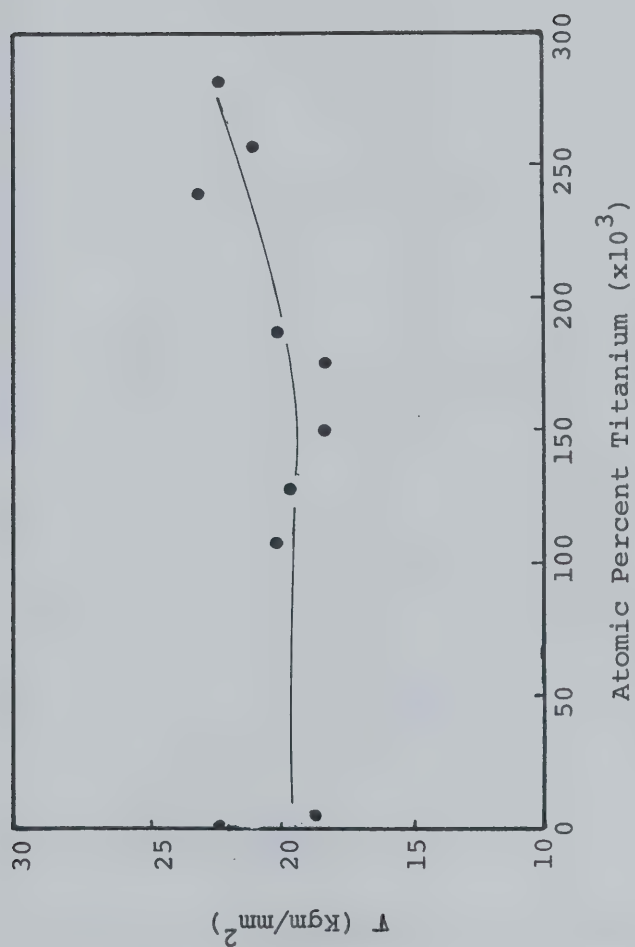
FIGURE 28. Bend Strength, γ, as a function of composition for alloys formed at 1675 ± 75°C and 5 ± 1 torr.
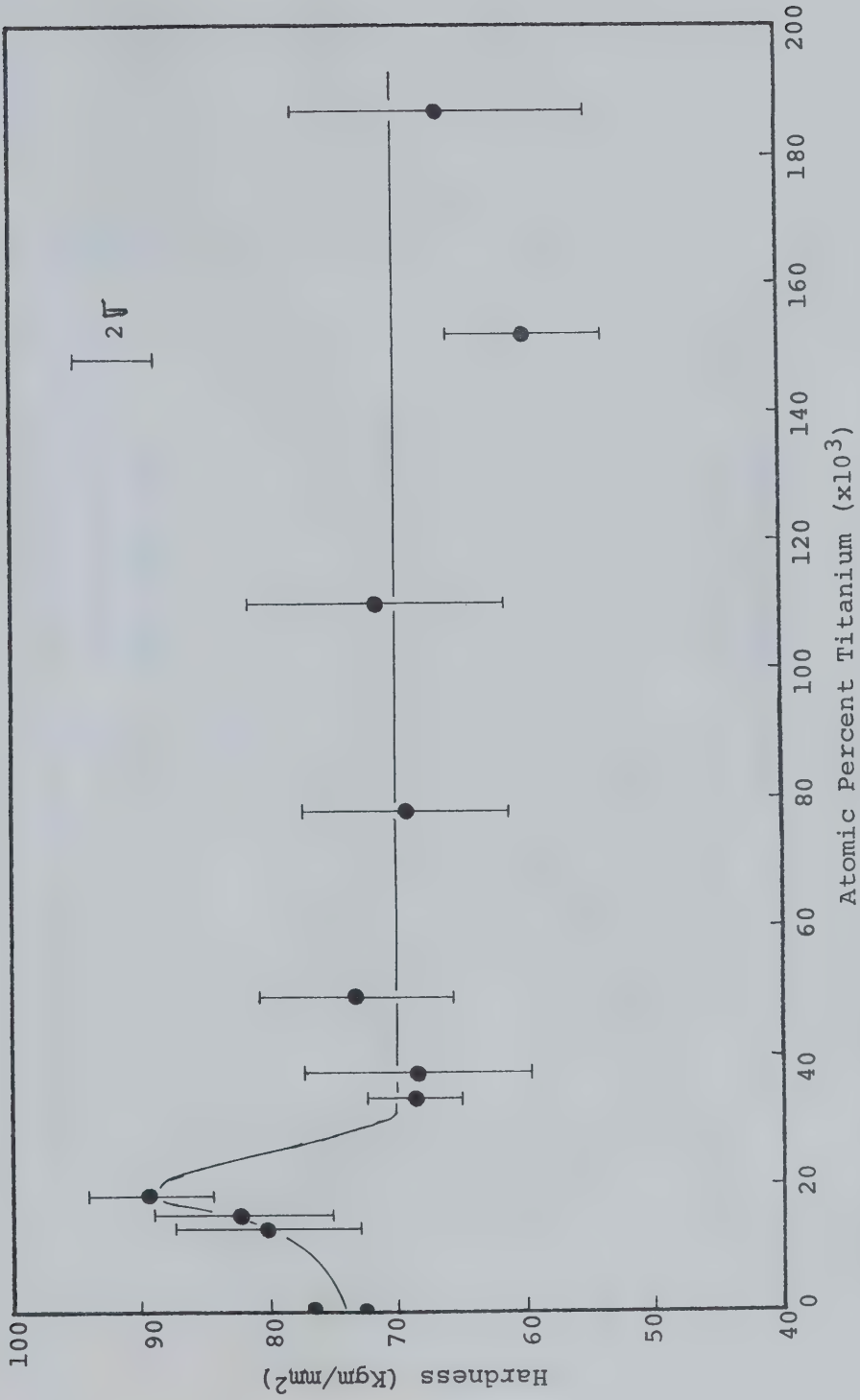
FIGURE 29. Microhardness on planes perpendicular to basal planes for alloys formed at 1675 ± 75°C and 5 ± 1 torr.
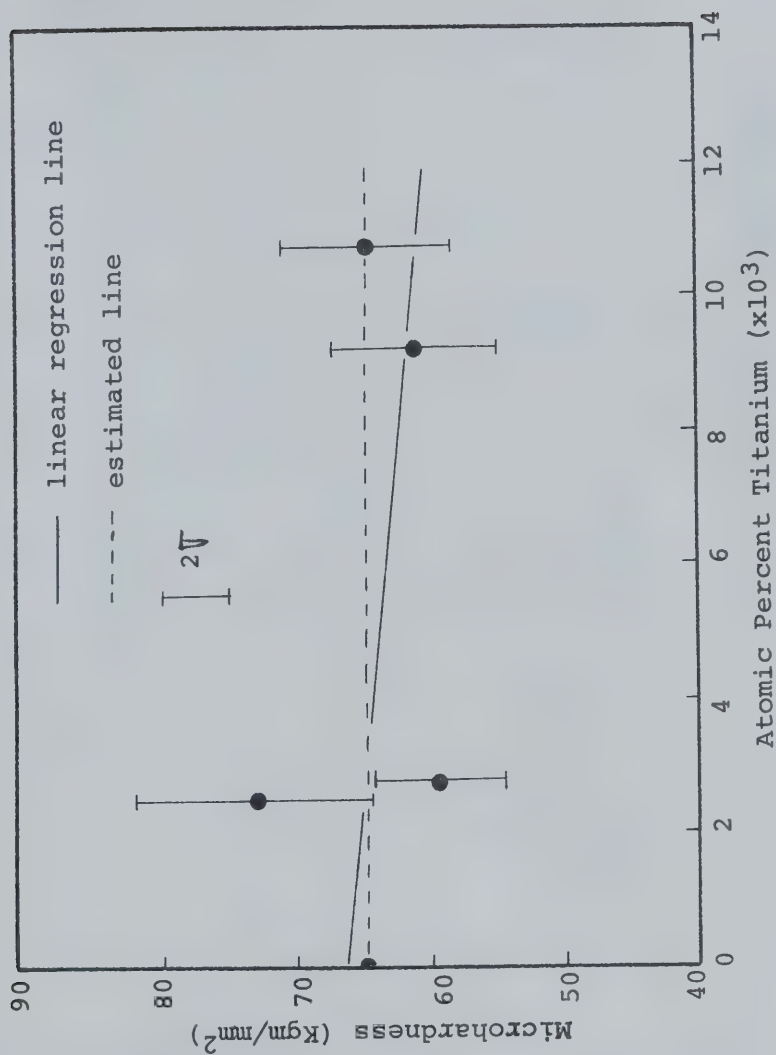
FIGURE 30. Microhardness on planes perpendicular to basal planes for alloys formed at 1975 ± 35°C and 5.5 ± 1.5 torr.
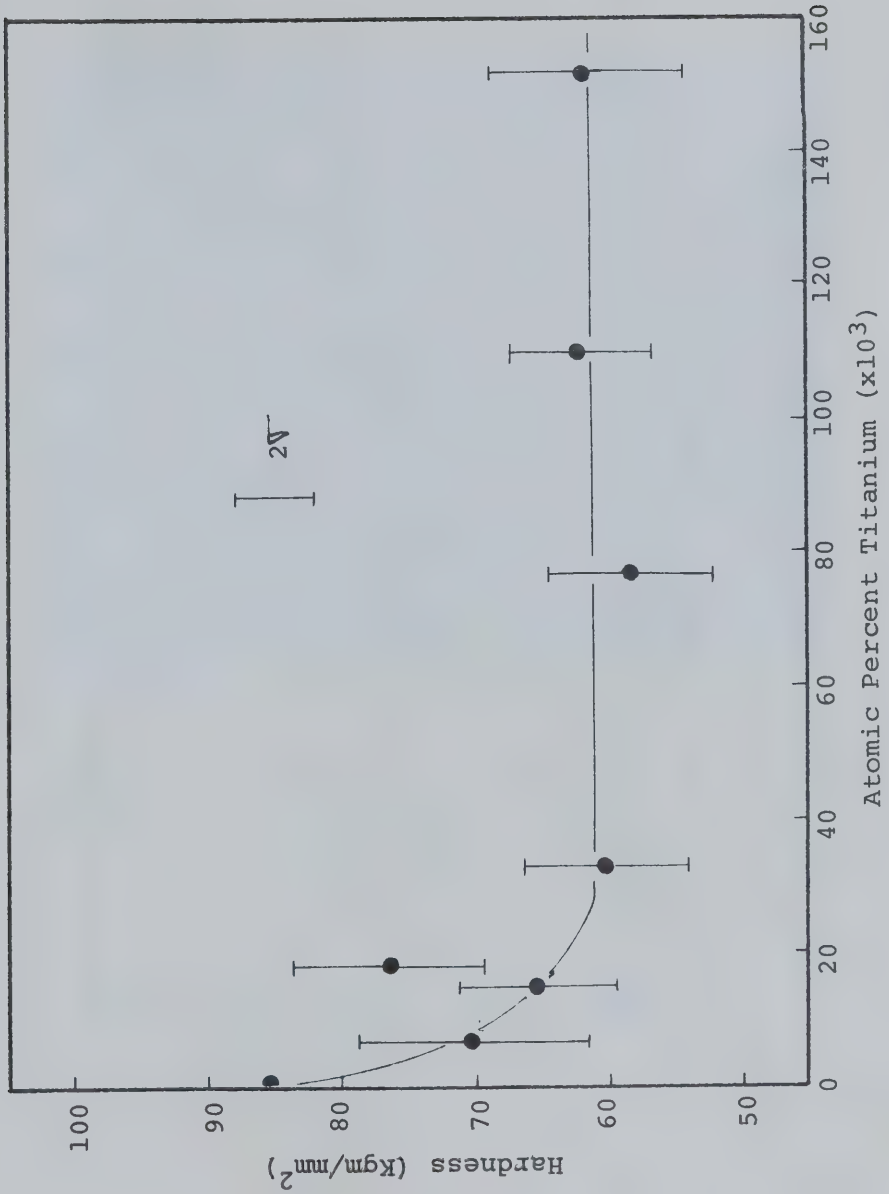
FIGURE 31. Microhardness on basal planes for alloys formed at 1675 ± 75°C and 5 ± 1 torr.
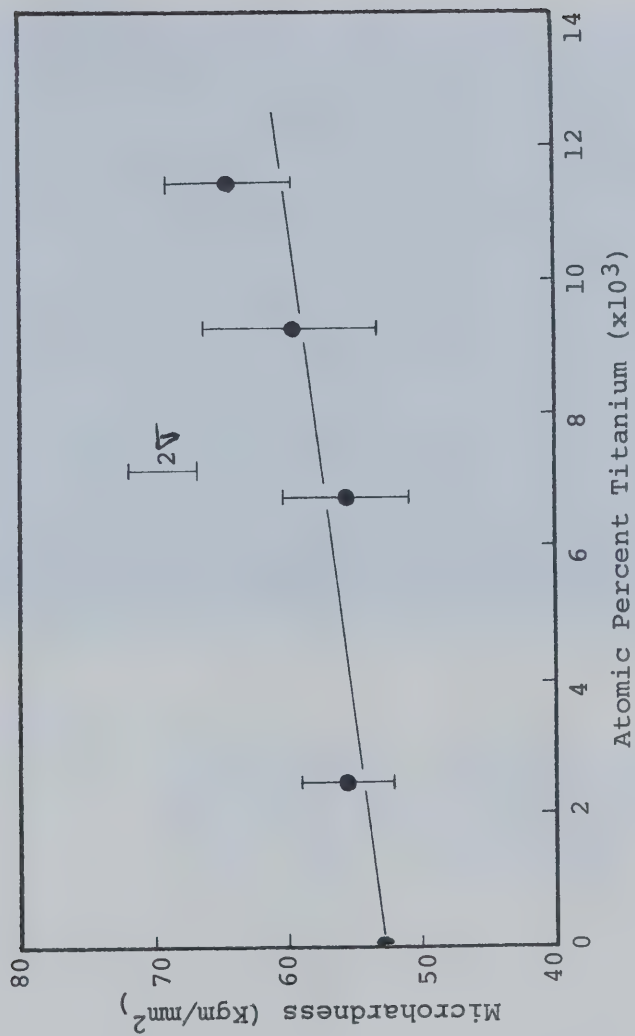
FIGURE 32. Microhardness on basal planes for alloys
formed at 1975 ± 35°C and 5.5 ± 1.5 torr.

FIGURE 33. Electron microprobe scan on planes
perpendicular to basal planes of a
pyrolytic graphite-0.037 a/o titan-
ium alloy deposited at 1675 ± 55°C
and 5 torr.   Approximately 150X

FIGURE 34. Electron microprobe scan on basal
planes of a pyrolytic graphite-
0.18 a/o titanium alloy deposited
at 1650 ± 20°C and 5 torr.
Approximately 1,000X.
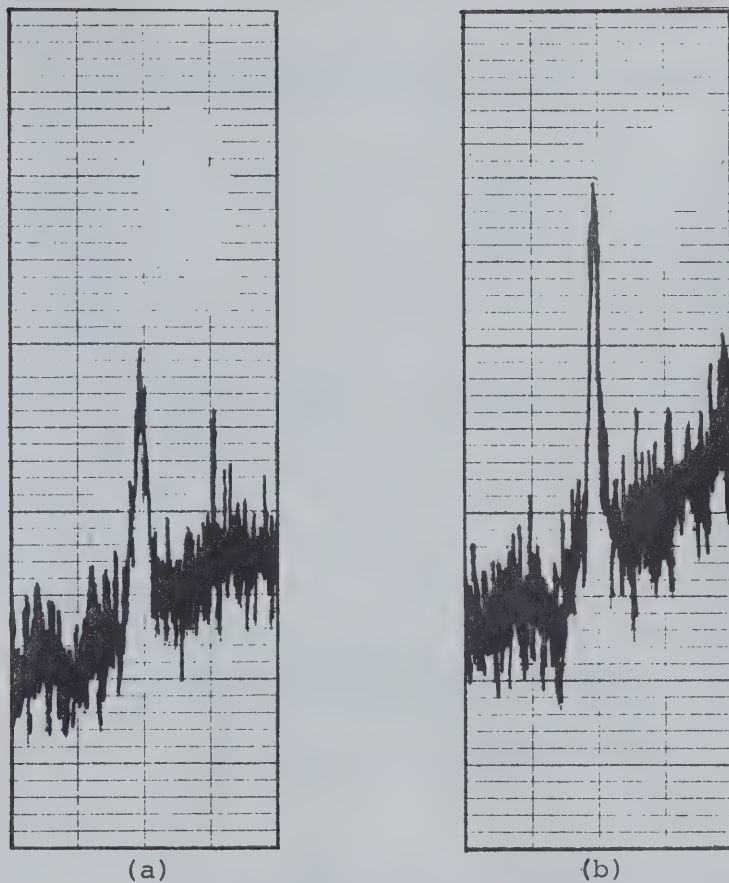
FIGURE 35.   (111) diffraction peak of titanium carbide.

(a)   as deposited 0.018 a/o titanium alloy.
(b)   heat treated 0.013 a/o titanium alloy.
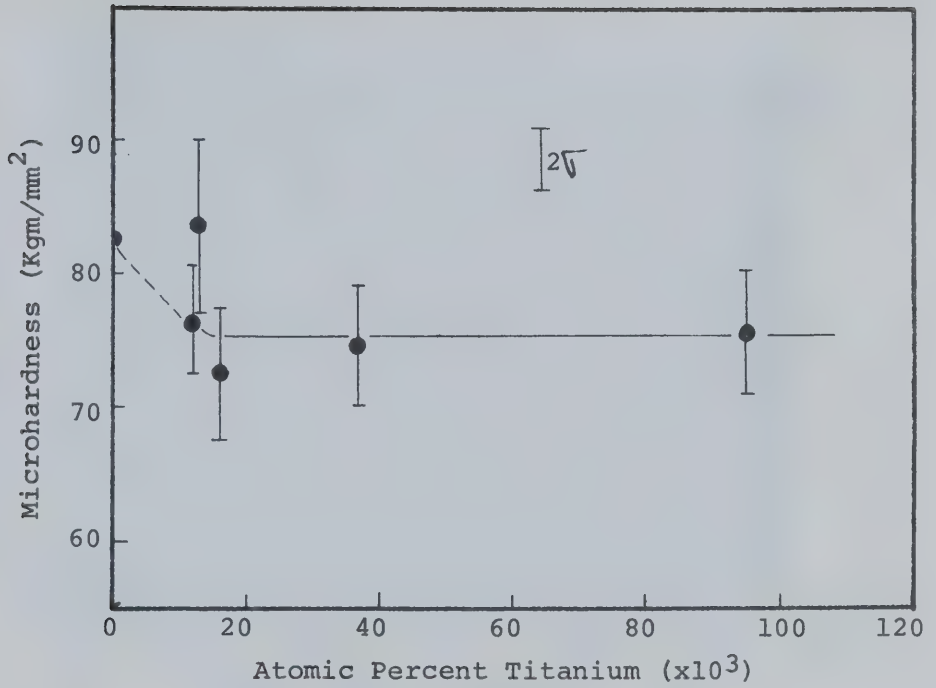
FIGURE 36. Microhardness on planes perpendicular to basal planes for alloys formed at 1675 ± 75°C and heat treated at 1600 ± 100°C for 20 hours.
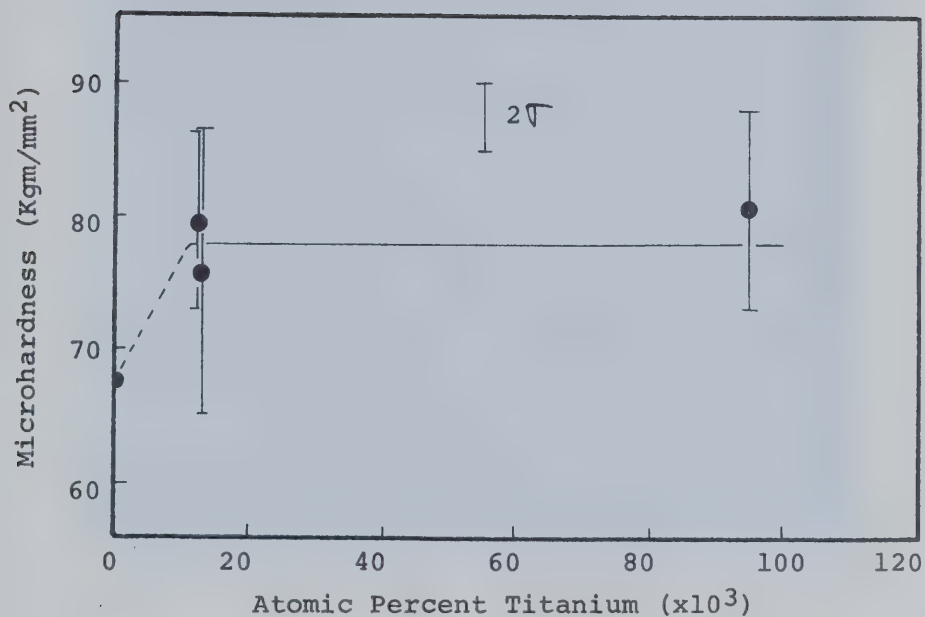
FIGURE 37.   Microhardness on basal planes for
alloys formed at 1675 ± 75°C and
heat treated at 1600 ± 100°C.

FIGURE 38. Electron microprobe scan of titanium
distribution. 0.037 a/o titanium
alloy formed at 1675 ± 75°C and heat
treated at 1600 ± 100°C for 20 hours.
Scan is of planes perpendicular to
basal planes. Approximately 150X.

FIGURE 39. Electron microprobe scan of titanium
distribution. Alloy contains 0.013
a/o titanium and was formed at 1675
± 75°C and subsequently heat treated
for 20 hours at 1600 ± 100°C. Scan
is of basal planes. Approximately
150X.
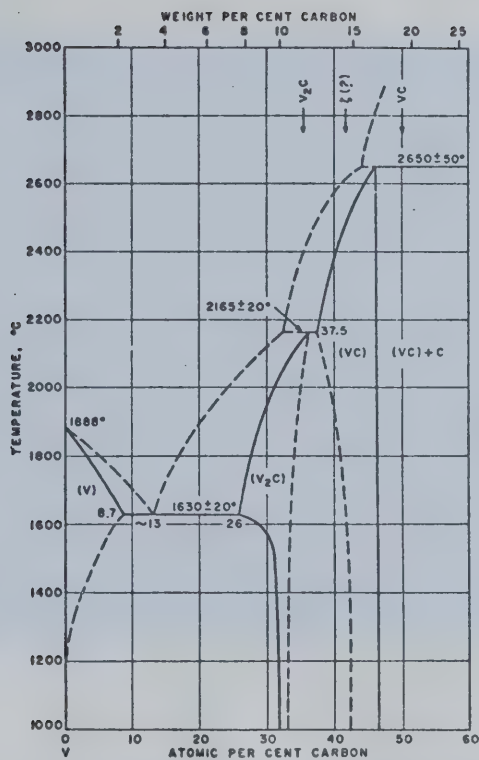
FIGURE 40. Carbon-vanadium phase diagram.

Taken from F. A. Shunk, _Constitution of Binary Alloys_, Second Supplement, McGraw Hill Co., New York, 1969.

FIGURE 41. Singularly nucleated pyrolytic
graphite-<0.001 a/o vanadium
alloy formed at 1800 ± 20°C and
5 torr. 80X, polarized light.

FIGURE 42.   Non basal planes of a pyrolytic
graphite-<0.001 a/o vanadium
alloy formed at 1700 ± 30°C and
8+ torr.   80X, polarized light.

FIGURE 43. Carbon plume growths on
substrate formed at
1700 ± 30°C and 8+ torr.

(a)
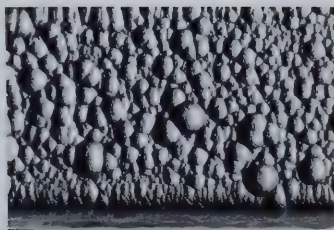
(b)
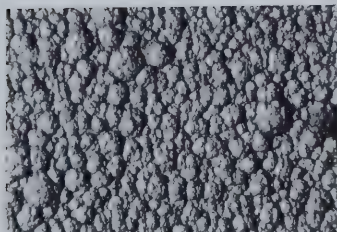
(c)

FIGURE 44.   Top view of basal planes of graphite-
             vanadium alloys.   6X

        (a)   Typical basal plane of pure
              pyrolytic graphite.
        (b)   Basal plane of alloy formed at
              1790 ± 50°C and 5 torr.
        (c)   Basal plane of alloy formed at
              1550 ± 100°C and 14 torr.
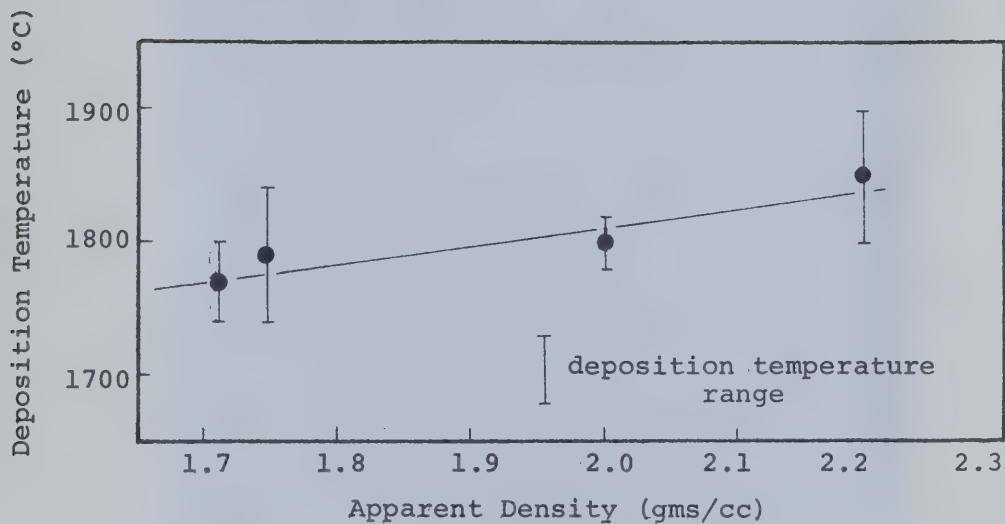
FIGURE 45. Apparent density as a function
of deposition temperature for
pyrolytic graphite alloys con-
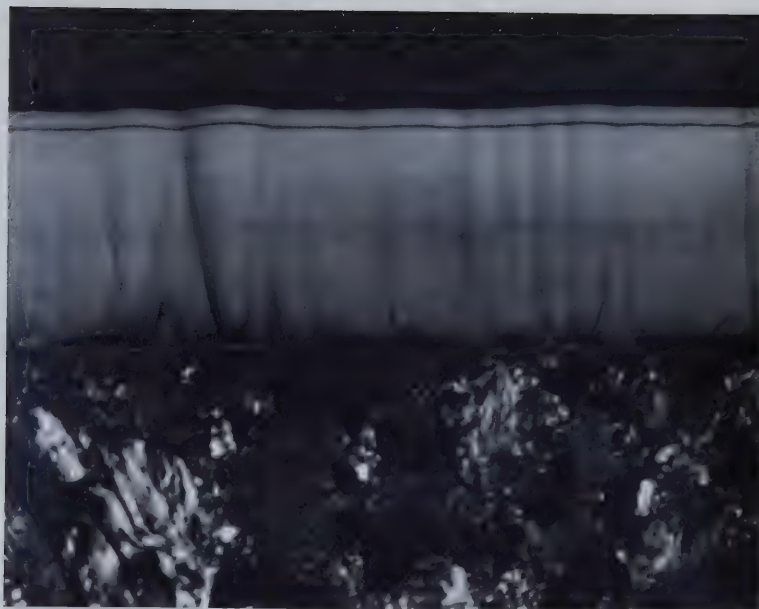taining <0.001 a/o vanadium
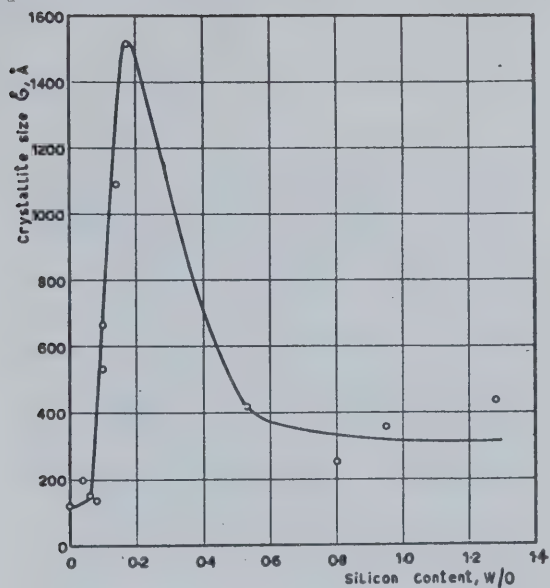and formed at 5 torr.

FIGURE 46.   Singularly nucleated pyrolytic
             graphite-0.003 a/o nickel alloy
             formed at 1620 ± 20°C and 6.5
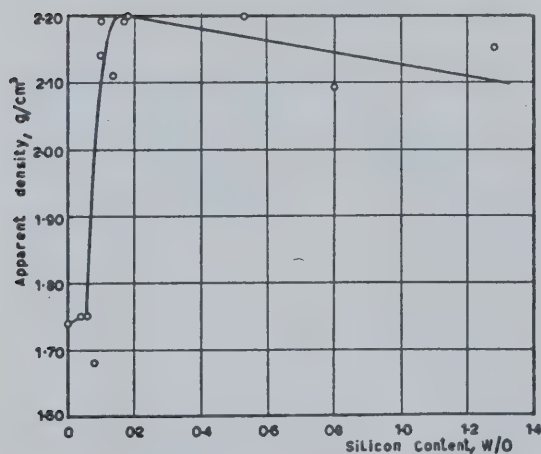   torr.   80X, polarized light.

FIGURE 47.   Electron microprobe scan of
nickel in a pyrolytic graph-
ite alloy containing 0.003
a/o nickel.

Dependence of the crystallite height on
silicon content.

Density of silicon-containing pyrocarbon
against silicon content.

FIGURE 48. Results taken from Marinkovic et al,
Carbon 8, 1970, p. 283. Peak values
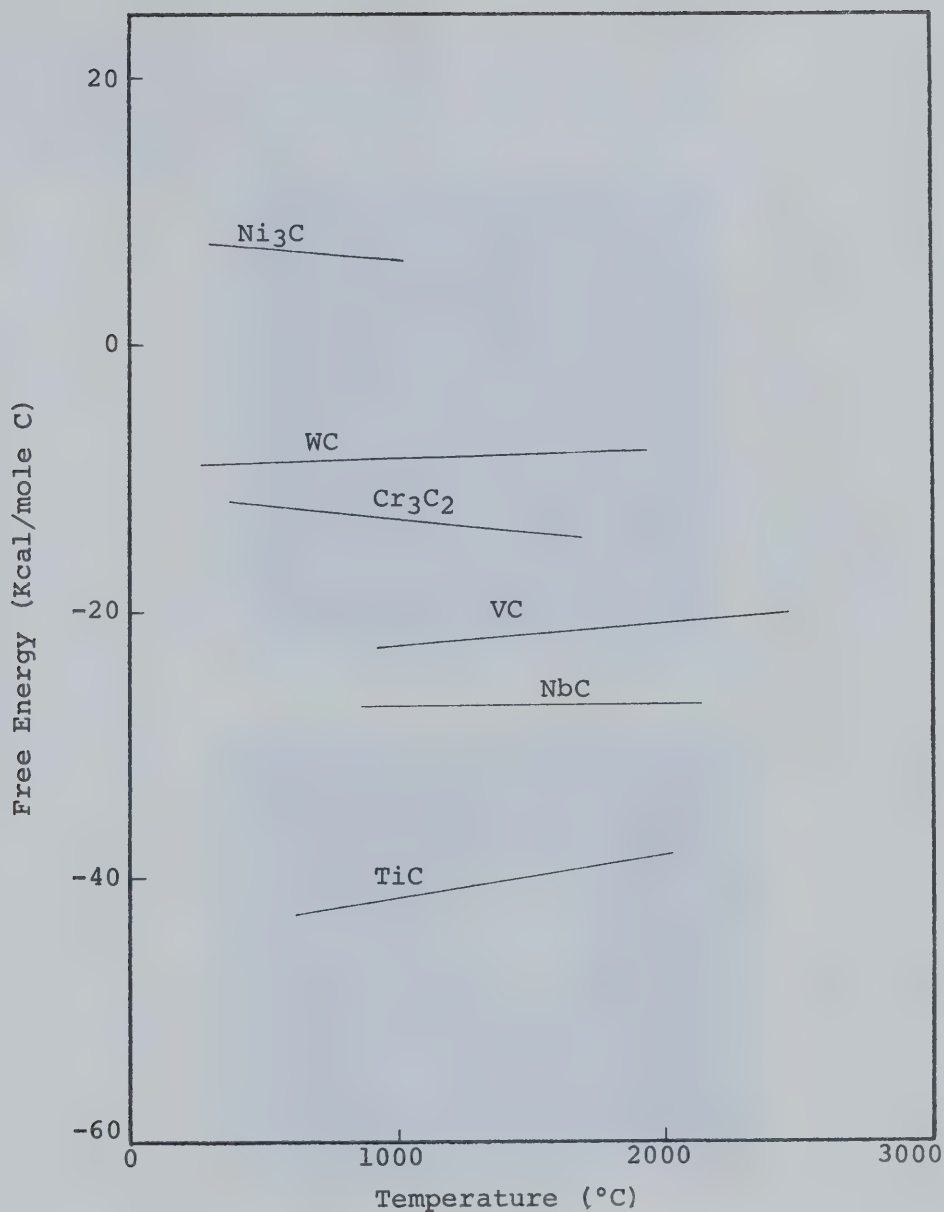are interpreted as the limit of
solid solubility.

FIGURE 49. The standard free energies of formation
of carbides per mole of graphite.
Data taken from O. Kubaschewski, E. L.
Evans and C. B. Alcock, Metallurgical
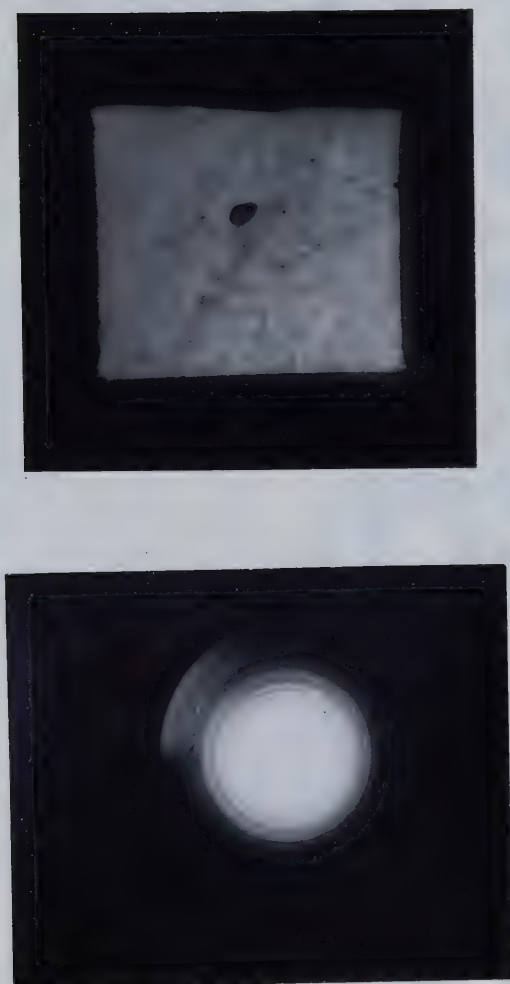Thermochemistry, Pergamon Press, 1967.

FIGURE 50. Precipitate in pyrolytic graphite-
titanium alloy with [110] zone
planes perpendicular to graphite
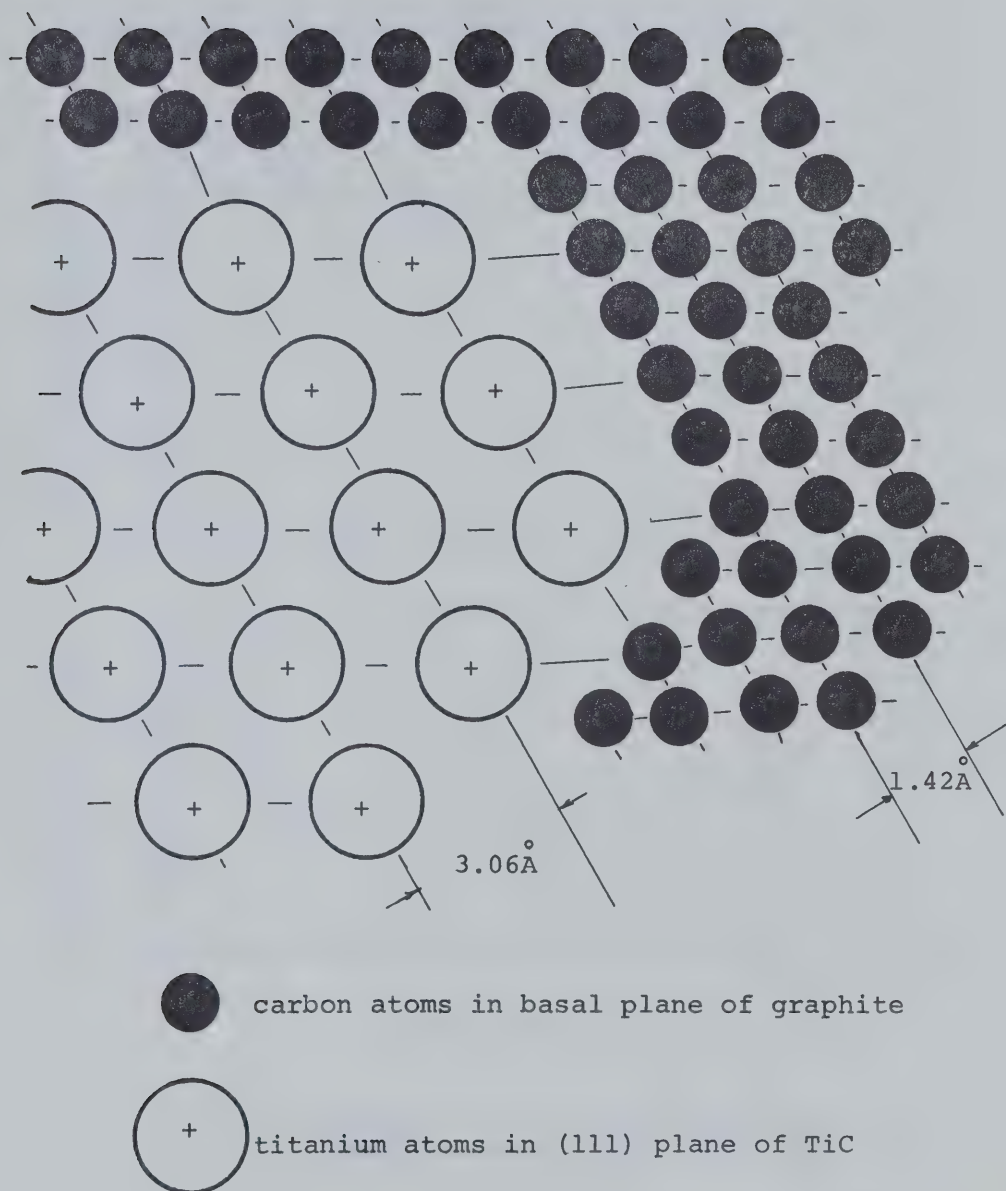basal planes.

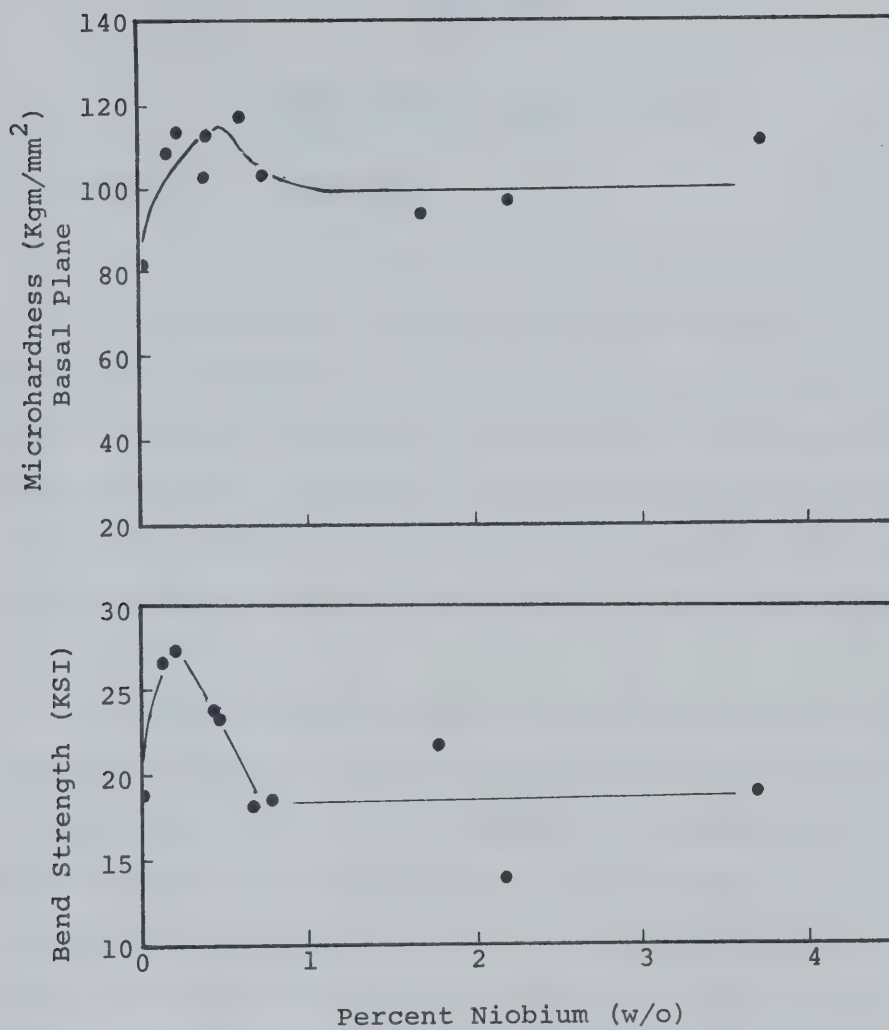FIGURE 51. Semi-coherent interface between
titanium carbide and graphite.

FIGURE 52.   Properties of pyrolytic carbon-
            niobium alloys. Data taken from
            U.S. Patent 3,464,843.

APPENDIX A

Experimental Error Analysis

1. Deposition Temperature

Deposition temperature was monitored by a Latronics
Infred pyrometer and a chromel-alumel thermocouple. The
pyrometer is sensitive to radiation between 1.8 and 2.7
microns and thus atmosphere, water vapor, and quartz glass
absorption bands are avoided. The emissivity of the sub-
strate and deposit was found to be very dependent on temp-
erature and an emissivity calibration of the pyrometer had
to be carried out.

The pyrometer calibration was done by first depositing
pyrolytic graphite on a substrate. With the emissivity of
the pyrometer set at 0.5, the substrate was heated to a
desired temperature and allowed to equilibriate. The emis-
sivity was then varied and the corresponding temperature
noted. Another temperature at emissivity 0.5 was then
selected and the process repeated until the series of curves
given in Figure A1 was obtained. Next, metallic materials
were suspended one at a time over the substrate and their
melting point determined with the pyrometer emissivity set
at 0.4. The metals used were:

```
nickel          mp - 1453°C
zircalloy #2    mp - 1800-1830°C
niobium         mp - 2468°C
```

Figure A2 represents the curve obtained for melting tempera-
ture versus observed pyrometer temperature. Now, taking the
observed temperature from Figure A2 and locating that temp-
erature on Figure Al at an emissivity of 0.4, a curve could
be drawn parallel to existing curves, the actual temperature
was found on this curve, and thus the emissivity setting
required to give the actual temperature could be determined.
It is estimated that with care, temperature inaccuracies
would be no more than 2 or 3 percent. Pyrometer accuracy is
given as ±1%.

Difficulties, however, occurred with excessive sooting
in the deposition chamber. Some soot settled out on the
quartz sight glass and prevented use of the pyrometer. This
occurred even though the glass was protected by a shutter.
A sheathed thermocouple in the vicinity of the deposition
substrate could then be employed to monitor deposition temp-
erature. Quite often, the fogging over of the sight glass
occurred late in the deposition run. It was then possible
to monitor temperature by keeping the rate of change of
temperature, as indicated by the thermocouple, constant with
what it had been previously. In instances where the sight
glass became useless almost immediately, previous experience

was used to keep the temperature indicated by the thermo-couple in line with the deposition rate. Such instances probably resulted in a temperature error of ±10%.

Rough controls on the power source resulted in temp-erature fluctuations. Reported temperatures are thus given over a range, and any errors due to the pyrometer being out of calibration are thereby less important.

2.   Chemical Analysis

With care, errors in spectroscopy determinations should be low, especially where there are no interfering ions or compounds. However, to check on the reliability of the chemical analysis of graphite-metal alloys, several alloys were analyzed by a commercial firm.* A comparison of the results is given in Table Al and it can be seen that with the exception of vanadium all the results between the two analyses are approximately the same and even vanadium results differ only at low concentrations where inhomogeneity in the alloy deposit could be more of a factor than the actual analysis.

---

* Commercial analysis done by Chicago Spectro Service Laboratory, Inc., Chicago, Illinois.

3.   Density Measurements

Densities were determined to five place figures with four place figure significance. Density checks were performed on several alloy deposits and agreement within ±0.003 gm/cc was found for samples selected from the same region of the deposit. Density of the deposit was found to vary from top to bottom in the deposit--the bottom of the deposit being most dense. For this reason, only an apparent density could be cited.

4.   X-ray Measurements

X-ray diffractometer measurements were recorded to the nearest thousandth of a degree but calculations were done only on two decimal place accuracy. The root mean square lattice strain values are somewhat questionable for this reason. Lattice c parameter determination was done by averaging results from four sets of fore and back scans. Weighted peak radiation length was used in the calculations.

5.   Microhardness Measurements

Reported experimental microhardness values were obtained by taking eight or more values from a single sample and subjecting the results to statistical analysis. A large number of results were rejected in this manner and it was thought

that perhaps microhardness might vary with load in the 100 gm load range. Figure A3 shows that above a load of 40 grams, microhardness values are constant with increasing load. Variations in microhardness values must therefore be related to local microstructural differences in the deposits. Figure A3 shows this could be the case as all reported values, except the 100 gm load value, are from single hardness readings.

TABLE A1

Comparison of Chemical Analyses

w/o Alloy Element

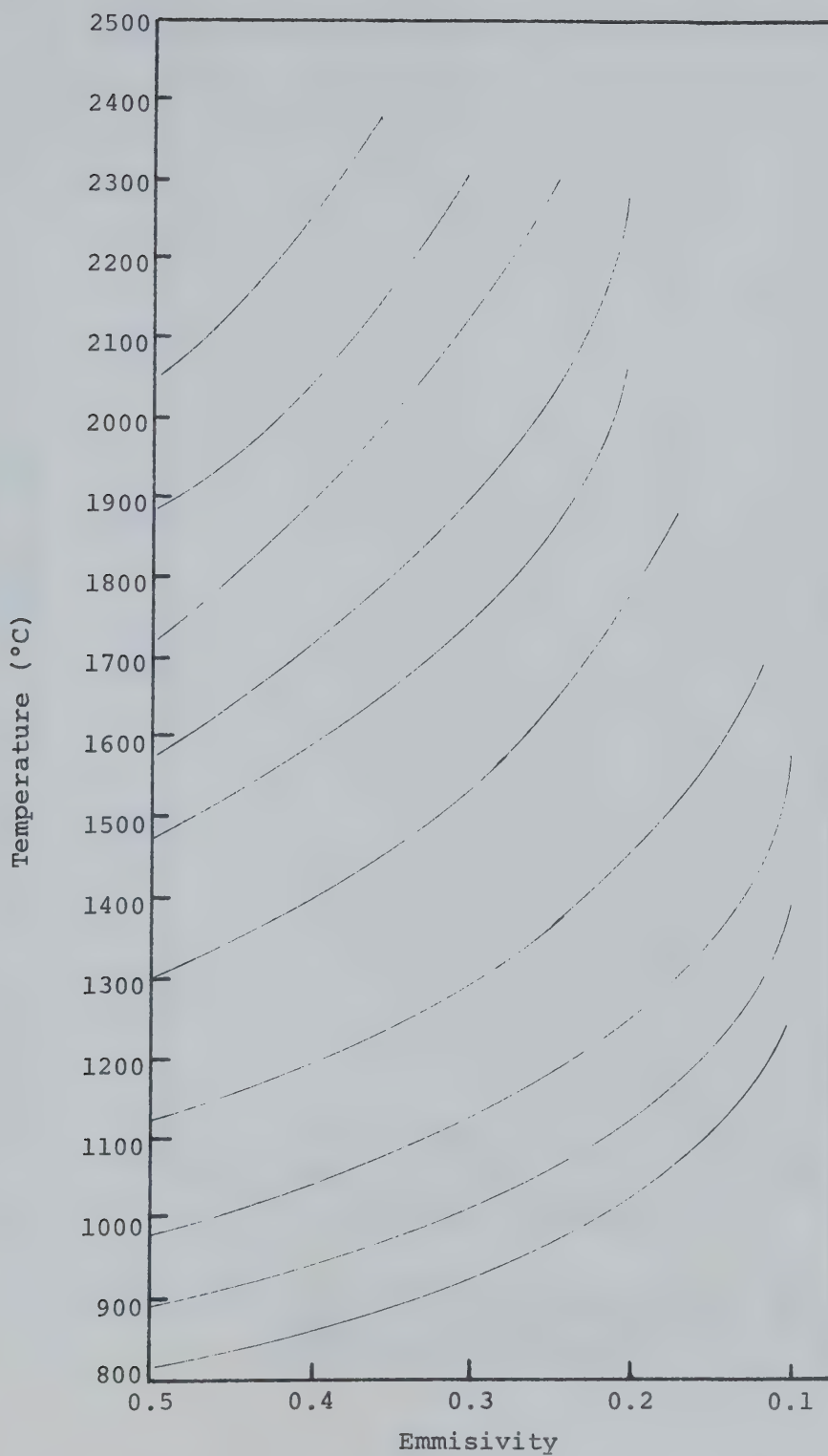| Sample Number	Analysis by Author	Commercial Analysis
37PCTi	0.050	0.0520
2PCV	0.008	<0.005
2PCNi	0.014	0.0150

FIGURE A1. Pyrometer temperature reading as
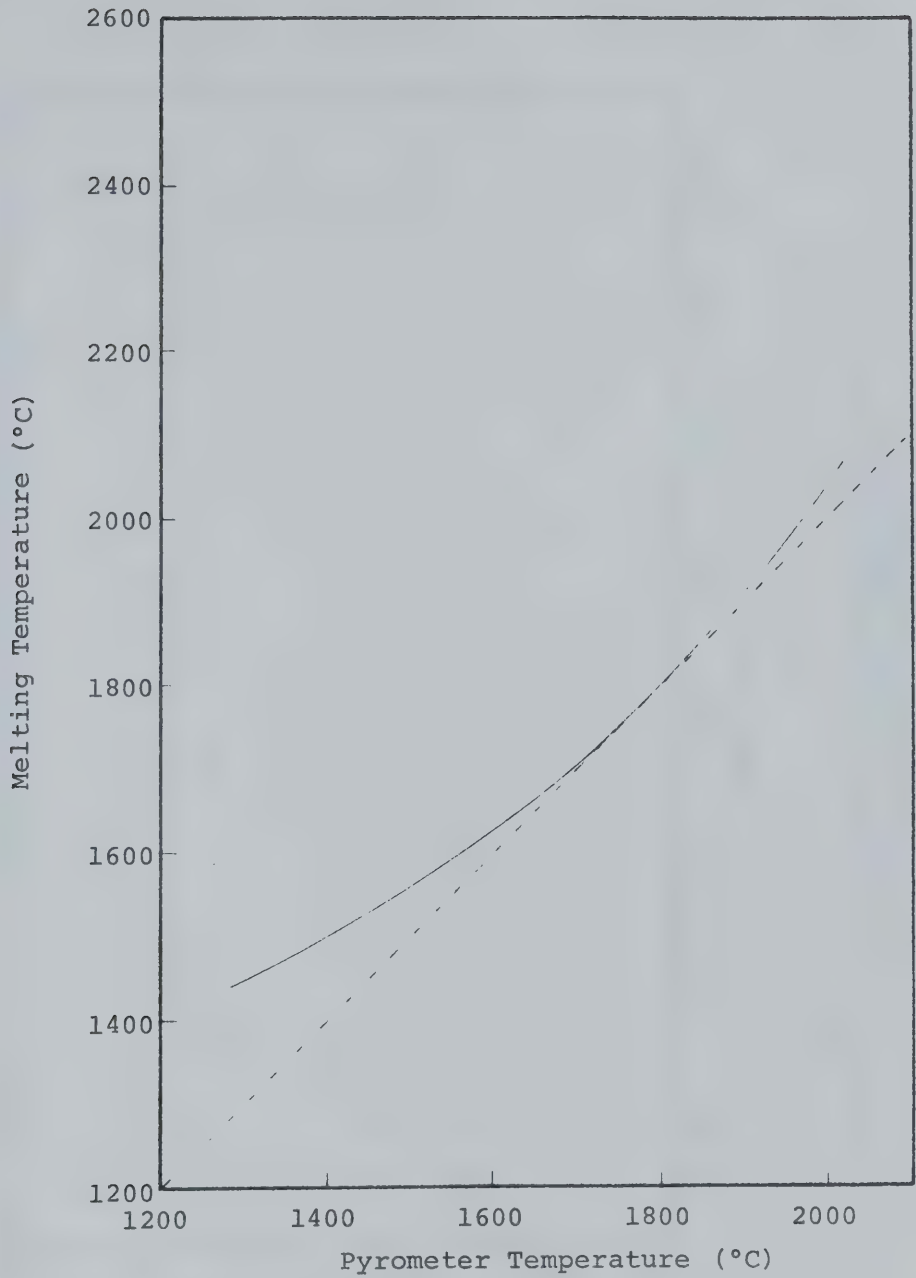
FIGURE A2.   True temperature as a function of
             observed pyrometer temperature for
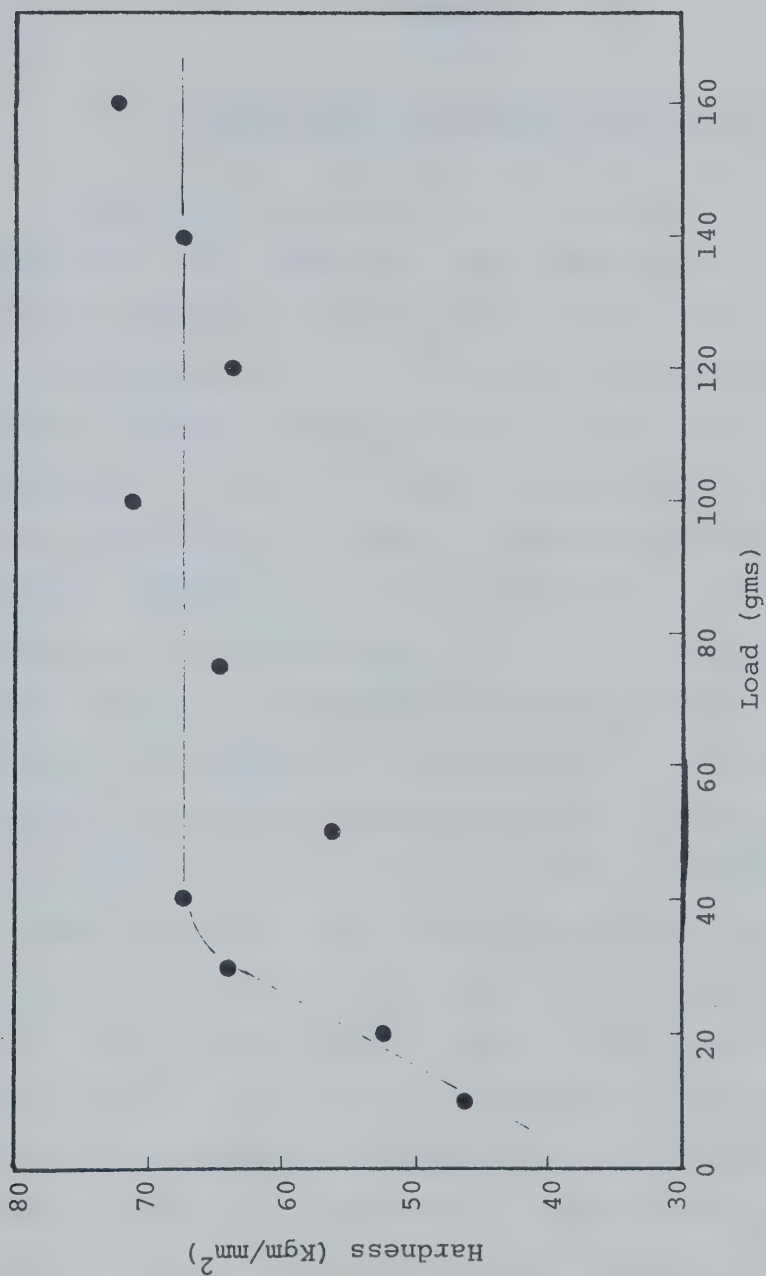   an emissivity setting of 0.4.

FIGURE A3. Microhardness on planes perpendicular to basal planes as a function of applied load for sample #8PC.

APPENDIX B

Evaluation of Reported Solubilities

The solubility limit of 0.3 a/o nickel in graphite reported in the literature[1] was determined by examining graphite grown in a liquid nickel bath. The graphite was subsequently analyzed in situ by an electron probe. Extraction of graphite crystals from the nickel matrix followed by conventional chemical analysis on the graphite was not found to be practical or reliable. The graphite crystals were, however, examined by electron microscopy and found to be uniform to a resolution of 100 $\overset{\circ}{A}$. It is unfortunate that no X-ray structure determination was done on the graphite to determine its degree of graphitization. In a study[2] of graphite grown in an iron-silicon melt, it was found that the graphite had a lattice parameter, c, smaller than that of ideal graphite. This graphite contained both iron and silicon but, after etching, only silicon remained. Also, after etching, the graphite gave an ideal lattice spacing of 3.3538 $\overset{\circ}{A}$. This led to the conclusion that iron creates an internal pressure of approximately 100 Kg/cm^2 to give a lower c value. Such may also be the case with graphite grown in nickel melts so that standard conditions do not exist for any reported solubility. The determination in

situ using an electron microprobe can also give an errone-
ously high nickel concentration as the probe excites fluor-
escence from a volume rather than a surface.

The solubility of vanadium in well crystallized graph-
ite has been reported as 0.088 a/o vanadium.[3] This was
obtained by examining, with an electron microprobe, a glassy
carbon on which vanadium carbide had been melted. The vana-
dium rapidly diffused into the carbon. As vanadium is known
to catalyze graphitization, a measurement of vanadium con-
centration in an area of the carbon which had been graphit-
ized by molten vanadium carbide was taken as the solubility
limit. These findings on solubility are not really convin-
cing as the authors produce a fluorescent X-ray image of the
area in which solubility was determined. This photo shows
clustering of vanadium. A photomicrograph of the area shows
a mixture of vanadium carbide and graphite. Furthermore,
this work was done on glassy carbon which is not graphite.
Experiments with pyrolytic graphite showed very little
penetration of the graphite by vanadium or vanadium carbide
and experiments with natural graphite showed no reaction at
all. It would appear then that the reported solubility is
too high and may not be generalized to other conditions.
The authors also state, "the solubility of vanadium in dis-
ordered carbon ought to be smaller [than in crystalline
graphite] but there seems to be no experimental way of

confirming this." This statement appears to be in direct opposition to their experimental findings and also to the findings of other investigators.[4,5]

Thus it appears that the two reportings of solid solubility for transition metals in graphite are perhaps orders of magnitude too large.